1 2 9 0

UNIVERSIDADE Ð
COIMBRA

Inês Vasconcelos Miranda-Santos

**ANALYSIS OF METABOLIC HETEROGENEITY
OVER CELL DIVISION CYCLE
IN NON-SYNCHRONIZED YEAST**

A ^{13}C BASED EXPERIMENTAL-COMPUTATIONAL APPROACH

Outubro de 2019

Faculdade de Ciências e Tecnologia

Inês V. Miranda-Santos
0000-0002-5467-2756

3rd edition

Coimbra

Outubro de 2019

1 2 9 0

UNIVERSIDADE Ð
COIMBRA

Faculdade de Ciências e Tecnologia

Inês V. Miranda-Santos

0000-0002-5467-2756

2nd edition

Coimbra

Setembro de 2019

Faculdade de Ciências e Tecnologia

ANALYSIS OF METABOLIC HETEROGENEITY OVER CELL DIVISION CYCLE IN NON-SYNCHRONIZED YEAST
a ^{13}C based experimental-computational approach

Inês Vasconcelos Miranda-Santos

Agosto de 2018

1 2 9 0

UNIVERSIDADE Đ
COIMBRA

À minha MÃE e

Ao meu PAI,

Ao JOÃO

  Em gratidão.

Ao GASPAR

Ao ANTÓNIO

Ao MATIAS,

Ao INÁCIO

Ao JOAQUIM

  Em esperança.
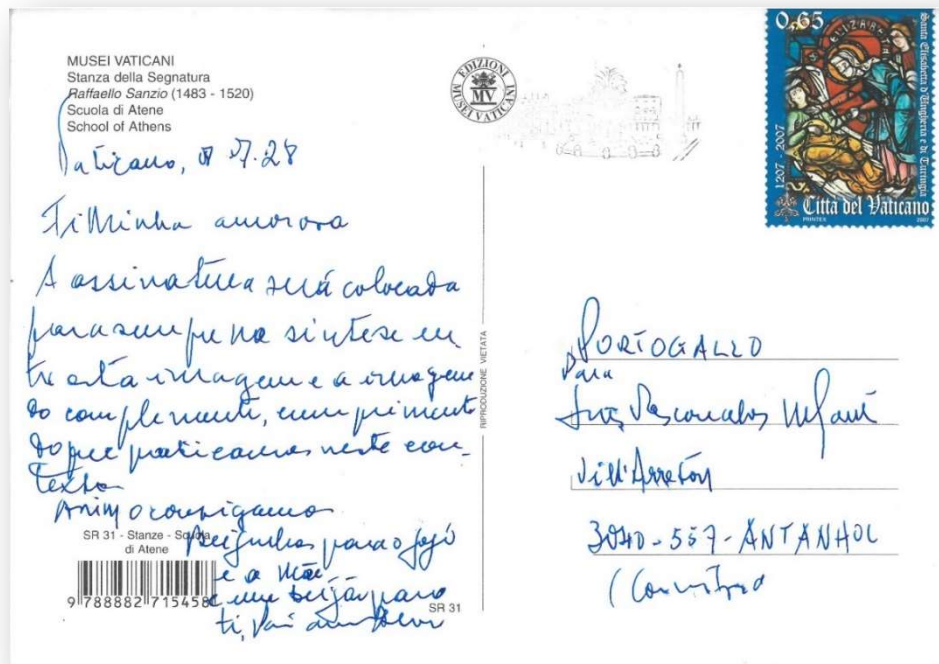
MUSEI VATICANI
Stanza della Segnatura
Raffaello Sanzio (1483 - 1520)
Scuola di Atene
School of Athens

Vaticano, 07.28

Ti Minha amorosa

A assinatura será colocada
para sempre na síntese en
tre esta imagem e a imagem
do complemento, cumprimento
do que praticares neste con-
texto.

Assim o consigamos!

PORTOGALLO
Para

3040-557-ANTANHOL
(Coimbra)

"A assinatura será colocada para sempre na síntese entre esta imagem
e a imagem do complemento, cumprimento do que praticares neste contexto. Assim o consigamos!"
"The signature will be forever stamped in the synthesis between this image
and the image of its complement, fulfilment of whatever you practice under this scope." Dare we make it!"

"De que vale ao homem ganhar o mundo inteiro

Se vier a perder a sua alma?"

"For what does it profit a man to gain the whole world and forfeit his soul?"

Mc 8, 36

"Porque onde estiver o vosso tesouro, aí estará também o vosso coração."

"Because where your treasure is, there your heart will be also."

Mt 6, 21

ACKNOWLEDGEMENTS

Agradeço
ao meu Irmão, João
pela cumplicidade fraterna, a disponibilidade e presença incondicionais
sem perguntas nem delongas.

Agradeço
à minha Madrinha Paula
pela fraternidade, pela confiança e esperança em mim e pelo apoio
deligente.

Agradeço
ao Gaspar, ao António, ao Matias, ao Inácio e ao Joaquim
por não se deixarem levar pelas dificuldades da vida – sim, bebés e
crianças também têm dificuldades na vida, oh! se têm! –
e serem para mim exemplo a seguir de determinação, confiança, coragem
e perseverança para todas as fases da vida

Agradeço,
à Sónia pelo apoio fraterno partilhado.

Agradeço
à minha família tios e primos e afilhados
por gostarem de mim como eu sou.

I acknowledge
my friends in Saarbrücken
for being my family and my home
particularly you who sheltered and fed me.

Agradeço
à SinCera
por me recordar e fazer sentir que somos fermento na massa,
que não estou sózinha na Missão Comum.

Agradeço
à CVX e à Companhia de Jesus,
particularmente ao Padre Vasco Pinto de Magalhães
por, com paciência paternal, me treinarem no buscar o caminho do MAIS.

Agradeço
ao Dr. Francisco Allen Gomes
por cuidar de mim e me *"puxar as orelhas".*

Agradeço
ao escutismo e particularmente ao Agrupamento 603 do Corpo Nacional de Escutas
por serem a minha escola de vida e o meu porto seguro.

Agradeço
a ti, sim, por sempre me chamares ao essencial: *Força, Foco e Fé.*
...e que foi determinante na prolongada recta final.

Deo gratias!

RESUMO

Há cada vez mais evidências sobre alterações metabólicas significativas ao longo do ciclo de divisão celular (CDC) em células eucarióticas. No entanto, devido a limitações técnicas, não há informação quantitativa sobre a distribuição dos fluxos metabólicos (DFM) nas fases distintas do CDC. Nomeadamente, os métodos de sincronização do CDC perturbam o metabolismo sendo propensos a artefactos e os métodos de separação de células têm baixa eficiência e uma capacidade limitada para separar adequadamente as células de acordo com o CDC. Procurando ultrapassar estas limitações, idealizámos uma metodologia para marcar e seguir o perfil de distribuição de fluxos metabólico (DFM) de células eucarióticas numa fase específica do CDC, contornando a necessidade de sincronização ou de separação de células. A metodologia idealizada assenta no uso de marcadores isotópicos para seguir o metabolismo intermediário partindo da abundância dos isótopos de monómeros constituintes dos biopolímeros que são polimerizados apenas durante as fases-alvo do CDC. Como estudo preliminar para validar o conceito, analisámos a abundância de isótopos de desoxinucleósidos e nucleósidos a partir de DNA nuclear e RNA citoplasmático, respectivamente, de *Saccharomyces cerevisiae* cultivada com glicose marcada com ^{13}C afim de determinar o metabolismo na fase S e fora da fase S, respectivamente, do CDC.

Neste sentido, primeiro implementámos uma abordagem baseada em GC-MS para elucidar isotopómeros posicionais dos desoxinucleósidos e nucleósidos de DNA e RNA, inspeccionando os espectros de fragmentação de seus derivados de trimetilsilil. Identificámos a porção do ião molecular que constitui os respectivos fragmentos, focando particularmente nos átomos de carbono do esqueleto molecular. Os nucleósidos fragmentados ao nível da ligação N-glicosídica geram nucleobases e / ou iões de fragmentos de ribose ou desoxirribose e seus fragmentos. Também se observaram fragmentos de nucleósidos compostos pela nucleobase e alguns carbonos do anel de ribose. No total, atribuímos inequivocamente 31 fragmentos.

A fim de avaliar a viabilidade da determinação da DFM em estudo a partir de informações obtidas a partir do método GC-MS anteriormente descrito e optimizar as condições experimentais, desenvolvemos um modelo computacional do metabolismo intermediário de *S. cerevisiae*; é um modelo desenvolvido a partir de levantamento genómico e adequado à investigação da DFM ao longo do CDC. Conceptualizámos duas subpopulações de células – células em fase S e fora da fase S do CDC. O modelo é viável e está terminado, pronto para ser usado para uma análise de sensibilidade meticulosa tendo

como fim o desenho de experiências e a respectiva análise dos fluxos metabólicos por marcação com ^{13}C (^{13}C-MFA).

S. cerevisae foi cultivada em cultura contínua em meio enriquecido com [1,2-^{13}C] glicose. Os desoxinucleósidos e nucleósidos de DNA e RNA, respectivamente, foram isolados separadamente e a distribuição dos isótopos de massa (DIM) dos seus fragmentos foi medida por GC-MS. Uma análise qualitativa dessa DIM mostrou que: i) a porção de ribose dos nucleosídeos pirimidínicos foi biossintetizada via ramo oxidativo da via das pentoses juntamente com vai-e-vem no ramo não oxidativo; ii) desoxirribose de desoxinucleósidos pirimidínicos foram biossintetizados via glicólise e ramo não oxidativo da via das pentoses; iii) as nucleobases das desoxipirinas foram biossintetizadas via através de um fluxo concertado de vai-e-vem entre a glicólise e o ramo não oxidativo da via das pentoses seguindo-se fluxo pelo ramo oxidativo da via da pentoses; iv) o DIM da nucleobases da citidina, desoxicitidina e timidina revelam atividade do ramo oxidativo da via das pentoses, carboxilase do piruvate e ciclo dos ácidos tricarboxílicos. Esta evidência de multiplicidade de vias metabólicas contribuintes para a biosíntese de nucleobases da citidina, desoxicitidina e timidina pode ser resultante de um tempo de meia vida mais longo dos reservatórios de aspartato. A atividade combinada da carboxilase do piruvato e do ciclo dos ácidos tricarboxílicos pode dever-se à necessidade de satisfazer o recrutamento simultâneo de biossíntese de aminoácidos e ácidos gordos a partir dos intermediários do ciclo dos ácidos tricarboxílicos, exigindo, assim, um ciclo dos ácidos tricarboxílicos activo e o reabastecimento dos seus respectivo reservatórios. Os isotopómeros ^{13}C dos monómeros do DNA diferem dos do RNA, indicando que uma DFM heterogénea ao longo do CDC.

PALAVRAS-CHAVE: metabolismo de células proliferativas, proliferação celular, ciclo metabólico, análise de fluxos metabólicos por ^{13}C, modelação metabólica, espectrometria de massas, nucleósidos

ABSTRACT

There is increasing evidence of extensive metabolic changes over the division cycle of eukaryotic cells. However, quantitative information about how flux redistributes in distinct phases of this cycle is lacking, due to technical difficulties. Namely, cell division cycle (CDC) synchronization methods disrupt metabolism, and are thus artifact-prone, and cell sorting methods have low throughput and a limited ability to adequately separate cells by CDC. Seeking to bypass these shortcomings, we devised a methodology to profile the metabolic flux distribution (MFD) of eukaryotic cells in a specific phase of CDC without requiring CDC synchronization or cell sorting. The general principle consists in using isotopic tracers to back trace intermediary metabolism from the isotopomer abundances of building-blocks of biopolymers that are polymerized only during the target phases of the CDC. As a proof of principle, we analyzed the isotopomer abundances of building-blocks from nuclear DNA and cytoplasmic RNA of Saccharomyces cerevisiae *grown on ^{13}C-labeled glucose to profile the metabolism in S phase and non-S-phase (respectively) of the CDC.*

Towards this goal, we first implemented a Gas Chromatography – Mass Spectrometry (GC-MS) based approach to elucidate positional isotopomers of nucleosides from RNA and DNA by screening the fragmentation spectra of their trimethylsilyl derivatives. We identified the molecular ion moieties retained in the respective fragment ions, focusing particularly on the carbon backbone. Nucleosides fragmented at the N-glycosidic bond provide nucleobase and/or ribose or deoxyribose fragment ions and fragments thereof. Nucleoside fragments composed of the nucleobase plus some carbons of the ribose ring were also observed. In total, we unequivocally assigned 31 fragments.

In order to assess the viability of determining the sought MFD from information obtainable from the previous GC-MS method and to optimize the experimental conditions, we developed a customized genome-wide computational model of intermediary metabolism of S. cerevisiae*. Its design accounts for two sub-populations of cells – in and out of S-phase of the CDC. The model is feasible, ready to be used for a meticulous sensitivity analysis, to design further experiments and to perform ^{13}C-metabolic flux analysis (^{13}C-MFA).*

A continuous culture of S. cerevisae *was fed with [1,2-^{13}C]glucose. deoxynucleosides and nucleosides from DNA and RNA, respectively, were isolated separately and the mass isotopomer distribution (MID) of their fragments was measured in GC-MS. A qualitative analysis of these MID showed that: i) the ribose moiety of pyrimidinic nucleosides was biosynthesized via the oxidative branch of pentose phosphate*

pathway (PPP) followed by shunting back and forward in the non-oxidative branch of PPP; ii) deoxyribose of pyrimidinic deoxynucleosides was biosynthesized via glycolysis followed by the non-oxidative branch of PPP; iii) nucleobases of deoxypurines were biosynthesized via a concerted flux of shunting back and forward between glycolysis and non-oxidative PPP followed by the oxidative branch of PPP; iv) the MID of nucleobases of cytidine, deoxycytidine and thymidine reveal activity of the oxidative branch of PPP, PC and TCA cycle. This would come from the longer turnover of TCA cycle related pools. The concerted activity of PC and TCA cycle may satisfy the joint demand for amino acids and fatty acids biosynthesis from the intermediaries of TCA cycle, thus requiring an active TCA cycle and the respective replenishing of its pools. The ^{13}C-isotopomers of DNA building blocks differ from those of RNA, indicating that the MFD is heterogeneous over CDC.

ABBREVIATIONS

^{13}C-MFA	^{13}C-metabolic flux analysis
aa	amino acid
ASP	aspartate
CDC	cell divison cycle
CDW	cell dry weight
CLE	carbon labeling experiments
cRNA	cytosolic RNA
CTHF	N5,N10-methylenetetrahydrofolate
DEPC	diethylpyrocarbonate
DNA	deoxyribonucleic acid
dNMP	2'-deoxynucleosides monophosphate
DR	dilution rate
DT	doubling time
EDTA	Ethylenediaminetetraacetic acid
EC	enzyme classification
F6P	fructose-6-phosphate
FBA	flux balance analysis
FISH	fluorescent *in situ* hybridization
FTHF	N10-formyltetrahydrofolate
GA3P	glyceraldehyde-3-phosphate
GC	gas chromatography
GSS	Glycine/serine system
HPLC	high pressure liquid chromatography
LC	liquid chromatography
MFD	metabolic flux distribution
MID	mass isotopomer distribution
MS	mass spectrometry
MSTFA	N-methylsilyl-trifluoroacetamide
mtDNA	mitochondrial DNA
mtRNA	mitochondrial RNA
nDNA	nuclear DNA
NMP	nucleosides monophosphate
OAA	oxaloacetate

OD_{600}	optical density at 600 nm
ON	overnight
PPP	Pentose Phosphate Pathway
PPPnon-ox	Non-oxidative branch of Pentose Phosphate Pathway
PPPox	Oxidative branch of Pentose Phosphate Pathway
PC	pyruvate carboxylase
R5P	ribose-5-phosphate
RNA	ribonucleic acid
RT	retention time
SIM	seletctive ion monitoring
TCA cycle	tricarboxylic acid cycle
xch	exchange flux
YMC	Yeast metabolic cycle
YPD	Yeast Extract Peptone Dextrose Agar

CONTENTS

1 | Introduction

1.1| METABOLIC HETEROGENEITY OVER CELL DIVISION CYCLE IN PROLIFERATING CELLS

Metabolism of proliferating cells differs from that of quiescent and its characterization has been subject of great interest given the relevance for tumor therapy and regenerative medicine. In the 20's of last century, Otto Warburg found evidence that tumor cell metabolism relies on lactic fermentation, rather than in oxidative phosphorylation, regardless of the presence of O_2 (Warburg, 1924, 1956) – The Warburg effect. More recently, it has been described that metabolic pathway activities are targets of key regulatory signaling pathways altered in tumor cells (DeBerardinis et al., 2008; Hsu and Sabatini, 2008; Vander Heiden, Cantley and Thompson, 2009). Indeed, a common understanding is that there is a metabolic phenotype characteristic of the proliferating state, presenting a reconfiguration of the metabolism as compared to quiescent state and conferring proliferating advantage (Lunt and Vander Heiden, 2011; Deberardinis and Chandel, 2016; Pavlova and Thompson, 2016).

Alternatively, the number of significant metabolic differences between proliferating and quiescent cells can be looked at as the metabolism being different in different phases of the cell division cycle (CDC), i. e., each phase of CDC may have its proper metabolic profile. A proliferating cell culture is indeed a mixture of cells in different phases of the CDC, thus, with different metabolic profiles. In such a case, the metabolic profile observed in proliferating populations may result from the combination of the metabolic profiles and cell abundances of each phase of the CDC. This hypothesis is supported by the evidence of heterogeneous metabolism in asynchronous growing human leukemia T cell population and by the metabolic oscillations observed in proliferating synchronized cultures. Carbon labeling experiments (CLE) in asynchronous proliferating human leukemia T cells resulted in ^{13}C isotopomer distribution of several metabolites that could not come from metabolic processes taking place simultaneously in the same macrocompartments, cells. The profiling of the metabolism of such cell population suggested that the culture is constituted by several sub-populations in relation to phases of the CDC (Miccheli et al., 2006b). Proliferating synchronized yeast cultures show oscillations in pO_2, which are coupled to CDC phases and accompanied by oscillations in metabolic gene expression and metabolite concentrations (Tu et al., 2005). Considering that the proliferating cell continuously cycles over the different phases of the CDC, the metabolic heterogeneity may be due, at least in part, to the metabolic reconfiguration associated to the distinct phases of the CDC.

Few studies have so far investigated whether and how metabolism is different at distinct phases of the CDC. Evidences of metabolic heterogeneity coupled to the CDC have been observed at transcriptomic and metabolomic levels (Tu et al., 2005; Chen et al., 2007; Slavov and Botstein, 2011), but the metabolic flux distribution (MFD) has not. Therefore, we aimed at studying the phase specific activity of intermediary metabolism in

asynchronous cell population. We used CLE and focused particularly in S-phase as proliferating cells spend a considerable fraction of CDC in this phase and DNA is specifically biosynthesized at this stage. Therefore, the ^{13}C isotope distribution in the monomers of DNA reports the MFD during S-phase. For proof-of-principle we used budding yeast *Saccharomyces cerevisiae* as model of eukaryotic proliferating cell.

1.2| OBJECTIVES

1. To investigate whether and how the metabolic flux distribution of the intermediary metabolism during S-phase differs from that of the average of the other phases of CDC, in asynchronous *S. cerevisiae* population.

2. Achieving this general objective required these other accessory objectives:

    2.1. To develop a GC-MS based methodology to determine ^{13}C isotopomers of deoxynucleosides and nucleosides isolated from DNA and RNA.

    2.2. To develop a ^{13}C-MFA computational model of proliferating asynchronous population of *S. cerevisiae* to perform *in silico* forward simulation of intermediary metabolism and to estimate metabolic flux distribution.

1.3| METABOLIC OSCILLATIONS IN THE YEAST AND THEIR RELATIONSHIP WITH THE CELL DIVISION CYCLE

The strongest evidence for the metabolic heterogeneity over the CDC comes from the correlation between metabolic oscillations in synchronized yeast cultures and the CDC. For this reason, here we review this topic in some detail.

It has been known since the mid 1950's that yeast cell populations in continuous culture can exhibit sustained oscillations of O_2 consumption (Finn and Wilson, 1954). Early observations showed that the oscillations in dissolved O_2 were accompanied by oscillations in culture cell density, dissolved CO_2, and pH (Finn and Wilson, 1954; Kaspar von Meyenburg, 1973; Harrison and Topiwala, 1974; Bandyopadhyay and Ghose, 1982). Later, it was also observed that the concentration of acetate, ethanol, pyruvate, glycogen, ATP, NADH (Satroutdinov, Kuriyama and Kobayashi, 1992), glutathione (Murray *et al.*, 1999), amino acids and trehalose (Hans, Heinzle and Wittmann, 2003) changed cyclically, orchestrated with the oscillatory rates of respiration and fermentation. This orchestration permitted to conveniently follow the metabolic oscillations by monitoring dissolved O_2 and/or NADH concentration and to identify an oxidative and a reductive phase, corresponding to low and high dissolved O_2 respectively. More recently, it was shown that over half of the gene transcripts, mainly coding for metabolic enzymes (Tu *et al.*, 2005; Murray, Beckmann and Kitano, 2007), the majority of the metabolome (Murray, Beckmann and Kitano, 2007; Tu *et al.*, 2007) and the activity of many transcription factors (Rao and Pellegrini, 2011) oscillate with the same period as, but various phase shifts from, the dissolved O_2 oscillation.

1.3.1| Yeast Metabolic Cycle

The oscillations in gene expression cluster according to the above-mentioned phase shifts into three major groups which are also functionally distinct. In the oxidative cluster, which maximum of expression is at the sudden decrease in dissolved O_2, the most upregulated genes relate to amino acid, purine, pyrimidine and lipid biosynthesis, sulfur uptake and metabolism, RNA metabolism and translation initiation factors. The reductive/building cluster follows the oxidative cluster and its gene expression peaks when the dissolved O_2 reaches the minimum and begins to accumulate. Its genes code for oxidative phosphorylation, tricarboxylic acid (TCA) cycle, mitochondrial biogenesis, DNA replication, histones, spindle pole and cell division. Finally, the reductive/charging cluster consists of genes that reach maximal expression at the maximum of dissolved O_2. They code for enzymes of glycolysis and the breakdown of storage carbohydrates, recruitment of ethanol for acetyl-CoA feeding into the TCA cycle, fatty-acid oxidation, methylcitrate cycle, glyoxylate cycle, amino acid catabolism, production of NADPH, peroxisome,

ubiquitin/proteasome, vacuole and protein degradation (Tu *et al.*, 2005). Given the broad span of these oscillations, this phenomenon is nowadays referred as the yeast metabolic cycle (YMC).

The majority of the metabolome oscillates during the YMC and the metabolite oscillations cluster at distinct phases of the YMC. However, the correlation of metabolite clusters with the metabolic function or pathway activity is not complete. For instance, different types of amino acids show maximal concentration at the three different phases of the YMC. Overall, it can be said that nucleotides, NADH, pyruvate and other glycolytic intermediaries, succinate and other TCA cycle intermediates cluster together; intermediaries of pentose phosphate pathway (PPP), trehalose and other storage carbohydrates form another cluster of accumulation of metabolites (Murray, Beckmann and Kitano, 2007; Tu *et al.*, 2007). Different authors reached different conclusions about the correlation between the phase shift of the metabolite clusters, the transcript clusters and the oxidative/reductive phases. Tu et al. (2007) stated that the maximum of metabolite accumulation coincides with the maximum of gene expression of the enzymes that catalyze the respective pathways, whereas Klevecz et al. (2004), Murray, Beckmann, and Kitano (2007) showed that the metabolite concentrations peak following the peak in the transcriptional activation of the pathway. At present there is no direct information about how metabolic fluxes relate to these oscillations.

The metabolic oscillations are only observed under specific conditions of low glucose concentration, low dilution rates (DR) and high O_2 concentration (Furukawa, Heinzle and Dunn, 1983; Porro *et al.*, 1988). There was substantial work devoted to identify the culture parameters that influence the oscillations. Nitrogen sources, namely ammonium and urea, specific substrate concentration and DR or duration of budding cycle are described to be determinant for observable oscillations (Kaspar von Meyenburg, 1969; Borzani, Gregori and Vairo, 1977; Agrawal *et al.*, 1982).

The first mathematical model developed that could fully describe the sustained oscillation included biomass, growth rate, O_2 concentration, yield and activity of storage/hydrolysis of carbohydrate as variables (Heinzle *et al.*, 1983).

1.3.2| Yeast Metabolic Cycle, constitutive or conditional?

The fact that whole-culture oscillations are detectable only under some conditions can be interpreted in two fundamentally different ways, namely, (i) these oscillations occur in individual cells <u>at all times</u> but are macroscopically observable only under those conditions when full synchronization of the cell culture is achieved – *constitutive oscillation hypothesis*; or (ii) the oscillations occur in individual cells <u>only under those</u>

conditions – *conditional oscillation hypothesis*.[1] As first evidence for the *constitutive oscillation hypothesis* Silverman et al. (2010) determined by fluorescence *in situ* hybridization (FISH) the single-cell expression level of four distinct genes under conditions where culture-level metabolic oscillations were not observed. The pair of transcripts that belonged to the same YMC cluster as per Tu et al. (2005) was expressed simultaneously in the same cell, whereas the pair that belonged to distinct YMC clusters was not. These results on transcription at the single cell level support the above-mentioned hypothesis that metabolism is different in different phases of the CDC.

Moreover, the induction of sustained glycolytic oscillations in isolated cells showed that the oscillations are not a collective property requiring high cell density, they are rather a single cell phenomenon, not requiring synchronization (Gustavsson *et al.*, 2014). In these experiments, individual cells were positioned in arrays within a microfluidic flow chamber such that all the cells were subjected to the same environment but not synchronized. This setup allowed NADH autofluorescence measurement at single-cell level. Given that oscillations occurred only upon induction, rather than spontaneously, this experiment still does not answer the primary question whether YMC is an intrinsic property of proliferating yeast cells. Attempts to inspect the metabolome and metabolic pathway activity at the single cell level were so far unsuccessful, mostly due to experimental limitations of either keeping oscillations in a cell isolated from an oscillating population or achieving oscillations at very low cell density (De Monte *et al.*, 2007; Poulsen, Petersen and Olsen, 2007; Chandra, Buzi and Doyle, 2011; Aon *et al.*, 2019).

Another approach to inspect intermediary metabolism used stable-isotope tracer experiments in asynchronous proliferating leukemia T cell population. It was possible to infer the activity of PPP, TCA cycle and amino acid metabolism (Miccheli *et al.*, 2006a). The flux ratios estimated from the pattern of ^{13}C enrichment of lactate, alanine, glutamate, proline, serine, glycine, malate and the ribose-5-phosphate (R5P) moiety of the nucleotides showed that the metabolic processes described could not take place simultaneously in the same macro compartment (cell). These observations are evidence for a heterogeneous metabolism in the asynchronous population.

1.3.3| Yeast Metabolic Cycle & Cell Division Cycle

Evidence for a correlation between the metabolic cycle and the CDC has accumulated since very early. The mean generation time of the cells was one of the first parameters identified as correlating with the periodicity of the metabolic oscillations (Kaspar von Meyenburg, 1969). In metabolically oscillating cultures, the budding index also oscillates between 10 and 60% (Porro *et al.*, 1988). Prior to budding, ethanol

---

[1] It should be noted that these are two extreme and not mutually exclusive hypotheses. *I.e.*, it may happen that metabolism oscillates in single cells in many conditions where culture-level synchronization does not occur, and there are also conditions where oscillations stop at the single-cell level as well.

production is enhanced and cells grow on ethanol (Porro *et al.*, 1988); glucose uptake reaches its maximum during budding (Chen and McDonald, 1990). DNA replication, the most readily identifiable CDC event, is gated by the reductive phase: DNA is only replicated during the reductive phase (Klevecz *et al.*, 2004; Tu *et al.*, 2005), but cells can undergo the reductive phase without engaging in DNA replication. Indeed, it was suggested that the YMC and the CDC are related but distinct cycles, i.e., budding yeast cells can undergo YMC without division (Slavov *et al.*, 2011). The metabolic oscillations were observed during the growing phase before cells were ready to cross the G1/S check point and thus enter the CDC. Nonetheless, CDC-related gene transcripts clustered by expression and this cluster oscillated with the same period as the transcription clusters of the reductive/oxidative cycle (Klevecz *et al.*, 2004; Tu *et al.*, 2005). At present the mechanisms coupling the CDC and YMC and the physiological significance of this coupling remain incompletely understood.

1.4| METABOLIC FLUX DISTRIBUTION IN NON-SYNCHRONIZED YEAST CULTURE BY ^{13}C TRACING

1.4.1| 13C-Metabolic Flux Analysis and metabolic modelling

Fluxomics aims at estimating the reaction rates of a substantial number of metabolic pathways (fluxes). However, most metabolic fluxes cannot be directly measured. Rather their values can only be inferred from indirect measurements. The most commonly used formalisms for metabolic (quasi) steady-state flux calculation are flux balance analysis (FBA) (Savinell and Palsson, 1992; Vallino and Stephanopoulos, 1993), ^{13}C-isotopomer analysis (Malloy *et al.*, 1987) and ^{13}C-metabolic flux analysis (^{13}C-MFA) (Wiechert, 2001; Sauer, 2006; Zamboni *et al.*, 2009).

^{13}C-MFA is considered the "gold standard" of fluxomics because it presents great advantages over both FBA and ^{13}C-isotopomer analysis in the detailed and absolute quantification of intracellular fluxes. More precisely, ^{13}C-MFA: i) resolves parallel reaction steps, metabolic cycles and forward *vs.* backward directions in bidirectional reactions (Wiechert and Graaf, 1997); ii) it does not require assumptions about cellular energy state (e.g. P/O ratio, thorough accounting of metabolic reactions involving ATP/ADP and NAD(P)H/NAD(P)$^{+}$); iii) it does not require the *a priori* assumption of a cellular objective (objective function) (Wiechert *et al.*, 1997); iv) it allows in principle a comprehensive quantification of absolute intracellular metabolic fluxes (Wiechert, 2001).

In ^{13}C-MFA, fluxes are calculated from the metabolite isotopic enrichments upon CLE and from the experimentally measurable metabolic rates and exchange fluxes (xch) between the intracellular and extracellular media, and by inference using computational tools (Wiechert *et al.*, 1997). CLE is a common approach for the study of metabolism based on the use of stable isotopes. In CLE the fed substrate is selectively enriched in ^{13}C and is normally metabolized in the cell as its natural abundance labeled counterpart (T.Gregg *et al.*, 1973). As the substrate is metabolized it undergoes the molecular transformations proper of each reaction resulting in the distribution of the ^{13}C isotope through the metabolic network according to the activity of the metabolic pathways. Hence, the downstream metabolite pools become enriched in ^{13}C in accordance with the carbon rearrangement specific of the respective metabolic reactions. The enrichment in ^{13}C is assessed as isotopomer[2] abundance. Therefore, the metabolic routes through which metabolites are produced are traced back from the isotopomer abundances of the metabolite pools. The ^{13}C

---

[2]The term "isotopomer" derives from isotope+isomer and refers to molecules of the same compound that differ in the position and number of a certain isotope. In the case of ^{13}C, a molecule presents 2^n isotopomers, *n* being the number of carbons of the molecule. E. g. lactate has 3 carbons in its molecular structure, in total it has 8 isotopomers: [1-^{13}C] lactate, [2-^{13}C] lactate, [3-^{13}C] lactate, [1,2-^{13}C] lactate, [1,3-^{13}C] lactate, [2,3-^{13}C] lactate, [1,2,3-^{13}C] lactate, [U-^{12}C] lactate, where the numbers in between brackets designate the carbon numbering where the ^{13}C isotope is localized and U stands for uniformly labeled, i.e. all the carbons are ^{13}C.

positional isotopomer abundances, i.e. the ^{13}C tracer distribution, resultant from a CLE indicates the specific pathways generating the analyzed metabolite, and the fractional abundance of the positional isotopomers of that metabolite permits inferring the activity of each intervenient pathway.

The estimation of metabolic fluxes by ^{13}C-MFA requires mathematical models of metabolite isotopomer abundances as function of the metabolic reaction rates. Such models integrate the metabolic network topology, the stoichiometry and the carbon atom mapping of the reactions, the isotopomer balances of the network, the reaction rate constraints and the input substrate composition (Wiechert *et al.*, 2001; Nöh, Droste and Wiechert, 2015). The metabolic network topology is surveyed at genome-wide level and together with the respective stoichiometry builds up the reconstruction of the metabolic network. The carbon mapping refers to the description of the carbon rearrangements from substrates to products taking place in each reaction; the carbon labelling transitions are represented in the model, based on the knowledge of which substrate carbon atom becomes which product carbon atom in the reaction (Wiechert and Graaf, 1997). The isotopomer balance is computed in matrix notation from the network reconstruction and the carbon mapping. (Wiechert *et al.*, 1999).

The mathematical model quantitatively describes the relation between the metabolic reaction rates and the ^{13}C tracer distribution and enrichment of the metabolites. Given a set of metabolic rate values, the mathematical model predicts the respective isotopomer abundance. Conversely, the model can be used to estimate metabolic rates from experimentally determined isotopomer abundances. Therefore, in ^{13}C-MFA fluxes are estimated by fitting the model to the experimentally measured ^{13}C isotopomer distribution under appropriate flux constraints. The implementation of ^{13}C-MFA for large metabolic networks is challenging because there are 2^n balance equations per reaction, being *n* the number of carbons of the metabolites involved in the reaction. Parameter estimation is based on matrix calculations, applying non-linear regression and the least squares estimator (Wiechert and de Graaf, 1996; Wiechert *et al.*, 1997). In brief, ^{13}C-MFA unfolds as follows (Wiechert *et al.*, 2001): i) ^{13}C isotope distributions of metabolites are simulated *in silico* from sets of metabolic flux rates and from a substrate with a given ^{13}C labelling, complying with the imposed model constraints. The initial guesses of the fluxes for these forward simulations are derived from experimental determinations and plausibility considerations. ii) The discrepancies between model-predicted and the measured isotopic distributions are calculated and iteratively minimized using the weighed least squares method. Goodness of fit statistics are then used to evaluate the confidence with which the metabolic flux rates were inferred from the data in view of their precision. The ability of ^{13}C-MFA to resolve flux distributions is restricted to cases where the reactions under investigation lead to rearrangement of carbon backbone, and that the ^{13}C isotopomer distribution of the analyzable metabolites is distinguishable by NMR or MS. Besides the technical limitations, the application of ^{13}C-MFA can be discouraged due to the high cost of tracer substrates and

the requirement of MS or NMR analytics. Moreover, in addition to metabolic steady-state, ^{13}C-MFA also requires isotopic (quasi)steady-state over the course of the analysis.

An appropriate design of the metabolic network model may permit overcoming most of the above mentioned limitations. Thus, a separate chapter (*cf* Chapter 3) is dedicated to the topic of design of metabolic network models.

1.4.2| Characterization of metabolic flux distribution in S-phase and out of S-phase

The determination of the metabolic fluxes related to CDC is not straightforward. To investigate how the metabolic fluxes relate to CDC-specific events we needed to overcome limitations of the current methodologies. An ideal method should preserve the whole characteristics of an unperturbed cell and be compatible with metabolic flux studies. Synchronization methods are based either in starvation (G0 arrest) or inhibition of certain cellular processes (arrest in a specific phase of CDC). Starvation results in synchronization of the population *via* certain manipulations of the cell metabolism. When cell metabolism is the subject of study starvation may introduce artifacts. On the other hand, synchronization methods do not exactly select any specific CDC stage. Rather they yield sets of starting cells exhibiting some common characteristics that do not perfectly correlate with the CDC phase, e.g. DNA content. Moreover, this so called synchrony rapidly fades out due to the variability among cells (Cooper, 2003) and even in cultures considered to be synchronized it is noticeable sub-populations, one going through the CDC and the other does not (Burnetti, Aydin and Buchler, 2016). Methods of cell sorting with respect to CDC phases are also not adequate because of the low cell throughput, of they also being based on properties only partially coupled to CDC, they are incompatible with narrow time frames required for metabolic studies sample preparation and does not apply to extracellular metabolites.

An ideal method should be non-invasive and able to report on metabolic fluxes in specific CDC phases without requiring cell cycle synchronization or cell sorting. Metabolic flux analysis based on isotopic (e.g. ^{13}C) tracing is a well-established and powerful approach for estimating metabolic fluxes. This methodology may be adopted for the intended purpose as long as informative isotopically traceable metabolic intermediates can be found that are only synthesized in specific CDC phases. These can be the monomers of biopolymers that are synthesized only in those phases. Examples are the aminoacyl residues from some histones or the 2'-deoxynucleotides from nuclear DNA (nDNA).

For a proof of principle, we chose to investigate the S-phase specific metabolism in comparison with the average metabolism in the other phases. In proliferating cells, nucleosides incorporated in DNA and RNA mainly originate from *de novo* biosynthesis (Cohen *et al.*, 1983). The ^{13}C tracer distribution in the deoxynucleosides from nDNA

probes S-phase metabolism, as nDNA is only synthesized in this phase. In turn, the ^{13}C tracer distribution in nucleosides from cytosolic RNA (cRNA) probes the other phases of CDC, when this RNA is synthesized.

The isotopic distribution of the deoxynucleosides and nucleosides at the moment of their biosynthesis becomes imprinted from that of their precursors. In turn, the isotopomer abundance of the precursors, which are intermediary metabolites, reflects the MFD of the cells fed with labeled substrates. Thus, the isotopic distribution in deoxynucleosides reports the MFD during S-phase and the isotopic distribution in nucleosides report the average metabolic distribution of the other phases of CDC. Moreover, the precursors of deoxynucleosides and nucleosides are positioned in very informative branches of the intermediary metabolism. The carbon backbone of pyrimidine deoxynucleosides and nucleosides are derived from aspartate (ASP) and carbamoyl phosphate, whereas that of purine deoxynucleosides and nucleosides is derived from glycine, HCO_3^- and N10-formyltetrahydrofolate (FTHF). ASP exchanges with oxaloacetate (OAA), which in turn is an intermediary of the TCA cycle. Carbamoyl phosphate originates from HCO_3^-. Glycine and FTHF originate from serine, C1-C2 and C3, respectively, which belong to the serine-glycine system. In both deoxynucleosides and nucleosides, the carbon backbone of the ribose moiety is derived from R5P. R5P is an intermediary of the PPP. In Figure 1.1 we depicted the intermediary metabolites precursors or pyrimidine and purine nucleosides and the respective carbon equivalence.
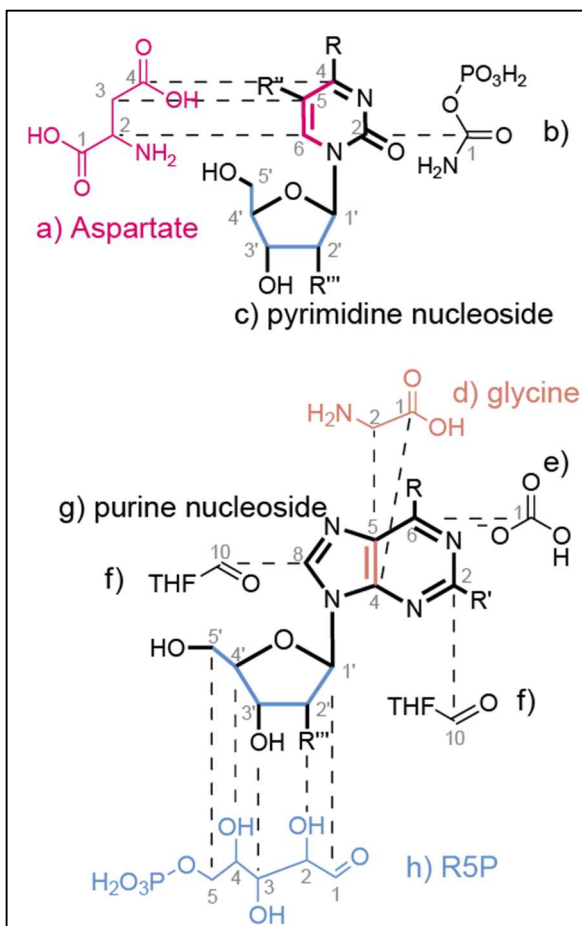
Figure 1.1 – Schematic representation of the formation of pyrimidine and purine nucleosides from the respective precursors. a) aspartate, b) carbamoyl-phosphate, c) pyrimidine nucleoside, d) glycine, e) bicarbonate, f) formyl tetrahydrofolate, g) purine nucleoside, h) ribose-5-phosphate. Dashed lines depict carbon correspondence between nucleosides and precursors. R, O or NH. R', NH_2 or H. R", H or CH_3. R, is O in thymidine, uracil and NH_2 in deoxycytidine. R' is H in deoxyadenosine and NH_2 in deoxyguanosine.; R" is H in cytidine and CH_3 in thymidine.

1.5| 13C ISOTOPOMER ANALYSIS BY MASS SPECTROMETRY

1.5.1| Analysis of mass isotopomer of fragments of deoxynucleosides and nucleosides

The Mass Spectrometry (MS) methodology separates compounds, analytes, based on their mass/charge (m/z) ratio and quantifies the abundance of each detected m/z. In metabolic flux determination, the analytes are the free metabolites or the monomers of any biopolymer that, after extracted from cells, are prepared for analysis and measured in the mass spectrometer. In the vast majority of the cases, mass spectrometers are in line with a chromatographic preparative system, either liquid or gas chromatography (GC). In case of using a GC-MS system, the non-volatile analytes must be derivatized. The analytes are thus injected in the mass spectrometer at their own chromatographic retention time (RT). Once in the mass spectrometer, the analytes are ionized and the resulting molecular ions fly through the quadrupoles towards the detector. The ionization energy also dissociates the energetically unstable molecular ions yielding fragment ions. Fragment ions are identified by their respective m/z together with the parent ion.

The presence of heavier isotopes, e.g. ^{13}C, in a compound results in the increase of its m/z, which is observable by a mass shift in proportion to the total number of ^{13}C atoms present in the compound. Ions of the same metabolite but differing in the total number of ^{13}C isotopes are designated by mass isotopomers. Therefore, a metabolite with n carbons can have up to $n+1$ ^{13}C mass isotopomers, namely m+0, m+1, … m+n. For any given parent ion or fragment, MS distinguishes only their mass isotopomers but not their positional isotopomers; e. g., in MS it is possible to distinguish [1,2-^{13}C] lactate from [1-^{13}C] lactate but not [1,2-^{13}C] lactate from [2,3-^{13}C] lactate.

However, the accuracy of metabolic flux determination based on ^{13}C tracing improves with the increasing resolution of the ^{13}C distribution in the labeled metabolites, *i. e.,* with the assessment of fractional abundance of positional isotopomers (Wittmann and Heinzle, 1999; Antoniewicz, Kelleher and Stephanopoulos, 2007; Choi, Grossbach and Antoniewicz, 2012; Rühl *et al.*, 2012). In many cases, metabolite pools are fed by several metabolic pathways that differ in the carbon rearrangements through their respective metabolic reactions. The positional isotopomers of a metabolite permit the distinction of the multiple pathways feeding its pool and their relative activity.

Although MS only provides information about the mass isotopomers of parent and fragments ions, the positional isotopomers can be determined by exploring the fragmentation spectrum of the metabolite and by analyzing the mass isotopomers of both

the parent and the fragment ions. Exploring the fragmentation spectrum[3] the carbon composition of the fragments and their moiety in the molecular ion are elucidated. The fragment ions retain the ^{13}C enrichment respective of their moiety of the parent ion. Therefore, the ^{13}C isotopes are positioned in the moieties whose fragments present a shift in their *m/z*. Methods have been developed to elucidate the carbon composition of the fragments (Choi, Grossbach and Antoniewicz, 2012; Wegner *et al.*, 2014; Miranda-Santos *et al.*, 2015) and to estimate fluxes using the mass isotopomer distributions (MID) of the molecular ion and of its respective fragments (Wiechert, 2001; Weitzel *et al.*, 2013). The mass isotopomers of amino acids have been exploited to flux estimation (Christensen and Nielsen, 1999; Wittmann, Hans and Heinzle, 2002; Antoniewicz, Kelleher and Stephanopoulos, 2007) but mass isotopomers of deoxynucleosides or nucleosides and of their fragments had not been before our work (Miranda-Santos *et al.*, 2015).

---

[3] Fragmentation spectrum is the unique pattern in the mass spectrum that is characteristic of the respective molecule ionized with a specific ionization energy. It is like a mass spectral fingerprint of the molecule.

2| Material and Methods

2.1| CHEMICALS

Unless otherwise stated, chemicals were purchased from Sigma-Aldrich (St. Louis, MO, USA).

[U-^{13}C] glucose and [1,2-^{13}C] glucose 99.0% purity were purchased from Cambridge Isotope Laboratories (Andover, MA, USA).

RNAase-free pipette tips were purchased from Axigen, Corning Incorporated Life Sciences (Tewksbury, MA, USA).

N-methylsilyl-trifluoroacetamide was purchased from Macherey-Nagel GmbH & Co (Düren, Germany).

Zymolyase was purchased from Seigaku Corp., Japan.

DNase turbo, RNase A and RNase T1 were purchased from Thermo-Scientific (Fremont, CA, USA).

Saccharomyces cerevisiae haploid, prototrophic strain CEN.PK113-7D was courtesy Dr. Peter Kötter from Frankfurt University.

Culture incubator was a Multitriton from Infors AG, Bottmingeen.

Bioreactor was a Vario 1000 Mini-Reaktoren from Meredos, Bovenden, Deutschland.

Spectrophotometer for measuring optical density at 660 nm (OD_{660}) was a NovaspecR from Pharmacia Biotech.

Bioreactor control unit was a FCE 03 from FairMenTec, Wald, Switzerland.

Bioreactor temperature was controlled by a circulating thermostat MV-4 from Julabo, Seelbach, Germany.

Bioreactor pH was controlled by a 405 DPAS-SC-K8S / 225 from Mettler Toledo, Giessen, Germany.

Bioreactor partial O_2 pressure was monitored by a polarographic probe Oyxprobe from Broadley James, Bedford, England, and controlled by a WMR Compact 4, Brooks Instruments, Veenedaal, The Netherlands.

2.2| CELL CULTURE

2.2.1| Batch culture of *Saccharomyces cerevisiae*

S. *cerevisiae* strain CEN.PK113-7D were grown on Yeast Extract Peptone Dextrose Agar (YPD-agar) plates (10 g/L yeast extract, 20 g/L peptone, 20 g/l glucose in 2% agar) at 30 °C for 48 h. The pre-cultures and main cultures were carried out in a defined medium (Verduyn *et al.*, 1992; Velagapudi *et al.*, 2006) containing 37.8 mM $(NH_4)_2SO_4$, 147 mM KH_2PO_4, 2.03 mM $MgSO_4$, 51.3 µM EDTA, 40.5 µM $CaCl_2$. Minerals and vitamins from stock solutions, 1000 × concentrated, were added to the following final concentrations: (minerals) 16.0 µM $ZnSO_4$, 1.26 µM $CoCl_2$, 5.05 µM $MnCl_2$, 1.2 µM $CuSO_4$, 10.8 µM $FeSO_4$, 1.83 µM $NaMoO_4$, 16.2 µM H_3BO_3, 0.602 µM KI and (vitamins) 0.2 µM biotin, 4.6 µmM Ca-pantothenate, 8.1 µmM nicotinic acid, 0.14 mM myo-inositol, 2.7 µM thiamine HCl, 4.7 µM pyridoxine HCl, and 1.5 µM p-aminobenzoic acid. Glucose at a concentration of 111 mM (20 g/L) was the sole carbon source. In tracer experiments, naturally labeled glucose was substituted by [U-^{13}C] glucose, or [1,2-^{13}C] glucose in their respective main cultures. The final pH of the medium was set to 5 by the addition of 1 N NaOH. Cultivations were performed in baffled shake flasks at 30 °C and 230 rpm. For the pre-culture a single colony from the agar plate was inoculated in the medium as described above and incubated overnight (ON). The main cultures were prepared from an inoculum of the pre-culture, giving an initial optical density (OD) of 0.1. Cell growth was measured by monitoring the optical density at 660 nm (OD_{660}) in a spectrophotometer (NovaspecR, Pharmacia Biotech). Specific growth rate (µ) was determined by fitting an exponential function to the OD data *versus* time. OD_{660} was converted into Cell Dry Weight (CDW), a measure of biomass concentration using a standard curve (Schneider, 2011).

$$CDW \ (g/L) = \ 0.5065 \ \times \ OD_{660} \qquad (2.1).$$

OD_{660} was converted into number of cells per volume using a standard curve.

$$Conc_{cells} \ (cell/mL) = 2 \ \times \ 10^7 \ \times \ OD_{660} \qquad (2.2).$$

Data represent the average of at least three different main cultures.

2.2.2| Continuous culture of *Saccharomyces cerevisiae*

The continuous culture of *S. cerevisiae* was carried out in Vario 1000 mini-reactors (Meredos, Bovenden, Germany). Prior to continuous culture, a main culture was carried out in the bioreactor, which was prepared as described in 2.2.1. The continuous culture was started when the preparative main culture reached an OD_{660} of 2.8. Cell density was monitored by optical density at 660 nm (OD_{660}) in a spectrophotometer (NovaspecR, Pharmacia Biotech).

The volume of continuous culture was 100 mL and culture was performed in a fermentor of 1 L, at a temperature of 30 °C and pH 5. The flow rate was 10 mL/h corresponding to a DR of 0.1 h^{-1}. The gassing rate was 1 vvm (compressed air) and the stirrer speed was 550 rpm. The continuous culture was carried out in a defined medium (Verduyn *et al.*, 1992; Velagapudi *et al.*, 2006) containing 37.8 mM $(NH_4)_2SO_4$, 147 mM KH_2PO_4, 2.03 mM $MgSO_4$, 51.3 µM EDTA, 40.5 µM $CaCl_2$. Minerals and vitamins from stock solutions, 1000 × concentrated, were added to the following final concentrations: (minerals) 16.0 µM $ZnSO_4$, 1.26 µM $CoCl_2$, 5.05 µM $MnCl_2$, 1.2 µM $CuSO_4$, 10.8 µM $FeSO_4$, 1.83 µM $NaMoO_4$, 16.2 µM H_3BO_3, 0.602 µM KI and (vitamins) 0.2 µM biotin, 4.6 µmM Ca-pantothenate, 8.1 µmM nicotinic acid, 0.14 mM myo-inositol, 2.7 µM thiamine HCl, 4.7 µM pyridoxine HCl, and 1.5 µM p-aminobenzoic acid. $[1,2-^{13}C]$ glucose at a concentration of 28 mM (5 g/L) was the sole carbon source. Table 2.1 summarizes the continuous culture conditions and parameters.

Temperature, pH and the stirring speed were monitored by the control unit FCE 03 (FairMenTec, Wald, Switzerland). Temperature was measured using a Pt100 platinum resistance thermometer, which calibration was performed by means of a 2-point calibration, at 0 °C and at the cultivation temperature of 30 °C. To control the reactor temperature, a circulating thermostat (MV-4, Julabo, Seelbach, Germany) was used. The regulation of the pH was carried out with an autoclavable glass potentiometric electrode (405 DPAS-SC-K8S / 225, Mettler Toledo, Giessen, Germany) and corrected by the addition of 0.2 M NaOH. The two-point calibration was performed before autoclaving at pH 4.01 and 6.81. The proportion of dissolved oxygen (pO_2) in the culture medium was determined using a polarographic probe (Oyxyprobe, Broadley James, Bedford, England). The calibration was carried out at culture conditions by means of a two-point calibration with nitrogen (0%) and compressed air (100%). The gassing rate was regulated by means of a separate control unit (WMR Compact 4, Brooks Instruments, Veenedaal, The Netherlands).

Table 2.1 - Continuous culture conditions and parameters

Parameters	Value	
Volume of reactor	100	mL
Flow rate	10	mL/h
DR μ^4	0.1	h^{-1}
DT^5	6.93	h
	415.9	min
pH	5	
Culture OD	2.8	
[glucose]$_{medium}$	0.028	M
	5	g/L
	0.5	%
CDW^6	1.42	mg/mL
[Cell]^7	5.60 × 10^7	cells/mL
Flow rate of cells^8	5.60 × 10^8	cells/mL h

---

[4] $DR = \dfrac{\text{flow rate } (\frac{mL}{h})}{\text{reactor volume (mL)}} \equiv \mu$

[5] $DT = \dfrac{\ln 2}{\mu}$

[6] Cell dry weigth $= 0.507 \left(\frac{mg}{mL}\right) \times OD$

      OD – optical density.

      0.507 was determined by weighing the dry mass of culture samples of different O.D.

[7] Cell concentration $= 2.0 \times 10^7 \left(\frac{cell}{mL}\right) \times OD$

      2.0×10^7 was determined by counting under the microscope the cell number from culture samples of different O.D.

[8] Flow rate of cells $= [cell] \left(\frac{cell}{mL}\right) \times Flow\ rate \left(\frac{mL}{h}\right)$

2.3| PREPARATION OF DEOXYNUCLEOSIDES AND NUCLEOSIDES FOR ^{13}C ISOTOPOMER ANALYSIS

2.3.1| Estimation of the necessary amount of cell and nucleic acids

The preparation of the deoxynucleoside and nucleoside sample for GC-MS analysis required the estimation of the amount of biological material required. We used chemical standards of deoxynucleosides and of nucleosides to build a calibration curve and identified their concentration range at which signal/noise would be above 0.2 and below saturation. We set the concentration of each deoxynucleosides and nucleosides in 1 mM and the sample volume in 50 µL. Therefore, each sample to be analyzed in GC-MS must contain 50 nmol of each deoxynucleoside or nucleoside. Table 2.2 summarizes the calculation of the required amounts of biological material for preparation of the GC-MS samples. The required mass of DNA and RNA was estimated from the average molecular mass of dNMP and NMP, 327.0 g/mol and 339.5 g/mol respectively, and considering a yield of digestion of nucleic acids to their monomers of 50%. We estimated to need 0.13 mg of DNA and 0.14 mg of RNA. The required amount of cells from where to extract the nucleic acids was calculated based on their relative fraction of biomass. The required biomass was 186.86 mg for nDNA, 2.72 mg for cRNA, 436.00 mg for mtDNA and 452.67 mg for mtRNA.

2.3.2| Nuclear DNA extraction

To the best of our knowledge, the available protocols to extract DNA (usually devoted for molecular biology purposes) use a much lower number of cells and yield an amount of DNA insufficient for our needs. In order to obtain enough DNA, we needed to use more cells per extraction and therefore, scaled up the process.

Total DNA was isolated and purified following the protocol reported by Holm (Holm *et al.*, 1986). Ice cold samples containing 7×10^9 cells (approximately 100 mL of a cell suspension of $OD_{660}=3.5$) were washed with 5 mL of ice cold ultrapure water and spun down at 1500 *g*, 4 C for 5 min. Supernatant was discarded and the pellet resuspended in 2.1 mL of ice cold SCE buffer (1 M Sorbitol, 0.1 M $NaCH_3COO$, 60 mM EDTA, pH 7). Cell suspension was treated with 150 µL of Zymolyase solution (2000 U/mL Zymolyase 20T, 10% 2-mercaptoethanol in SCE buffer) and incubated ON at 37 $^{\circ}$C to promote spheroplast formation.

Table 2.2 – Required amount of (deoxy)nucleosides, nucleic acids and cells for DNA and RNA extraction and digestion for (deoxy)nucleosides preparation.

	description	amount	
GC-MS sample	$C_{\text{each (deoxy)nucleoside}}$	1.00	mM
	V_{sample}	50.00	µL
	$n_{\text{each (deoxy)nucleoside}}$	**50.00**	**nmol**
Nucleic acids	(deoxy)nucleoside $\xrightarrow{\text{yields}}$ (deoxy)NMP		
	$n_{\text{each (deoxy)NMP}}$	50.00	nmol
	$\text{total}_{\text{(deoxy)NMP}}$	4x	
	$n_{\text{total (deoxy)NMP}}$	200.00	nmol
	$\overline{M}_{\text{(NMP)}}$	339.50	g/mol
	$\overline{M}_{\text{(deoxyNMP)}}$	327.00	g/mol
	yield of digestion	~50 %	
	m_{RNA}	**0.14**	**mg**
	m_{DNA}	**0.13**	**mg**
Cell culture	$\text{biomass}_{\text{cRNA}}$	5.00	%
	$\text{biomass}_{\text{nDNA}}$	0.07	%
	$\text{biomass}_{\text{mtRNA}}$	0.03	%
	$\text{biomass}_{\text{mtDNA}}$	0.03	%
	CDW	1.42	mg/mL
	biomass for cRNA	2.72	mg
	biomass for nDNA	186.86	mg
	biomass for mtRNA	452.67	mg
	biomass for mtDNA	436.00	mg
	volume of culture for cRNA	**1.91**	**mL**
	volume of culture for nDNA	**131.63**	**mL**
	volume of culture for mtRNA	**318.87**	**mL**
	volume of culture for mtDNA	**307.13**	**mL**
	Total	**759.54**	**mL**
^{13}C enrichment	µ	0.1	h^{-1}
	DT	6.93	h
	duplication to reach 0.8 % of non-labelled DNA[9]	7.0	
	Enrichment time	48.28	h
	Enrichment volume of culture	**485.8**	**mL**

The spheroplasted cells were spun down at 1500 *g* for 1 min and the resulting pellets were well drained. The pellet was slowly resuspended in 2.1 mL of a Guanidine-HCl (GuHCl) solution (4.5 M GuHCl, 0.1 M EDTA, 0.15 M NaCl, 0.05% sodium lauryl sarcosinate, pH 8.0) and then incubated at 65 °C for 10 min with occasional swirling to lyze spheroplasted cells. After cooling to room temperature, 2.1 mL of ice cold ethanol were added, and the mixture was centrifuged at 16000 *g* for 5 min. The supernatant was discarded and the pellet was then well drained. The pellet was slowly resuspended in 4.2 mL of Tris-EDTA (TE) buffer 10×. Our best results in resuspending this pellet came by

---

[9] Number of duplications to reach a minimum % of non-enrichment $= \log_2\left(\frac{100}{\%}\right)$

swirling it with vortex. Since pure DNA was desired, samples were treated with 2800 U of RNAse A and 108 kU of RNase T1 at 37 °C for 1 hr. This incubation was followed by incubation with 12 U of proteinase K at 37 C for 30 min. Samples were then extracted twice with 1.7 volumes of phenol-chloroform-isoamyl-alcohol (P:C:I), 25:24:1, pH 8, pre-equilibrated with 0.5 M Tris-HCl pH 8; in detail, approximately 7 mL of P:C:I were added, the solution was mixed in vortex for 1 min and centrifuged at 1600 g for 5 min. After the second extraction, in order to precipitate DNA, the aqueous phase was made 0.3 M in $NaCH_3COO$, pH 8, and 2.5 volumes of ethanol were added. Samples were mixed by inversion and incubated at -70 °C for, at least, 15 min. The DNA was spun down at 16000 g for 30 min and supernatant was discarded. The DNA pellet was resuspended in ethanol 70% and spun down again at 16000 g for 30 min. The supernatant was discarded; the DNA pellet was well dried and resuspended in 100 μL of ultrapure water. DNA was analyzed on a 1% agarose gel for integrity and purity. When some vestigial amounts of RNA were still present, samples were re-incubated with RNase A and T1 in TE buffer 10×, 37 C O.N.. After incubation, DNA was precipitated with $NaCH_3COO$ and ethanol as before. DNA was quantified by absorbance at 260 nm using a Nanodrop 2000c device (Thermo Scientific, USA). The $A_{260/280}$ and $A_{260/230}$ ratios were examined for protein and solvent contamination. For all the extractions, the values of $A_{260/280}$ ratio were in the range of 1.9 - 2.0 and the values of $A_{260/230}$ ratio were in the 2.0 - 2.3 range. We obtained 130 μg of DNA per extraction, on average, representing 0.075% of the biomass. DNA samples were stored at -20 ºC.

2.3.3| Cytosolic RNA extraction

Total RNA was isolated and purified following the basic protocol from (Collart and Oliviero, 2001) with some modifications. RNA extractions were handled in the sterile bench, pipette's tips were RNase free, microcentrifuge tubes and flasks were autoclaved and all the solutions were prepared in RNase free water. RNase free water was prepared incubating ultrapure water made 0.1% in diethylpyrocarbonate (DEPC) at 37 ºC, O.N. and followed by autoclaving to remove DEPC. Samples containing 100×10^6 cells (approximately 1.5 mL of cell suspension at $OD_{660}=3.5$) were washed with 1 mL of ice cold RNase free water, spun down at 1500 g, 4 ºC for 5 min and supernatant was discarded. In order to disrupt cells, cell pellet was resuspended in 400 μL TES buffer (10 mM Tris-HCl, pH 7.5, 10 mM EDTA, 0.5% SDS). Immediately, 400 μL of acid phenol:chloroform 5:1, pH 5.1, pre-heated to 65 ºC, were added and vigorously mixed in vortex for 10 sec to promote protein denaturation and prevent RNA degradation. Extensive cell lysis and protein denaturation was achieved by incubation at 65 ºC for 60 min and agitating in vortex for 10 sec every 10 min. After cooled down in ice for 5 min, samples were centrifuged at 16000 g, 4 ºC for 5 min. The aqueous phase was then extracted twice with equal volume of chloroform; in detail, the aqueous upper phase was transferred to a clean microcentrifuge tube and an equal volume of chloroform was added. Samples were mixed in vortex for 20 sec and centrifuged at 16000 g, 4 ºC for 5 min. After the second extraction, in order to

precipitate RNA the aqueous phase was made 0.3 M in $NaCH_3COO$, pH 5.3, and 2.5 volumes of ethanol were added. Samples were mixed by inversion, incubated in -20 ºC for at least 30 min and centrifuged at 16000 g, 4 ºC for 15 min. Supernatant was discarded, 1 mL of ethanol 70% was added and agitated in vortex briefly to resuspend the pellet. After centrifugation at 16000 g, 4 ºC for 5 min, supernatant was discarded, the RNA pellet was well dried and resuspended in 100 µL RNase free water. RNA was analyzed on 1% agarose gel for integrity. RNA was quantified by absorbance at 260 nm using a Nanodrop® 2000c device (Thermo Scientific, USA). The $A_{260/280}$ and $A_{260/230}$ ratios were examined for protein and solvent contamination. For all the extractions, the values of $A_{260/280}$ ratio were in the range of 1.9 - 2.0 and the values of $A_{260/230}$ ratio were in the 2.0 - 2.3 range. We obtained 180 µg of RNA per extraction in average, representing 4.5% of the biomass. RNA samples were stored at -70 C.

2.3.4| Mitochondrial DNA and RNA

Mitochondria were isolated following the scale up of a published protocol (Defontaine, Lecocq and Hallet, 1991). Except otherwise stated, all procedures were taken at 4 ºC. Ice cold samples containing 1.78×10^{10} cells (approximately 320 mL of a cell suspension of $OD_{660}=2.8$) were washed twice with 50 mL of ice cold ultrapure water and spun down at 500 g for 10 min. Supernatant was discarded, the pellet resuspended in 50 mL of washing solution (1.2 M sorbitol, 2% mercaptoethanol, 50 mM EDTA, pH 7) and spun down at 500 g for 10 min. Pellet was resuspended in 35 mL of solution A (0.5 M sorbitol. 10 mM EDTA, 50 mM Tris, pH 7.5) with mercaptoethanol 2% and added 400 U of Zymolyase 20T and incubated at 37 °C to promote spheroplast formation. Incubation was considered complete when we observed a 95% depletion in OD_{660}). The spheroplasted cells were spun down in the ultracentrifuge Bekman Coulter Optima L-90K, rotor type 45 Ti at 15000 g for exactly 15 min to avoid the formation of extra hard pellet. The pelleted mitochondria crude was resuspended in 35 mL of solution A (without mercaptoethanol) and spun down in the same ultracentrifuge at 15000 g for 15 min. The washing procedure with solution A was done three times. The mitochondria pellet was resuspended in 1.5 mL of solution A. Half of the mitochondria resuspension was further proceeded to be extracted mitochondrial DNA (mtDNA) and the other half to be extracted mitochondrial RNA (mtRNA). Mitochondria resuspension for DNA extraction was added 5 U of DNase turbo to remove traces of nDNA. Mitochondrial resuspension for RNA extraction was added 2800 U of RNAse A and 108 kU of RNase T1 to remove traces of cRNA. Incubations took O.N. at 37 ºC. Proteinase K 12 U were added to both mitochondria resuspension and digestion was promoted at 37 ºC for 30 min. Incubation was stopped by the addition of 25 mL of solution A with 2% mercaptoethanol to each mitochondrial extraction. Mitochondria were spun down in the ultracentrifuge at 15000 g for 15 min. The pellet washed four times in 35 mL of solution A without mercaptoethanol and spun down in the ultracentrifuge at 15000 g for 15 min. Before the fourth centrifugation, an aliquot of mitochondrial resuspension was taken for protein quantification by Bradford method. After the fourth

centrifugation the mitochondria pellet was resuspended in 4 mL of solution B (100 mM NaCl, 10mM EDTA, 1% sarkosyl, 50 mM Tris) and incubated for 1 h at room temperature to promote mitochondria lysis. mtDNA and mtRNA were extracted following the extraction protocol for cDNA and nRNA.

2.3.5| Digestion of nucleic acids into the respective monomers

Nucleic acid digestion was scaled up from (Quinlivan and Gregory, 2008). Briefly, 100 µg of nucleic acids at a final concentration of 0.2 µg/mL were incubated O.N. at 37 ºC with 0.5 U/mL Benzonase, 0.3 mU/mL Phosphodiesterase and 0.4 U/mL Alkaline Phosphatase in the digestion buffer composed of 10 mM NH_4HCO_3, 50 mM NaCl and 10 mM $MgCl_2$ pH 7.9. Benzonase required to be subjected to buffer substitution as it was provided by the manufacturer in a solution containing glycerol, glycerol is derivatized also by N-Methyl-N-(trimethylsilyl) trifluoroacetamide (MSTFA) resulting in a giant signal in GC-MS; after microfiltration with a 3 kDa cutoff membrane, Benzonase was recovered in 20 mM NH_4HCO_3, 20 mM NaCl, and 2 mM $MgCl_2$, pH 8. Phosphodiesterase I was prepared from powder in 100 mM NH_4HCO_3, pH 8.9 and Alkaline Phosphatase in 10 mM NH_4HCO_3, 0.1 mM $ZnCl_2$ and 1 mM $MgCl_2$, pH 8. NH_4HCO_3 buffer was always prepared prior to digestion and with fresh ultrapure water. After digestion, a microfiltration with a cutoff membrane of 3 kDa was performed. The concentration of each sample (deoxy)nucleosides was determined by high pressure liquid chromatography (HPLC) and the filtrate was freeze-dried.

2.3.6| Derivatization of nucleosides for GC-MS analysis

(Deoxy)nucleosides, either standard or digested from nucleic acids, were derivatized with MSTFA (Orata, 2012). The derivatization was promoted in pyridine:MSTFA (50:50) at 80 C for 30 min.

In detail, standard (deoxy)nucleosides were solubilized separately in pyridine:DMF (50:50). Guanosine and 2'-deoxyguanosine were warmed up at 80 ºC for 5 – 10 min, with occasional vortexing, until complete solubilization. Samples were diluted with pyridine to 2× the final concentration and MSTFA was added in a volume equal the pyridine fraction. Derivatization was promoted.

(Deoxy)nucleosides from nucleic acid digestion were extracted from the freeze-dried powder with pyridine:DMF (50:50). As the freeze-dried powder had a significant amount of salt, 200 µL of pyridine:DMF was used to completely wet the sample. After warmed up for 10 min at 80 ºC with occasional vortexing, samples were centrifuged for 10 min in bench top centrifuge at maximum speed (16000 g). Supernatant was collected

and dried under vacuum. Samples were first solubilized in pyridine and an equal volume of MSTFA was then added. The volume was calculated to obtain a final concentration of 0.8 mM in cytidine and 0.2 mM in thymidine, keeping a 50:50 pyridine:MSTFA ratio. Derivatization was promoted as described above.

2.4| GC-MS ANALYSIS OF NUCLEOSIDES AND THEIR FRAGMENT MOIETIES

2.4.1| Gas-Chromatography-Mass Spectrometry

GC-MS measurements were carried out on a HP6890 GC system using a Mass Selective Detector 5973 (Agilent Technologies, Waldbronn, Germany). We used a HP5MS UI capillary column (5%-phenyl)-methylpolysiloxane Ultra Inert 60 m × 250 μm × 0.25 μm, Agilent Technologies, Waldbronn, Germany). For electron impact ion generation, a 70 eV electron beam was used followed by mass analysis using a quadrupole. The optimized conditions for the measurement of nucleosides were as follows. One μL of sample was injected splitless for 2 min using a PTV with an initial temperature of 130 °C and a temperature gradient of 12 °C/s, up to 320 °C. Carrier gas flow was helium at 1.1 mL/min. The temperature gradient for the separation of nucleosides was 130 °C held for 1 min and 10 °C/min up to 325 °C held for 4 min. Temperatures of ion source and transfer liner were 230 and 320 °C. Full scan (SCAN) ranging from 50 to 700 Da using a scan rate of 9 scans/s and selective ion monitoring (SIM) were carried out with optimized settings for each analyte. In the SIM mode we set the ions corresponding to the mass isotopomers of every fragment assigned and according to the number of C belonging to the number of molecular carbons. For a fragment with n carbons in the carbon backbone we set the ions from m+0 m/z to m+n m/z. Every sample was measured in SCAN and SIM mode. Table 2.3 lists the exact m/z of the selected ions.

2.4.2| GC-MS spectral analysis

The criteria used for spectral analysis were as follows:

1. Identification of the nucleosides in the scan measurement:

   a. RT at which the spectrum presents the m/z characteristic of the respective nucleoside. In cases where the chromatographic signal presented shoulder and/or was underneath other signals, the extracted-ion chromatogram tool (XIC), which shows only the chromatographic signals of the extracted ions, permitted the unambiguous identification of the respective RT.

Table 2.3 – List of ions measured in SIM mode. Exact *m/z* of the ions selected to be measured in the SIM mode for each fragment of the (deoxy)nucleosides.

		m+0	m+1	m+2	m+3	m+4	m+5	m+6	m+7	m+8	m+9	m+10
deoxyribose		245.2	246.2	247.2	248.2	249.2	250.2					
deoxythymidine nucleobase		255.2	256.2	257.2	258.2	259.2						
deoxycitidine nucleobase		240.2	241.2	242.2	243.2	244.2						
		254.2	255.2	256.2	257.2	258.2						
deoxyadenosine	(192.1)*	193.1	194.1	195.1	196.1	197.1	198.1					
	(452.4)*	453.4	454.4	455.4	456.4	457.4	458.4	459.4	460.4	461.4	462.4	463.4
	(467.4)*	468.4	469.4	470.4	471.4	472.4	473.4	474.4	475.4	476.4	477.4	478.4
deoxyguanosine		295.2	296.2	297.2	298.2	299.2	300.3					
		540.5	541.5	542.5	543.5	544.3	545.3	546.5	547.5	548.5	549.5	550.5
		555.5	556.5	557.5	558.5	559.5	560.5	561.5	562.5	563.5	564.5	565.5
Uridine		224.2	225.2	226.2	227.2	228.2	229.2	230.2				
		245.2	246.2	247.2	248.2	249.2						
		339.3	340.3	341.3	342.3	343.3	344.3	345.3	346.3	347.3		
		348.3	349.3	350.3	351.3	352.3	353.3					
		401.4	402.4	403.4	404.4	405.4	406.4	407.4	408.4			
		517.5	518.5	519.5	520.5	521.5	522.5	523.5	524.5	525.5	526.5	
Adenosine		245.2	246.2	247.2	248.2	249.2						
	(322.3)*	323.3	324.3	325.3	326.3	327.3	328.3	329.3	330.3			
		348.3	349.3	350.3	351.3	352.3	353.3					
	(452.4)*	453.4	454.4	455.4	456.4	457.4	458.4	459.4	460.4	461.4	462.4	
	(540.5)*	541.5	542.5	543.5	544.5	545.5	546.5	547.5	548.5	549.5	550.5	551.5
Cytidine		184.1	185.1	186.1	187.1	188.1						
		223.2	224.2	225.2	226.2	227.2	228.2	229.2				
		245.2	246.2	247.2	248.2	249.2						
		348.3	349.3	350.3	351.3	352.3	353.3					
		516.5	517.5	518.5	519.5	520.5	521.5	522.5	523.5	524.5	525.5	
Guanosine		245.2	246.2	247.2	248.2	249.2						
		259.2	260.2	261.2	262.2	263.2	264.2					
		296.2	297.2	298.2	299.2	300.3	301.3					
		324.3	325.3	326.3	327.3	328.3	329.3	330.3				
		410.4	411.4	412.4	413.4	414.4	415.4	416.4	417.4			
		540.5	541.5	542.5	543.5	544.5	545.5	546.5	547.5	548.5	549.5	
		628.6	629.6	630.6	631.6	632.6	633.6	634.6	635.6	636.6	637.6	638.6
		643.6	644.6	645.6	646.6	647.6	648.6	649.6	650.6	651.6	652.6	653.6

*the fragments composed of nucleobase of adenosine and 2'-deoxyadenosine obtained from digestion of nucleic acids exhibited a shift of 1 Da in all their mass isotopomers.

2. Choosing the RT of different fragments in the SIM measurement:

   a. We used XIC for the fragment ions set in that SIM and for the ions of the respective molecular ion:

      i. When the different fragments of the respective molecular ion presented their maxima at the same RT, the spectrum was taken at that RT;

      ii. When the different fragments of the respective molecular ion presented their maxima at different RT, the spectrum was taken at the RT of the maximum of each fragment. The reasoning for this is the slightly different time that fragments of different masses take to reach the detector. This is also observed in the biological samples naturally labeled;

      iii. When the mass isotopomers of the same fragment presented maxima at different RT, the total spectrum of the RT maxima range was taken. The reasoning for this is the sensitivity of the spectrometer; although the spectrometer output does not discriminate *m/z* values of resolution beyond the 3rd decimal point, it has sensitivity to resolve these mass differences.

3. Confidence threshold of M.I.D. signal/noise ratio was 3. Noise intensity was determined from the average intensity of the spectral noise at a RT with no chromatographic signal. M.I.D. which signal/noise was between 3 and 2, it considered worth further spectral analysis. M.I.D. signal/noise below 2 was not considered.

3| Metabolic network modelling and simulations

3.1| METABOLIC MODEL OF PROLIFERATING YEAST

3.1.1| Genome-scale metabolic reconstruction of *Saccharomyces cerevisiae*

Building a metabolic model begins with the reconstruction of the metabolic network, which will define the metabolic network topology and its stoichiometry (*cf.* chapter 1.2.1). For a genome-scale reconstruction the reactions are surveyed from the genome of the organism (Förster *et al.*, 2003a). We consulted the KEGG PATHWAY database (Kanehisa and Goto, 2000), YeastPathways and the reconstruction by (Förster *et al.*, 2003a) to collect the metabolic genes of *S. cerevisiae*. The collected metabolic reactions are then implemented as a system of reactions, substrates and products, for which the respective stoichiometric matrix is computed. We used the Omix-visualization® (Droste *et al.*, 2011) software to assist both the reconstruction and implementation of the metabolic model and to visualize the network.

The comprehensiveness of the reconstruction depends on the range of metabolic pathways that are relevant for the question under investigation (Wiechert, 2001). In this case, we collected the metabolic reactions of *S. cerevisiae* that are relevant for cell proliferation, based on literature of budding yeast physiology. Proliferating yeast cells consume glucose, biosynthesize biomass to grow and divide, and produce acetate, ethanol, trehalose and glycogen (Lange and Heijnen, 2001). Therefore, the metabolic pathways included in the reconstruction were glycolysis, PPP, TCA cycle, gluconeogenesis, storage of carbohydrates, glyoxylate cycle, ethanol, acetate and CO_2 production and secretion, lipid, amino acid, purine and pyrimidine biosynthesis, the GSS and one-carbon pool metabolism (Figure 3.1).

3.1.2| Mapping of carbon atom derivation between metabolites

The network reconstruction is not yet a metabolic model. The next step is the establishment and implementation of the methodology to estimate the metabolic flux rates. We chose ^{13}C-MFA.
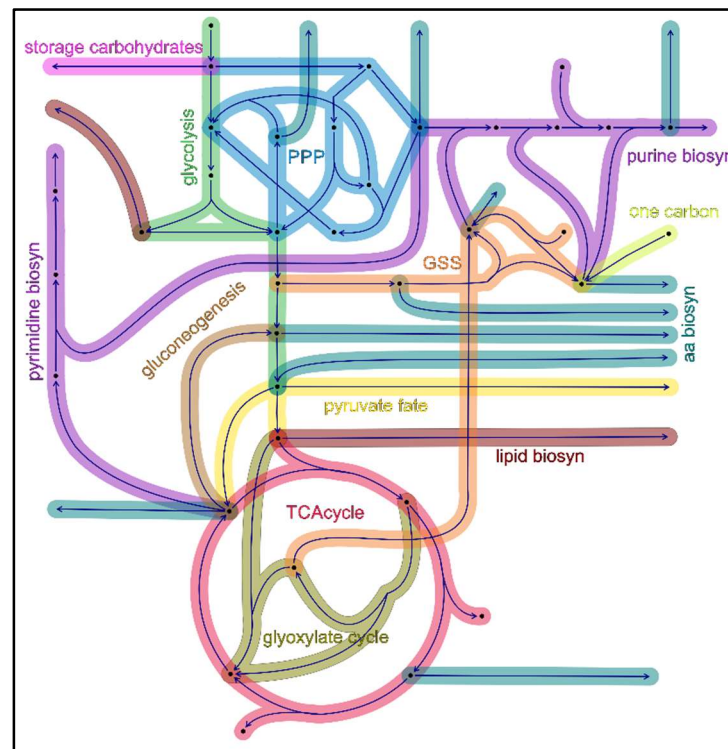
Figure 3.1 – Diagram of the metabolic pathways included in the metabolic reconstruction. Glycolysis/ gluconeogenesis, pentose phosphate pathway (PPP), tricarboxylic acid cycle (TCA cycle), biosynthesis/recruitment of storage of carbohydrates, glyoxylate cycle, pyruvate utilization for acetyl-CoA, OAA, ethanol and acetate (pyruvate fate), glycine/serine system (GSS), one-carbon pool metabolism (one carbon), purine biosynthesis (purine biosyn), pyrimidine biosynthesis (pyrimidine biosyn), recruitment of precursors for amino acid and lipid biosynthesis (aa biosyn; lipid biosyn).

Being a CLE based methodology, in ^{13}C-MFA metabolic rate estimation relies on the ^{13}C isotopomer balance of metabolites. Therefore, these models require the description of the carbon rearrangements occurring from substrates to products in each reaction of the metabolic network. This description is referred as the carbon mapping (Wiechert and Graaf, 1997) (Figure 3.2). The ^{13}C isotopomer balance is computed from the carbon mapping and from the stoichiometry of the metabolic network. The balance of ^{13}C isotopomers of metabolites depends on the reaction rate and carbon mapping of the respective metabolic reactions yielding the metabolite pool.

Eventually, metabolic rates are estimated by matrix calculations of the stoichiometric balance of ^{13}C isotopomers (*cf.* chapter 1.2.1) as function of the reaction rates and applying non-linear regression and least squares estimation (Wiechert and de Graaf, 1996).
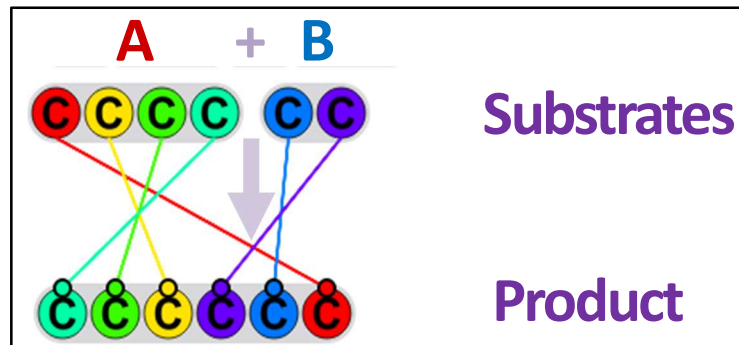
Figure 3.2 – Carbon mapping concept. Description of derivation of product carbons are from substrate carbons. Each carbon atom of the substrate will become a defined carbon of the product.

The majority of the metabolic reactions are reversible. Thus, the reaction rate (v) is the difference between the forward ($\vec{v}$) and the backwards rates ($\overleftarrow{v}$), net flux. Yet, the balance of metabolite ^{13}C isotopomers depends also on the extent of reversibility of the reactions. Therefore, (Wiechert and Graaf, 1997) established the concept of exchange (xch) flux. Exchange (xch) flux is the minimum rate between forward and backwards rates. The xch rate of an irreversible reaction is zero (Figure 3.3).
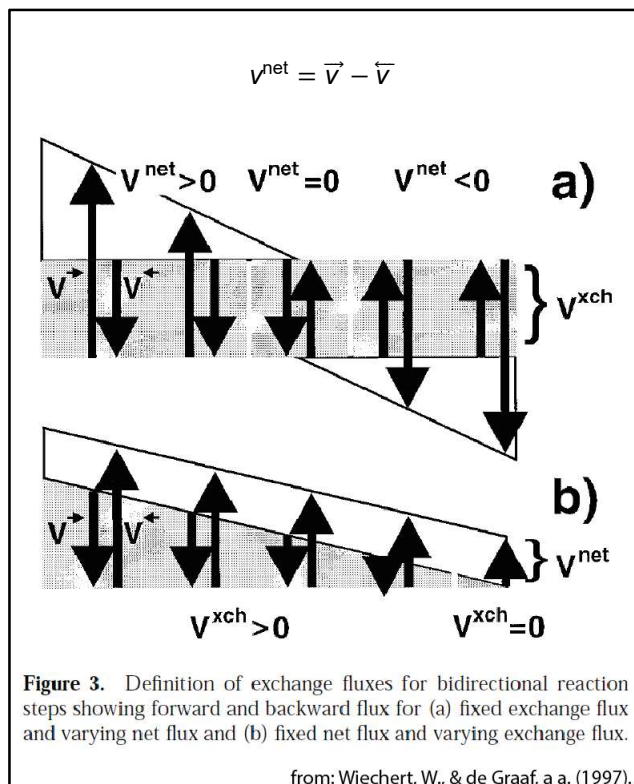
Figure 3.3 – Concept of net and xch flux. Net flux is the difference between the forward ($\vec{v}$) and the backwards rates ($\overleftarrow{v}$). Exchange (xch) flux is the minimum rate between forward and backwards rates. Figure 3 of Wiechert and Graaf, (1997) uses two extreme examples to illustrate the interplay between net and xch fluxes. In a) v^{xch} is fixed and v^{net} is variable. In b) v^{xch} is variable and v^{net} is fixed.

3.1.3| Simplification of the metabolic network

The simplification of the metabolic network seeks a judicious reduction of the number of variables. The reduction of the number of variable increases the determination of the system and reduces the demand on computational power and experimental assessments. (Varma and Palsson, 1993; Wiechert, 2001).

In Figure 3.4 we show the diagram of simplified metabolic network of proliferating *S. cerevisiae*. The simplification this metabolic network considered that:

i) the methodology used is ^{13}C-MFA;

ii) the biological system is a proliferating cell;

iii) we are investigating the intermediary metabolism;

iv) the experimental measurements are ^{13}C isotopomers of nucleosides and deoxynucleosides and uptake and secretion rates.

Therefore, attending to i) and iv) we lumped together consecutive linear reactions and redundant reactions. We also lumped together branched reactions which carbon mappings do not lead to distinguishable MID of nucleosides, deoxynucleosides and their fragments. In accordance to ii) we excluded reactions that are known to be inactive in proliferating yeast, e.g. salvage pathways. Following iii) we set as output reactions the reactions which products are outputs of the network and cannot be measured experimentally or are out of the scope of the study. These output reactions were implemented as sinks from the respective precursors. Output reactions are for example the recruitment of precursors for biosynthesis of lipids and amino acids. The one-carbon pool metabolism is involved in the purine and thymidine biosynthesis. It was simplified to the N^5,N^{10}-Methylene-tetrahydrofolate (CTHF) and N^{10}-Formyl-tetrahydrofolate (FTHF) pools. CTHF is C donor for thymidine biosynthesis whereas FTHF donates to purine biosynthesis. CTHF results from serine conversion to glycine and FTHF is formed from formate and CO_2 interchangeable pools. CTHF and FTHF are also interchangeable polls.

As a result of the model simplification, the metabolic rates are rates of single reactions or flux rates through clusters of reactions. Also, metabolite isotopomer abundance variables can concern a single metabolite pool or agglutinated pools. Hexokinase (E.C. 2.7.1.1) flux rate, implemented in the metabolic model as *gly1* is an example of a single reaction rate; whereas glucose-6-phosphatedehydrogenase, 6-phosphogluconolactonase and 6-phosphogluconate dehydrogenase (E.C.1.1.1.49, E.C.3.1.1.31 and E.C. 1.1.1.44) are example of clusters of reactions which flux rate is the variable *ppp1*. Likewise, Glc6P is the pool of glucose-6-phosphate only and the CITICIT pool aggregates the pools of citrate and of isocitrate.
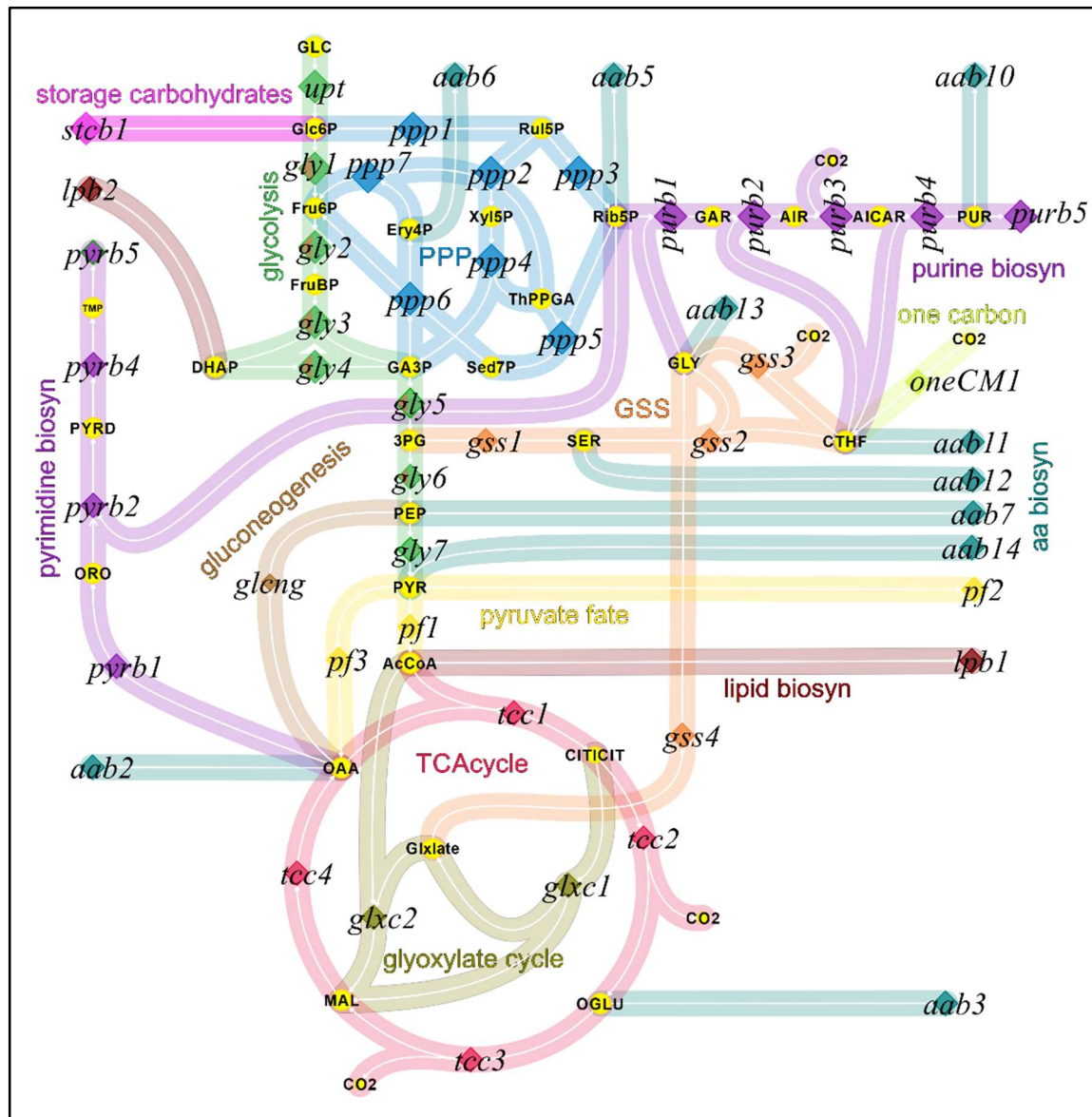
Figure 3.4 – Simplified genome-scale metabolic reconstruction of proliferating *S. cerevisiae*. Metabolic fluxes (single and clusters of metabolic reactions): *upt*, Hexokinase [EC:2.7.1.1]; *oneCM1*, Formate-tetrahydrofolate synthase [EC:6.3.4.3]. glycolysis/gluconeogenesis: *gly1*, Glucose-6-phosphate isomerase [EC:5.3.1.9]; *gly2*, 6-phosphofructokinase 1 [EC:2.7.1.11]; *gly3*, Fructose-bisphosphate aldolase [EC:4.1.2.13]; *gly4*, Triosephosphate isomerase [EC:5.3.1.2]; *gly5*, Glyceraldehyde-3-phosphate dehydrogenase [EC:1.2.1.12] + Phosphoglycerate kinase [EC:2.7.2.3]; *gly6*, 2,3-bisphosphoglycerate-dependent phosphoglycerate mutase [EC:5.4.2.11] + Enolase [EC:4.2.1.11];*gly7*, Pyruvate kinase [EC:2.7.1.40]; *glcng*, Phosphoenolpyruvate carboxykinase [EC:4.1.1.49]. PPP: *ppp1*, Glucose-6-phosphate 1-dehydrogenase [EC:1.1.1.49] + 6-phosphogluconolactonase [EC:3.1.1.31] + 6-phosphogluconate dehydrogenase [EC:1.1.1.44]; *ppp2*, Ribulose-phosphate 3-epimerase [EC:5.1.3.1]; *ppp3*, Ribose-5-phosphate isomerase A [EC:5.3.1.6]; *ppp4*, Transketolase [EC:2.2.1.1]; *ppp5*, Transketolase [EC:2.2.1.1]; *ppp6*, Transaldolase [EC:2.2.1.2]; *ppp7*, Transketolase [EC:2.2.1.1]. Pyruvate fate *pf1*, Pyruvate dehydrogenase complex [EC:1.2.4.1] + [EC:2.3.1.12] + Dihydrolipoamide dehydrogenase [EC:1.8.1.4]; *pf2*, Pyruvate decarboxylase [EC:4.1.1.1] + Alcohol dehydrogenase [EC:1.1.1.1] + [EC:1.1.1.2] + Aldehyde dehydrogenase [EC:1.2.1.3] + [EC:1.2.1.5] + Acetyl-CoA synthase [EC:6.2.1.1]; *pf3*, Pyruvate carboxylase [EC:6.4.1.1]. TCA cycle: *tcc1*, Citrate synthase [EC:2.3.3.1] + Aconitate hydratase [EC:4.2.1.3]; *tcc2*, Isocitrate dehydrogenase [EC:1.1.1.42] + Isocitrate dehydrogenase (NAD+) [EC:1.1.1.41]; *tcc3*, Oxoglutarate dehydrogenase [EC: 1.2.4.2] + Succinyl-CoA synthetase alpha subunit [EC:6.2.1.5] + Succinate

dehydrogenase (ubiquinone) flavoprotein subunit [EC:1.3.5.1] + Fumarate hydratase, class II [EC:4.2.1.2]; *tcc4*, Malate dehydrogenase [EC:1.1.1.37]. glyoxylate cycle: *glxc1*, Isocitrate lyase [EC:4.1.3.1]; *glxc2*, Malate synthase [EC:2.3.3.9]. glycine/serine system:*gss1*, Phosphoglycerate dehydrogenase [EC:1.1.1.95] + Phosphoserine aminotransferase [EC:2.6.1.52] + Phosphoserine phosphatase [EC:3.1.3.3]; *gss2*, Glycine hydroxymethyltransferase [EC:2.1.2.1]; *gss3*, Glycine cleavage system [EC:1.4.4.2] + [EC:2.1.2.10]; *gss4*, Alanine-glyoxylate transaminase [EC:2.6.1.44]. purine biosynthesis: *purb1*, Ribose-phosphate pyrophosphokinase [EC:2.7.6.1] + Amidophosphoribosyltransferase [EC:2.4.2.14] + Phosphoribosylamine-glycine ligase / Phosphoribosylformylglycinamidine cyclo-ligase [EC:6.3.4.13] + [EC:6.3.3.1]; *purb2*, Phosphoribosylglycinamide formyltransferase [EC:2.1.2.2] + Phosphoribosylformylglycinamidine synthase [EC:6.3.5.3] + Phosphoribosylamine-glycine ligase / Phosphoribosylformylglycinamidine cyclo-ligase [EC:6.3.4.13] + [EC:6.3.3.1]; *purb3*, Phosphoribosylaminoimidazole carboxylase [EC:4.1.1.21]; *purb4*, Phosphoribosylaminoimidazolecarboxamide formyltransferase + IMP cyclohydrolase [EC:2.1.2.3] [EC:3.5.4.10]; *purb5*, Purine nucleotide and deoxynucleotide demand. pyrimidine biosynthesis:*pyrb1*, Carbamoylphosphate synthetase/aspartate transcarbamylase [EC:2.1.3.2] + [EC:6.3.5.5] + Dihydroorotase [EC:3.5.2.3] + Dihydroorotate dehydrogenase (fumarate) [EC:1.3.98.1]; *pyrb2*, Orotate phosphoribosyltransferase [EC:2.4.2.10] + Orotidine-5'-phosphate decarboxylase [EC:4.1.1.23]; *pyrb4*, Thymidylate synthase [EC:2.1.1.45]; *pyrb5*, Pyrimidine nucleotide and deoxynucleotide demand; *lpb1 – 2*, Lipid biosynthesis; *aab2 - 14*, Amino acids biosynthesis; *stcb1*, Carbohydrate biosynthesis. Metabolites (single or clusters): 3PG – 3-phosphoglycerate; AICAR – 5-aminoimidazole-4-carboxamide ribonucleotide; AIR – 5'-phosphoribosyl5aminoimidazole AcCoA – acetylCoA; CITICIT – citrate+isocitrate; CO_2; CTHF – one carbon unit tetrahydrofolate (methylene, methyl, methenyl and formyl); DHAP – dihydroxyacetonephosphate; Ery4P – erythrose4phosphate; Fru6P – fructose-6-phosphate; FruBP – fructose-1,6-biphospate; GA3P – glyceraldehyde-3-phosphate; GAR – Glycineamide ribonucleotide; GLY – glycine; Glc6P – gluconate-6-phosphate; Glxlate – glyoxylate; MAL – malate; OAA – oxaloacetate; ORO – orotate; PEP – phosphoenolpyruvate; PYR – pyruvate; Rib5P – ribose-5-phosphate; Rul5P – ribulose-5-phosphate; SER – serine; Sed7P – sedoheptulose-7-phosphate; ThPPGA – 2 carbon units ketone intermediary of PPP; PYRD – pyrimidine; Xyl5P – xylulose-5-phosphate; PUR – purine; FTHF – formylthetrahydrofolate; OGLU – oxoglutarate; Acet/EtOH – acetate/etanol; TMP – thyminemonophosphate. XML script in chapter 8.1.

3.1.4| Conceptualization and design of the metabolic model of a non-synchronous population

In addition to collecting the reactions that occur in the organism and are relevant for the studied conditions, a metabolic model must be conceptualized and designed to depict as best as possible the biology and the investigated hypothesis. In our experimental condition the population of *S. cerevisiae* is proliferating and non-synchronous. Our hypothesis is that the MFD during S-phase differs from that of the other phases. Hence, despite our culture is constituted by one cell strain, it has two (metabolic) sub-populations, namely cells in S-phase and cells in the other phases of the CDC. Therefore, we conceptualized a model design that contemplates these two sub-populations, the S-phase sub-population and other the sub-population out of S-phase (non S-phase) (Figure 3.5).

According to the physiology of *S. cerevisiae* and based on the metabolic network reconstruction, some metabolites are secreted during proliferation. However, there is no evidence of accumulation of secreted metabolites in the extracellular medium (van Winden *et al.*, 2005). On the other hand, synchronized yeast cultures show oscillating concentrations of secreted metabolites, namely ethanol, acetate and trehalose (Hans, Heinzle and Wittmann, 2003; Tu *et al.*, 2005). Thus, the metabolites secreted by one cell sub-population can be taken up by cells of the other sub-population. Because the secreted metabolites are labelled from the ^{13}C labeled substrates feeding the culture, the secreted and re-uptaken metabolites become a ^{13}C tracer source in addition to that provided by the fed medium. The metabolic model design considering the two sub-populations permits taking into account this exchange of ^{13}C labelled substrates. The ^{13}C labelling of these internal substrates is unknown *a priori*, but predictable according to the MFD of the secreting cell. Figure 3.3 shows the metabolic model composed of two sub-populations, S-phase and non-S-phase populations, and the secreted and taken up metabolites. An example of such secreted metabolites is ethanol which is taken up and oxidized to acetate providing a source of NADPH alternative to PPP (van Winden *et al.*, 2005). The metabolic reconstruction of these two sub-populations is the same. The metabolic reactions of S-phase and non-S-phase cells were constrained and parametrized according to the metabolic specificities of the respective sub-population. For instance, in S-phase cell sub-population we parametrized the purine and pyrimidine biosynthesis according to the rate values of biosynthesis of DNA, whereas in non-S-phase cell sub-population we parametrized according to the rate values of biosynthesis of RNA.
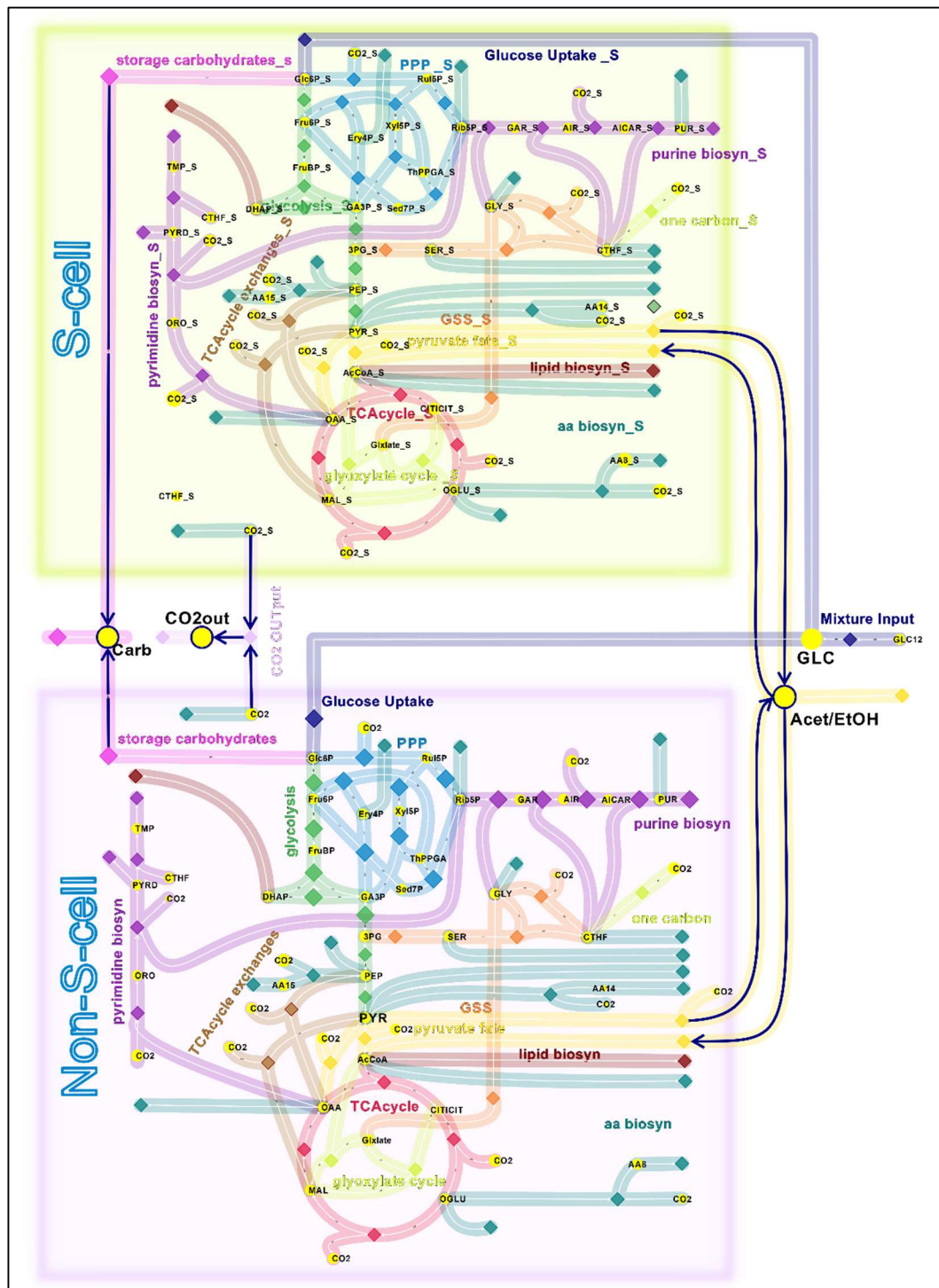
Figure 3.5 – Visualization of the model with the 2 subpopulations. Green compartment, S-phase cell subpopulation, purple compartments, non-S-phase cell sub-population; Large yellow metabolites can be secreted and taken up indiscriminately by either sup-population: Carb, storage carbohydrates; CO_{2out}, CO_2; Acet/EtOH, acetate/ethanol; PYR, pyruvate; GLC, glucose. Metabolic pathways (the suffix _S identifies the metabolic pathways belonging to the S-phase cell sub-population): Glycolysis/gluconeogenesis, pentose phosphate pathway (PPP), tricarboxylic acid cycle (TCA cycle), biosynthesis/recruitment of storage of carbohydrates, glyoxylate cycle, pyruvate utilization for acetyl-CoA, OAA, ethanol and acetate (pyruvate fate), glycine/serine system (GSS), one-carbon pool metabolism (one carbon), purine biosynthesis (purine biosyn), pyrimidine biosynthesis (pyrimidine biosyn), recruitment of precursors for amino acid and lipid biosynthesis (aa biosyn; lipid biosyn).

3.1.5| Constraining the variables of the metabolic network

The variables of the ^{13}C-MFA model are the flux rates and the ^{13}C isotopomer abundances. For each flux rate there are two variables, the net flux and the exchange (xch) flux (Wiechert and Graaf, 1997) (*cf.* Chapter 3.1.2). We established the independent variables based on the knowledge of the data that can be acquired, either experimentally or surveyed from literature. We set constraints for the independent variables that can be measured experimentally, e.g., uptake rates, isotopomer abundances, or that can be determined from cell culture parameters, e.g. specific growth rate. The very well determined thermodynamic properties of the reactions (Wiechert, 2007), e.g. directionality, are also used to constrain the respective independent variables (Weitzel *et al.*, 2013). The starting values for the not constrained independent variables are educated guesses obtained from literature, e.g. biomass composition, cell physiology (*cf.* chapter 3.2.1). The diagram in Figure 3.6 schematizes the categories of variables.
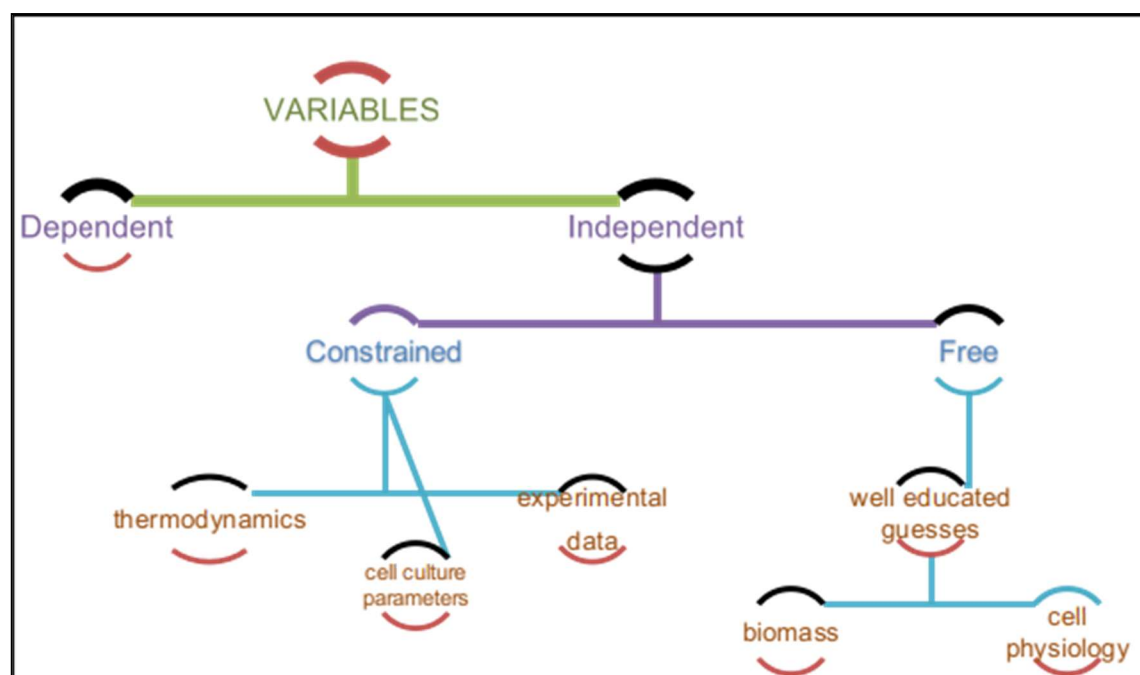
Figure 3.6 – Schematic diagram of the categories of the model variables and of their data. The variables of the metabolic model are either dependent or independent. Dependent variables are estimated from the independent ones. The independent variables are constrained in case that their values can be measured experimentally, can be calculated from the cell culture parameters or are a well-established property of the variable. Cell physiology and educated guesses are used to attribute starting values to the non-constrained, therefore free, independent variables.

The experimental conditions of the continuous culture are summarized in Table 3.1. The volume of the bioreactor was 100 mL and the flow rate of the continuous culture was 10 mL/h. This corresponds to a DR of 0.1 h^{-1} and a doubling time (DT) of 6.93 h. The glucose concentration in the medium was 0.028 M, which corresponds to a flow rate of glucose of 2.8×10^{-4} mol/h.

Table 3.1 – Parameters of the continuous culture in the bioreactor

Parameters	Value	
Volume of reactor	100	mL
Flow Rate	10	mL/h
DR [10]	0.1	h^{-1}
DT [11]	6.93	h
[glucose]$_{medium}$	0.028	M
	5	g/L
Flow rate of glucose[12]	2.80×10^{-4}	mol$_{glucose}$/h

In line with the conceptualized two sub-population model we needed to take into consideration the fraction of cells in S-phase and not in S-phase (Table 3.2). The data available in literature under the exact same conditions of our experiment (Tu *et al.*, 2005; Burnetti, Aydin and Buchler, 2016) reports the amount of time cells spend in S-phase and the DT of that population. Thus we could calculate that cells spent in S-phase 15% of DT. Knowing the DT of our culture we calculated the time length of S-phase as 1.09 h and of the other phases as 5.84 h (Table 3.1).

Table 3.2 – Fraction and duration of S-phase and of the other CDC phases with respect to total duration of CDC.

	Time fraction		Duration (h)
		DT	6.93
f$_{S-phase}$	0.15	S-phase	1.09
f$_{non-S-phase}$	0.85	Non-S-phase	5.84

Table 3.3 presents culture parameters measured experimentally and the values for independent variables calculated according to culture parameters. The culture OD was 2.8, corresponding to a CDW of 1.42 g/L and to a cell concentration of 5.6×10^7 cells/mL. The flow rate of cells was 5.6×10^8 cells/h and the biomass/cell was 2.54×10^{-11} g/cell. The measured glucose consumption rate was 2.5×10^{-4} mol/h corresponding to an average 4.46×10^{-13} mol/h cell, considering the cell flow rate of 5.6×10^8 cells/h. Considering the fraction of DT that cells spend in and out of S-phase (Table 3.1), and assuming that glucose uptake rate does not change over CDC we calculated an initial guess of glucose consumption of 7.02×10^{-14} mol/h S-phase cell and of 3.76×10^{-13} mol/h non-S-phase cell.

---

[10] DR = Flow Rate / Volume reactor. It is equivalent to specific growth rate (μ) in batch culture.

[11] DT = ln$_2$ / DR

[12] Flow rate of glucose (mol/h) = [glucose]$_{medium}$ × Flow Rate

Table 3.3 – Culture data measured experimentally and calculated accordingly, and independent variables calculated from the culture experimental data.

Parameters	Value		net flux
Culture OD_{600}	2.8		measured
CDW[13]	1.42	g/L	calculated
[cell][14]	5.60×10^7	cells/mL	calculated
Flow rate of cells[15]	5.60×10^8	cells/h	calculated
Biomass/cell[16]	2.54×10^{-11}	g/cell	calculated
mean glucose consumption$_{culture}$	1.83×10^{-3}	$mol_{glucose}$	measured
mean Glucose consumption/cell/h[17]	40.6×10^{-15}	$mol_{glucose}$/cell•h	calculated independent variable · $\dfrac{upt1}{2}$
Glucose consumption/S-phase cell[18]	6.38×10^{-15}	$mol_{glucose}$/h S-phase cell	$\dfrac{upt\_}{S}$
Glucose consumption/non-S-cell[19]	34.2×10^{-15}	$mol_{glucose}$/h non-S-phase cell	upt

In Table 3.4 we present the independent xch fluxes that were constrained according to the thermodynamic properties of the respective metabolic reaction. The xch flux of the irreversible reactions were constrained to zero. Worth of note is that constraining the xch flux to zero only sets the reaction as irreversible. It does not set the directionality of the flux. Therefore, the respective net flux must be set either greater or lower than zero to define the directionality of the reaction.

3.1.6| ^{13}CFlux2 & Omix-visualization suites

The mathematical models for estimation of metabolic fluxes by ^{13}C-MFA require appropriate computational suites to implement the metabolic network, compute the respective stoichiometric matrix and the isotopomer balance equations, and to estimate the metabolic fluxes. We chose the suite 13CFlux2(Weitzel *et al.*, 2013) among others (Zamboni, Fischer and Sauer, 2005; Ahmed *et al.*, 2013; Shupletsov *et al.*, 2014). 13CFlux2 permits the implementation of totally custom-made metabolic models. The

---

[13] CDW (g/L) = 0.5065 × $OD_{600.}$ (*cf* equation 2.1)

[14] [cell] (cell/mL) = 2×10^7 × OD_{600} (*cf* equation 2.2)

[15] Cell Flow Rate (cell/h)= [cell] × Flow Rate

[16] Biomass/cell (g/cell) = CDW / [cell]

[17] Glucose consumption/cell • h ($mol_{glucose}$/ cell • h) = mean glucose consumption$_{culture}$/cell number$_{culture}$/DT

[18] Glucose consumption/S-phase cell ($mol_{glucose}$/S-phase cell • h) =
= glucose consumption/cell • h ($mol_{glucose}$/ cell • h) × $f_{S-phase}$

[19] Glucose consumption/non_S-phase cell ($mol_{glucose}$/ non_S-phase cell • h) =

= Glucose consumption/cell • h ($mol_{glucose}$ /cell • h) × $f_{non-S-phase}$

network reconstruction is assembled from scratch, simplifications (*cf.* chapter 3.1.3) of the network e.g. clustering of reactions, assumptions and imposed constraints can be any to fully satisfy the experimental and mathematical requirements, and there are no boundaries for the model conceptualization and design. Despite more laborious to begin with, these features are rather an advantage because the resulting metabolic model fully matches the goals and particularities of the biological system and question under investigation. 13CFlux2 also comprehends features to run forward simulation, perform sensitivity analysis and statistical evaluation of flux estimation.

3.1.7| Parametrization of the metabolic network

The independent variables whose values are not directly assessable are given a guessed value. In our study cells are proliferating, therefore the reaction rates of biosynthesis of biomass were set as independent variables since their values can be appropriately guessed. A thorough and judicious survey in the literature was done to reliably find out the biomass composition in terms of the respective building blocks (Bruinenberg, Van Dijken and Scheffers, 1983; Verduyn, 1991; Gombert *et al.*, 2001; Lange and Heijnen, 2001; Förster *et al.*, 2003b; Daran-Lapujade *et al.*, 2004; Frick and Wittmann, 2005; von der Haar, 2008; Tummler, Kühn and Klipp, 2015) (Oura 1972, Alroy & Tannenbaum 1973, Dekkers 1981). The biomass parameter values used in our model were obtained from assessments performed in the same conditions of our culture (Table 3.1) and for the same *S. cerevisiae* strain CEN.PK113-7D. When data from the same conditions was not available, we exceptionally took values widely used in literature for the same goal of metabolic flux analysis or values proved to not change over the different culture conditions.

The actual composition of the biomass and respective building blocks of our cells was determined from the fractional composition of biomass of *S. cerevisiae* CEN.PK113-7D with respect to CDW. The fractional composition was calculated from the biomass parameters and respective CDW published for the surveyed experiments. Eventually we achieved the fractional biomass composition of *S. cerevisiae* and the fractional composition of the respective building blocks (Tables 3.4 – 3.6).

Table 3.4 – Fractional composition of amino acids in total protein

$f_{protein/biomass}$
0.407

amino acid	$f_{aa/t\ protein}$	amino acid	$f_{aa/t\ protein}$	amino acid	$f_{aa/t\ protein}$	amino acid	$f_{aa/t\ protein}$
Ala	0.0977	Gly	0.0889	Met	0.0114	Thr	0.0557
Arg	0.0386	His	0.0193	Orn	0.0024	Trp	0.065
Asp+Asn	0.0928	Ile	0.0589	Phe	0.0376	Tyr	0.0196
Cys	0.0014	Leu	0.0801	Pro	0.0422	Val	0.0733
Gln+Glu	0.1548	Lys	0.0657	Ser	0.0533		

(Lange and Heijnen, 2001)

Table 3.5 – Fractional composition of nucleosides and deoxynucleosides in respective total nucleic acid.

$f_{DNA/biomass}$		$f_{RNA/biomass}$	
0.004		**0.066**	
nucleosides	$f_{dnucl/t\ DNA}$	deoxynucleosides	$f_{nucl/t\ RNA}$
deoxyAMP	0.3090	AMP	0.3090
deoxyCMP	0.1917	CMP	0.1917
deoxyGMP	0.1920	GMP	0.1920
TMP	0.3016	UMP	0.3016

(Lange and Heijnen, 2001), (Otero *et al.*, 2010)

Table 3.6 – Fractional composition of lipids in total fat.

$f_{fat/biomass}$	
0.07	
lipid	$f_{lipid/t\ fat}$
palmitoleic acid	0.45
oleic acid	0.20
lauric acid	0.24
glycerol	0.11

(Oura 1972)

We prepared the biomass biosynthesis rates of our culture conditions based on the fractional composition of biomass (Tables 3.4 – 3.6) and in accordance to Equation 3.1.

$$rate_{monomer} = \frac{\left[\frac{f_{monomer/macromolecule} \times m_{macromolecule/cell}}{M_{monomer}}\right]}{CDCphase\ duration} \quad (mol/h \cdot cell) \quad (3.1)$$

Where $f_{monomer/macromolecule}$ is the fractional monomer composition *per* respective macromolecule (Tables 3.4 – 3.6), e.g. $f_{aa/t\_protein}$, fraction of aa per total protein; $m_{macromolecule/cell}$ is the total mass per cell of that macromolecule (Equation 3.2), e.g. $m_{protein/cell}$, mass of protein per cell;

$$m_{macromolecul\ /cell} = biomass/cell \times f_{macromolecule/cell} \quad (g) \quad (3.2)$$

$M_{monomer}$ is the molar mass of the monomer; and $CDC_{phase\ length}$ is the length of either S-phase or of the other phases (Table 3.2).

The biosynthesis of biomass is described in our model as sinks from the respective precursors, except in the case of deoxynucleosides and nucleosides. This means that the rate of biosynthesis is implemented as the rate of precursors' withdrawal (Table 3.7).

Table 3.7 – Monomers of biomass macromolecules, their respective metabolic precursors and flux variable.

Monomer	Precursor	Biomass sink variable
Ala	Pyr	*aab1*
Arg	OGlu + CO_2	*aab3* + *aab9*
Asp+Asn	OAA	*aab2*
Cys	SER	*aab12*
Gln+Glu	OGlu	*aab3*
Gly	Gly	*aab13*
His	R5P + PUR	*aab5* + *aab10*
Ile	OAA + [2,3Pyr-1CO_2]	*aab2* + *aab14*
Leu	AcCoA + [2,3Pyr-1CO_2] + [2,3Pyr-1CO_2]	*aab4* + *aab14*
Lys	[2,3,4,5OGlu-1CO_2] + AcCoA	*aab4* + *aab8*
Met	OAA + MetTHF	*aab2* + *aab11*
Orn	OGlu	*aab3*
Phe	E4P + PEP + [2,3PEP-1CO_2]	*aab6* + *aab7* + *aab15*
Pro	OGlu	*aab3*
Ser	SER	*aab12*
Thr	OAA	*aab2*
Thr	Gly	*aab13*
Trp	E4P + [2,3PEP- 1CO_2] + R5P + SER	*aab6* + *aab5* + *aab12* + *aab15*
Tyr	E4P + PEP + [2,3PEP- 1CO_2]	*aab6* + *aab7* + *aab15*
Val	Pyr + [2,3Pyr-1CO_2]	2 × *aab1*
palmitoleic acid	Acetyl-CoA	*lpb1*
oleic acid	Acetyl-CoA	*lpb1*
lauric acid	Acetyl-CoA	*lpb1*
glycerol	DHAP	*lpb2*

Several components of biomass share precursors. In such cases, the withdrawal rate equals the sum of the rates of biosynthesis. The resulting flux rate variables for biomass are presented in Table 3.8.

We assumed that during S-phase only DNA is biosynthesized (net fluxes *pyrb3_S, pyrb5_S* and *purb5_S*). Whereas the other components of biomass, protein, RNA and lipids were assumed to be biosynthesized during the other phases of CDC (net fluxes *aab1 – aab15, pyrb3, pyrb5, purb5, lpb1* and *lpb2*) (Table 3.8).

Some independent variables were missing additionally to the experimentally measured and educated guessed biomass biosynthesis rates. We picked metabolic fluxes positioned in critical spots of intermediary metabolism, namely the fork between glycolysis and PPP, the major reactions of TCA cycle, and the recruitment of pyruvate and GSS (Table 3.9). Their flux values were defined according to the physiological parameters of a culture of *S. cerevisiae* proliferating under the above mentioned experimental conditions. For flux etimation purposes these flux rates are taken as starting values which are adjustable

iteratively in response to the optimization of the data fitting. *gss3* flux rate was assumed to be devoted to purine biosynthesis.

Table 3.8 – NET Flux independent variables parametrized according to the guessed biomass demand. The notation (_S) respects to the designation of the variable in S-phase cell.

S-phase rate (mol/h.cell)	Biomass flux rate variable	Non-S-phase rate (mol/h.cell)	S-phase rate (mol/h.cell)	Biomass flux rate variable	Non-S-phase rate (mol/h.cell)
0	*aab1(_S)*	3.04×10^{-15}	0	*aab12(_S)*	1.48×10^{-15}
0	*aab2(_S)*	2.37×10^{-15}	0	*aab13(_S)*	2.92×10^{-15}
0	*aab3(_S)*	2.83×10^{-15}	0	*aab14(_S)*	4.06×10^{-15}
0	*aab4(_S)*	1.87×10^{-15}	0	*aab15(_S)*	1.16×10^{-15}
0	*aab5(_S)*	0.782×10^{-15}	0	*pyrb3(_S)*	0.436×10^{-15}
0	*aab6(_S)*	1.16×10^{-15}	0	*purb5(_S)*	0.406×10^{-15}
0	*aab7(_S)*	0.784×10^{-15}	5.81×10^{-17}	*pyrb3_S*	0
0	*aab8(_S)*	0.794×10^{-15}	8.77×10^{-17}	*pyrb5(_S)*	0
0	*aab9(_S)*	0.391×10^{-15}	1.38×10^{-16}	*purb5(_S)*	0
0	*aab10(_S)*	0.220×10^{-15}	0	*lpb1(_S)*	7.35×10^{-15}
0	*aab11(_S)*	0.135×10^{-15}	0	*lpb2(_S)*	0.313×10^{-15}

Table 3.9 – Starting values for free NET flux independent variables based on biomass production for the two subpopulation model.

	flux rate variable whole population	rate (mol/h.cell)	flux rate variable non-S-phase cell	rate (mol/h.cell)	flux rate variable S-phase cell	rate (mol/h.cell)
extracellular	*upt12*	40.6×10^{-15}				
	coOut	71.8×10^{-15}	*upt*	34.2×10^{-15}	*upt_S*	6.38×10^{-15}
	pf4	0				
intracellular			*gly1*	24.0×10^{-15}	*gly1_S*	4.47×10^{-15}
			gly5	47.9×10^{-15}	*gly5_S*	8.94×10^{-15}
			gly7	45.5×10^{-15}	*gly7_S*	8.76×10^{-15}
			pf1	15.7×10^{-15}	*pf1_S*	5.25×10^{-15}
			pf3	2.90×10^{-15}	*pf3_S*	2.00×10^{-15}
			tcc1	11.0×10^{-15}	*tcc1_S*	5.25×10^{-15}
			tcc3	7.71×10^{-15}	*tcc3_S*	3.68×10^{-15}
			tcc4	7.56×10^{-15}	*tcc4_S*	3.68×10^{-15}
			gss3	3.45×10^{-15}	*gss3_S*	0.8×10^{-15}

3.2| FORWARD SIMULATIONS

3.2.1| Analysis of the ^{13}C isotopomer populations in simulated extreme scenarios of metabolic profiles

In order to develop some intuition to guide the interpretation of subsequent results, below we examine how distinct metabolic profiles qualitatively influence the labelling of deoxynucleosides and nucleosides when the yeast are fed [1,2-^{13}C] glucose. We will then present quantitative simulations in the next chapter.

The pools of each precursor of deoxynucleosides and nucleosides are fed by several metabolic pathways. The isotopomer population of the precursor pools depends on the relative flux through each pathway and on the carbon rearrangement characteristic of the reaction – depicted in the carbon mapping. In some cases, different combinations of routes feed the metabolite pool. Thus, the isotopomer population of the pool will also depend on the array of the metabolic pathway routes – each array is a series of metabolic pathway activity. Nonetheless, some carbon mappings are, actually, a unique fingerprint meaning that certain ^{13}C isotopomers can only result of the activity of the respective metabolic reaction. In other cases, what is unique upon the activity of a metabolic pathway is the presence or absence of the ^{13}C isotope in particular positions of the carbon backbone, regardless of the labeling in the other carbons. Moreover, the pattern of ^{13}C labelling of the feeding substrates will narrow even more the fingerprint. Therefore, the analysis of the ^{13}C isotopomers of metabolite pools has, *per se*, potential to univocally elucidate whether there is, or not, activity of a given pathway.

On the other hand, the simulation of extreme MFD lets us identify unique patterns resulting from specific metabolic pathway activity and from the carbon mapping constraints. For instance, when [1,2-^{13}C] is the sole feeding substrate the only way to label C5'of R5P is through activity PPP$_{non-ox}$ bckw (towards R5P) upon glycolysis.

Following the carbon mapping respective of each metabolic reaction (Figure 3.7) we performed "pencil and paper" simulations of extreme scenarios of relative metabolic fluxes (Table 3.10).

The analysis of the ^{13}C isotopomer pools of the precursors of deoxynucleosides and nucleosides permitted the investigation of the impact of extreme scenarios of MFD in the MID of deoxynucleosides and nucleosides.
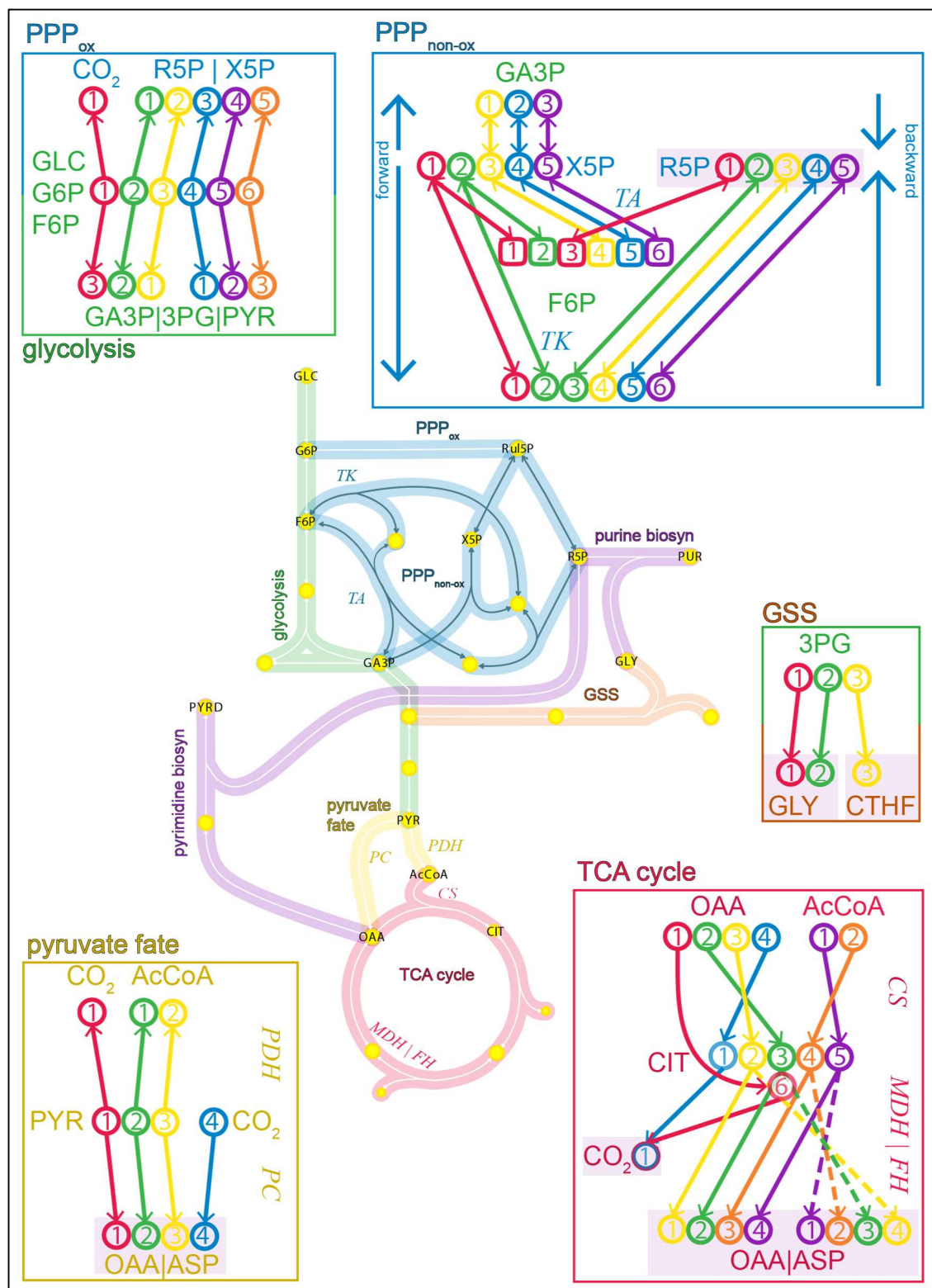
Figure 3.7 – Schematic diagram of the metabolic pathways considered in the extreme scenarios of metabolic profiles and carbon mapping of the precursor pools of deoxynucleosides and nucleosides. Central panel – metabolic pathways: glycolysis, pentose phosphate pathway oxidative and non-oxidative branches (PPP$_{ox}$ and PPP$_{non-ox}$, respectively), pyruvate fate, TCA cycle, glycine serine system (GSS), pyrimidine biosynthesis, purine biosynthesis. Boxes – carbon mappings: each circle depicts one carbon atom of the carbon backbone of the respective molecule, the number inscribed in the circle regards the IUPAC numeration of the carbon atoms in the respective molecule; metabolites,

glucose (GLC), glucose-6-phosphate (G6P), fructose-6-phosphate (F6P); glyceraldehyde-3-phosphate (GA3P); pyruvate (PYR), ribulose-5-phosphate (Rul5P); xylulose-5-phosphate (X5P); ribose-5-phosphate (R5P), acetyl-CoA (AcCoA); citrate (CIT); oxaloacetate (OAA); glycine (GLY), pyrimidine (PYRD), purine (PUR); shaded metabolites are the precursors of deoxynucleosides and nucleosides; reactions, transketolase (*TK*), transaldolase (*TA*), pyruvate carboxylase (*PC*), citrate synthase (*CS*), malate dehydrogenase, fumarate hydratase(*MDH|FH*).

Table 3.10 – Series of metabolic pathway activities simulated in the extreme scenarios of metabolic profiles.

Metabolic series
(1)   Glycolysis $\rightarrow$ PPP$_{non-ox}$ bckw
(2)   PPP$_{ox}$ $\rightarrow$ shunting PPP$_{non-ox}$ fwd $\leftrightarrow$ PPP$_{non-ox}$ bckw
(3)   Glycolysis + PPP$_{ox}$ $\rightarrow$ PPP$_{non-ox}$ fwd $\leftrightarrow$ PPP$_{non-ox}$ bckw
(4)   Glycolysis $\rightarrow$ TCA cycle
(5)   Glycolysis $\rightarrow$ PC + TCA cycle
(6)   PPP$_{ox}$ $\rightarrow$ PPP$_{non-ox}$ fwd $\rightarrow$ TCA cycle
(7)   PPP$_{ox}$ $\rightarrow$ PPP$_{non-ox}$ fwd $\rightarrow$ PC + TCA cycle

PPP$_{non-ox}$ fwd/bckw, non-oxidative branch of pentose phosphate pathway forward (towards F6P and GA3P)/backward (towards R5P/X5P); PPP$_{ox}$, oxidative branch of pentose phosphate pathway; TCA cycle, tricarboxylic acid cycle; PC, pyruvate carboxylase.

The ribose moiety of both nucleosides and deoxynucleosides has as precursor R5P, an intermediary of PPP. The pool of R5P can be fed either by the PPP$_{ox}$ or by the PPP$_{non-ox}$ in the direction towards R5P (PPP$_{non-ox}$ bckw). In turn, PPP$_{non-ox}$ bckw can be preceded by glycolysis (metabolic series (1)) or be part of the metabolic series (2). Therefore, the isotopomer population of R5P depends on the relative flux through the different series (1), (6)/(7), (2) and (3) of pathway activities. In Table 3.11 we show the pentose-5-phosphate isotopomers resulting from the activity of the four different series.

We can consider X5P and R5P metabolites as one single isotopomeric pool due to the equilibrium between their pools which is intermediated by the Rib5P pool. Although there are no carbon rearrangements in the reactions of PPP, the reversibility of the PPP$_{non-ox}$ branch (shunting forward and backward) and the interchange between pentose-5-phosphate pools permits multiple-labeled isotopomers like [1,2-^{13}C] R5P, [1,4,5-^{13}C] R5P, [2,4,5-^{13}C] R5P, [1,4,5-^{13}C] X5P. The activity of PPP$_{ox}$ yields less enrichment than glycolysis because *via* PPPox one ^{13}C of [1,2-^{13}C] glucose is passed into ^{13}CO$_2$. The isotopomer [1,2,4,5-^{13}C] X5P/R5P is results only of activity of glycolysis. In Table 3.12 we systematize the ribose moiety mass isotopomers. In no circumstance C3' becomes labeled with ^{13}C.

Table 3.11 – Predictable isotopomers of nucleoside's ribose and deoxyribose moieties generated after combination of different metabolic pathways. The number in between squared brackets regards the ^{13}C atom numbering, identifying the isotopomer. In bold are the isotopomers of the precursors of deoxynucleosides and nucleosides.

(1) Glycolysis → PPP$_{non-ox}$ bckw		
substrate	metabolite isotopomer yielded by	
	glycolysis	*PPP$_{non-ox}$ bckw*
[1,2]GLC	[1,2]F6P	[2,3]GA3P + GA3P	**R5P + [1,2]X5P + [1,2,4,5]X5P**

(2) PPP$_{ox}$ → shunting PPP$_{non-ox}$ fwd ←→ PPP$_{non-ox}$ bckw		
substrate	metabolite isotopomer yielded by	
	PPP$_{ox}$ (6) & (7)	*PPP$_{non-ox}$ fwd*	*PPP$_{non-ox}$ bckw*
[1,2]GLC	**[1]R5P + [1]X5P**	[1]F6P + [1,3]F6P	**[1]R5P + [2]R5P + [1,2]R5P + R5P + [1]X5P**

(3) Glycolysis + PPP$_{ox}$ → PPP$_{non-ox}$ fwd ←→PPP$_{non-ox}$ bckw		
substrate	metabolite isotopomer yielded by	
	Glycolysis ⁄ *PPP$_{ox}$*	*PPP$_{non-ox}$ fwd*	*PPP$_{non-ox}$ bckw*
[1,2]GLC	[1,2]F6P + [2,3]GA3P + GA3P	[1,3,5,6]F6P	**[1,4,5]R5P + [2,4,5]R5P + [1,2,4,5]R5P + [1]X5P + [1,4,5]X5P**
	[1]R5P + [1]X5P	[1]F6P + [1,3]F6P	**[1]R5P + [2]R5P + [1,2]R5P + R5P + [1]X5P**

PPP$_{non-ox}$ fwd/bckw, non-oxidative branch of pentose phosphate pathway forward (towards F6P and GA3P)/backward (towards R5P/X5P); PPP$_{ox}$, oxidative branch of pentose phosphate pathway.

Table 3.12 – Mass isotopomers of R5P moiety of deoxynucleosides and nucleosides imprinted from R5P and X5P.

Carbon mapping	**Pentose-5-phosphate isotopomer**	**R5P moiety mass isotopomer**
	R5P	m0
	[1]R5P [2]R5P [1]X5P	m1
	[1,2]R5P	m2
	[1,4,5]R5P [2,4,5]R5P [1,4,5]X5P	m3
	[1,2,4,5]R5P [1,2,4,5]X5P	m4

The purine moiety of both nucleosides and deoxynucleosides has as precursor glycine and formyltetrahydrofolate (FTHF). 3-Phosphoglycerate (3PG) is the glycolytic precursor of glycine. Therefore, the labeling in glycine will be influenced by the relative flux through glycolysis ((1) and (4)/(5) series) and PPP$_{non-ox}$ ((2) and (6)/(7) series). In Table 3.13 we present the combination of metabolic fluxes influencing glycine labeling and the resulting glycine ^{13}C isotopomers.
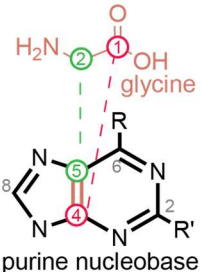
Table 3.13 – Predictable isotopomers of nucleoside's purine moieties generated after combination of different metabolic pathways. The number in between squared brackets regards the ^{13}C atom numbering, identifying the isotopomer. Deoxynucleosides and nucleosides precursor's isotopomers are in bold.

(1), (4) & (5) Glycolysis

substrate	metabolite isotopomer yielded by				
	glycolysis				
[1,2]GLC	[1,2]F6P	[2,3]GA3P + GA3P		**[2,3]3PG + 3PG**	**[2]GLY + GLY**

(2), (6) & (7) PPP$_{ox}$ → shunting PPP$_{non-ox}$ fwd ←→ PPP$_{non-ox}$ bckw

substrate	metabolite isotopomer yielded by				
	PPP$_{ox}$ (6) & (7)	*PPP$_{non-ox}$ fwd*			
[1,2]GLC	[1]R5P + [1]X5P	[1]F6P + [1,3]F6P	[3]GA3P + [1,3]GA3P + GA3P	**[3]3PG + [1,3]3PG + 3PG**	**GLY + [1]GLY**

(3) Glycolysis + PPP$_{ox}$ → PPP$_{non-ox}$ fwd

substrate	*Glycolysis* / *PPP$_{ox}$*	metabolite isotopomer yielded by			
		PPP$_{non-ox}$ fwd			
[1,2]GLC	[1,2]F6P + [2,3]GA3P + GA3P ——— [1]F6P + [1,3]F6P	[1,3,5,6]F6P ——— [1]F6P + [1,3]F6P	[1,3]GA3P + [2,3]GA3P + [3]GA3P + GA3P	**[3]3PG + [1,3]3PG + [2,3]3PG + 3PG**	**GLY + [1]GLY + [2]GLY**

PPP$_{non-ox}$ fwd/bckw, non-oxidative branch of pentose phosphate pathway forward (towards F6P and GA3P)/backward (towards R5P/X5P); PPP$_{ox}$, oxidative branch of pentose phosphate pathway.

The activity of either glycolysis or PPP upon feeding with [1,2-^{13}C] glucose yields either [1]GLY or [2]GLY and unlabeled glycine. Because glycine derives from C1 and C2, the labeling in C3 of 3PG is transferred into FTHF. Indeed, FTHF is also a precursors of purine nucleobase but its labeling is hardly predictable because it is in equilibrium with the other single carbon pools, namely formate, HCO_3, and the other tetrahydrofolate derivatives. Therefore, the mass isotopomers of purine nucleobase that we can predict are either m0 or m1 (Table 3.14).

Table 3.14 - Mass isotopomers of purine nucleobase deoxynucleosides and nucleosides imprinted from 3PG.

Carbon mapping	Glycine isotopomer	Purine nucleobase mass isotopomer
	GLY	m0
	[1]GLY [2]GLY	m1

The pyrimidine moiety both of deoxynucleosides and nucleosides has as precursor ASP which precursor is OAA, an intermediary of the TCA cycle. ASP (and OAA) isotopic distribution depends directly of the relative flux through TCA cycle and PC and indirectly of the activity of glycolysis and PPP as they influence the isotopic distribution of acetyl-CoA that will react with OAA to form citrate, another intermediary of TCA cycle. Table 3.15 shows the OAA pools resulting from the combination of the activities of glycolysis and either TCA cycle (4) or PC together with TCA cycle (5), and PPP and either TCA cycle (6) or PC together with TCA cycle (7). In Table 3.15 we highlight the sequential yielding of OAA isotopomers upon the consecutive rounds of TCA cycle. Each 4 series of metabolic pathway activity yield different starting pools of ^{13}C isotopomers of OAA.

The isotopomers [1,2,3], [2,3,4] and [1,2,3,4] are formed only upon glycolytic activity. The subsequent activity of PC yields directly the [2,3]OAA isotopomer. The isotopomers [1,3] and [2,4] results from the series PPP and TCA cycle or PC together with TCA cycle. The substrate [1,2-^{13}C] glucose did not yield a ^{13}C fingerprint to distinguish the activity of PC from that of TCA cycle. In Table 3.16 we present the mass isotopomers of pyrimidine nucleobase derived from OAA/ASP isotopomer pools.

3.2.2| Sets of fluxes used for forward simulations

Computational metabolic models permit *in silico* simulations of the ^{13}C isotopomer metabolite populations formed from sets of metabolic flux rates and concrete substrate ^{13}C labeling – *forward simulations*. The ^{13}C isotopomer populations of the metabolites to be analyzed are translated into their respective *in silico* MS spectra. The rates of one or two metabolic fluxes of those sets are scanned over a range of values.

We used forward simulations to rationalize the trend of the MID of deoxynucleosides and nucleosides in response to the scanned metabolic flux rates, and to explore the sensitivity of the biological system to concrete metabolic flux variables. The scanning of metabolic flux rates is expected to influence the ^{13}C isotopomer distribution and MID of deoxynucleosides and nucleosides. We will then use the rationalization to infer about the relative flux rates during S- and the other phases.

Table 3.15 – Predictable OAA isotopomers from different metabolic pathway series. The number in between squared brackets regards the ^{13}C atom numbering, identifying the isotopomer. Different colors distinguish different isotopomers. The isotopomers within the solid thick frame are exclusive of glycolysis or PPP$_{non-ox}$ (bold framed cells).

(4) Glycolysis → TCA cycle

OAA isotopomers	Acetyl-CoA isotopomers		TCA cycle "round"
	AcCoA	[1,2] AcCoA	
OAA	OAA	[1,2]OAA + [3,4]OAA	1st, 4th, nth.
[1,2]OAA	[2]OAA + [3]OAA	[1,2,3]OAA + [2,3,4]OAA	2nd, 4th, nth.
[3,4]OAA	[1]OAA + [4]OAA	[1,2,4]OAA + [1,3,4]OAA	
[2]OAA	[2]OAA + [3]OAA	[1,2,3]OAA + [2,3,4]OAA	
[3]OAA	[1]OAA + [4]OAA	[1,2,4]OAA + [1,3,4]OAA	
[1,2,3]OAA	[1,2]OAA + [3,4]OAA	[1,2,3,4]OAA	
[2,3,4]OAA	[1,2]OAA + [3,4]OAA	[1,2,3,4]OAA	
[1]OAA	OAA	[1,2]OAA + [3,4]OAA	3rd, 4th, nth.
[4]OAA	OAA	[1,2]OAA + [3,4]OAA	
[1,2,4]OAA	[2]OAA + [3]OAA	[1,2,3]OAA + [2,3,4OAA]	
[1,3,4]OAA	[1OAA] + [4OAA]	[1,2,4]OAA + [1,3,4]OAA	
[1,2,3,4]OAA	[1,2]OAA + [3,4]OAA	[1,2,3,4]OAA	4th, nth.

(5) Glycolysis → PC + TCA cycle

OAA isotopomers	Acetyl-CoA isotopomers		TCA cycle "round"
	AcCoA	[1,2] AcCoA	
[2,3]OAA	[1,2]OAA + [3,4]OAA	[1,2,3,4]OAA	1st,
[1,2]OAA	[2]OAA + [3]OAA	[1,2,3]OAA + [2,3,4]OAA	2nd, 3rd, 4th, nth.
[3,4]OAA	[1]OAA + [4]OAA	[1,2,4]OAA + [1,3,4]OAA	
[1,2,3,4]OAA	[1,2]OAA + [3,4]OAA	[1,2,3,4]OAA	
[2]OAA	[2]OAA + [3]OAA	[1,2,3]OAA + [2,3,4]OAA	
[3]OAA	[1]OAA + [4]OAA	[1,2,4]OAA + [1,3,4]OAA	
[1,2,3]OAA	[1,2]OAA + [3,4]OAA	[1,2,3,4]OAA	3rd, 4th, nth.
[2,3,4]OAA	[1,2]OAA + [3,4]OAA	[1,2,3,4]OAA	
[1]OAA	OAA	[1,2]OAA + [3,4]OAA	
[4]OAA	OAA	[1,2]OAA + [3,4]OAA	
[1,2,4]OAA	[2]OAA + [3]OAA	[1,2,3]OAA + [2,3,4OAA]	
[1,3,4]OAA	[1OAA] + [4OAA]	[1,2,4]OAA + [1,3,4]OAA	
OAA	OAA	[1,2]OAA + [3,4]OAA	4th, nth.

(6) PPP$_{ox}$ → PPP$_{non-ox}$ fwd → TCA cycle

	AcCoA	[2]AcCoA	TCA cycle "round"
OAA	OAA	[2]OAA + [3]OAA	1st, 4th,
[2]OAA	[2]OAA + [3]OAA	[2,3]OAA	2nd, 3rd, 4th,
[3]OAA	[1]OAA + [4]OAA	[1,3]OAA + [2,4]OAA	
[2,3]OAA	[1,2]OAA + [3,4]OAA	[1,2,3]OAA + [2,3,4]OAA	
[1]OAA	OAA	[2]OAA + [3]OAA	
[4]OAA	OAA	[2]OAA + [3]OAA	3rd, 4th, nth.
[1,3]OAA	[1]OAA + [4]OAA	[1,3]OAA + [2,4]OAA	
[2,4]OAA	[2]OAA + [3]OAA	[2,3]OAA	
[1,2]OAA	[2]OAA + [3]OAA	[2,3]OAA	
[3,4]OAA	[1]OAA + [4]OAA	[1,3]OAA + [2,4]OAA	4th, nth.
[1,2,3]OAA	[1,2]OAA + [3,4]OAA	[1,2,3]OAA + [2,3,4]OAA	
[2,3,4]OAA	[1,2]OAA + [3,4]OAA	[1,2,3]OAA + [2,3,4]OAA	
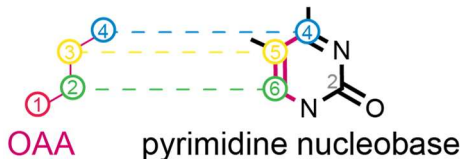
Table 3.15 (continued)

(7) PPP$_{ox}$ → PPP$_{non-ox}$ fwd → PC + TCA cycle			
	AcCoA	[2]AcCoA	TCA cycle "round"
[3]OAA	[1]OAA + [4]OAA	[1,3]OAA + [2,4]OAA	1st, 3rd, 4th,
[1]OAA	OAA	[2]OAA + [3]OAA	
[4]OAA	OAA	[2]OAA + [3]OAA	2nd, 3rd, 4th, nth.
[1,3]OAA	[1]OAA + [4]OAA	[1,3]OAA + [2,4]OAA	
[2,4]OAA	[2]OAA + [3]OAA	[2,3]OAA	
OAA	OAA	[2]OAA + [3]OAA	
[2]OAA	[2]OAA + [3]OAA	[2,3]OAA	3rd, 4th, nth.
[2,3]OAA	[1,2]OAA + [3,4]OAA	[1,2,3]OAA + [2,3,4]OAA	
[1,2]OAA	[2]OAA + [3]OAA	[2,3]OAA	
[3,4]OAA	[1]OAA + [4]OAA	[1,3]OAA + [2,4]OAA	4th, nth.
[1,2,3]OAA	[1,2]OAA + [3,4]OAA	[1,2,3]OAA + [2,3,4]OAA	
[2,3,4]OAA	[1,2]OAA + [3,4]OAA	[1,2,3]OAA + [2,3,4]OAA	

PPP$_{non-ox}$ fwd/bckw, non-oxidative branch of pentose phosphate pathway forward (towards F6P and GA3P)/backward (towards R5P/X5P); PPP$_{ox}$, oxidative branch of pentose phosphate pathway; TCA cycle, tricarboxylic acid cycle; PC, pyruvate carboxylase; OAA, oxaloacetate; AcCoA, Acetyl-CoA.

Table 3.16 - Mass isotopomers pyrimidine nucleobase imprinted from OAA.

Carbon mapping	OAA isotopomer	Pyrimidine nucleobase mass isotopomer
	OAA, [1]OAA	m0
	[4]OAA, [3]OAA, [2]OAA, [1,3]OAA, [1,2]OAA,	m1
	[3,4]OAA, [2,4]OAA, [2,3]OAA, [1,3,4]OAA, [1,2,4]OAA, [1,2,3]OAA,	m2
	[1,2,3,4]OAA, [2,3,4]OAA	m3

We performed forward simulations to gain insight on the impact of relative metabolic flux rates on the ^{13}C isotopomer precursor populations and, therefore, on the respective out coming MID of deoxynucleosides and nucleosides. In the forward simulations we aimed at scanning the rates of concurrent metabolic fluxes feeding the precursor pools of deoxynucleoside and nucleoside. Namely, R5P is fed by PPP$_{ox}$ and PPP$_{non-ox}$, glycine is fed by GSS and glyoxylate cycle and ASP/OAA is fed by TCA cycle and PC. Thus, the number of metabolic pathways directly involved in these forward simulations is less than in the complete metabolic model of proliferating cell metabolism. Hence, a reduced metabolic model is enough for forward simulations with such a purpose and given that simple sets of metabolic fluxes are required. Using a rather reduced metabolic model permits overcoming some limitations of the more comprehensive models. A very comprehensive metabolic model returns more detail about the system at the expense of more independent variables to be determined. On the one hand, it is not always possible

to determine all the required independent variables; and on the other hand, the level of detail may be beyond what is indeed required. Thus, the comprehensiveness of the metabolic model is a tradeoff between determination and discrimination power of the model. Therefore, for the purpose of the present forward simulations we established a one population, reduced metabolic model comprehending only the major intermediary metabolism pathways and the biosynthesis of purine and pyrimidine (Figure 3.8).
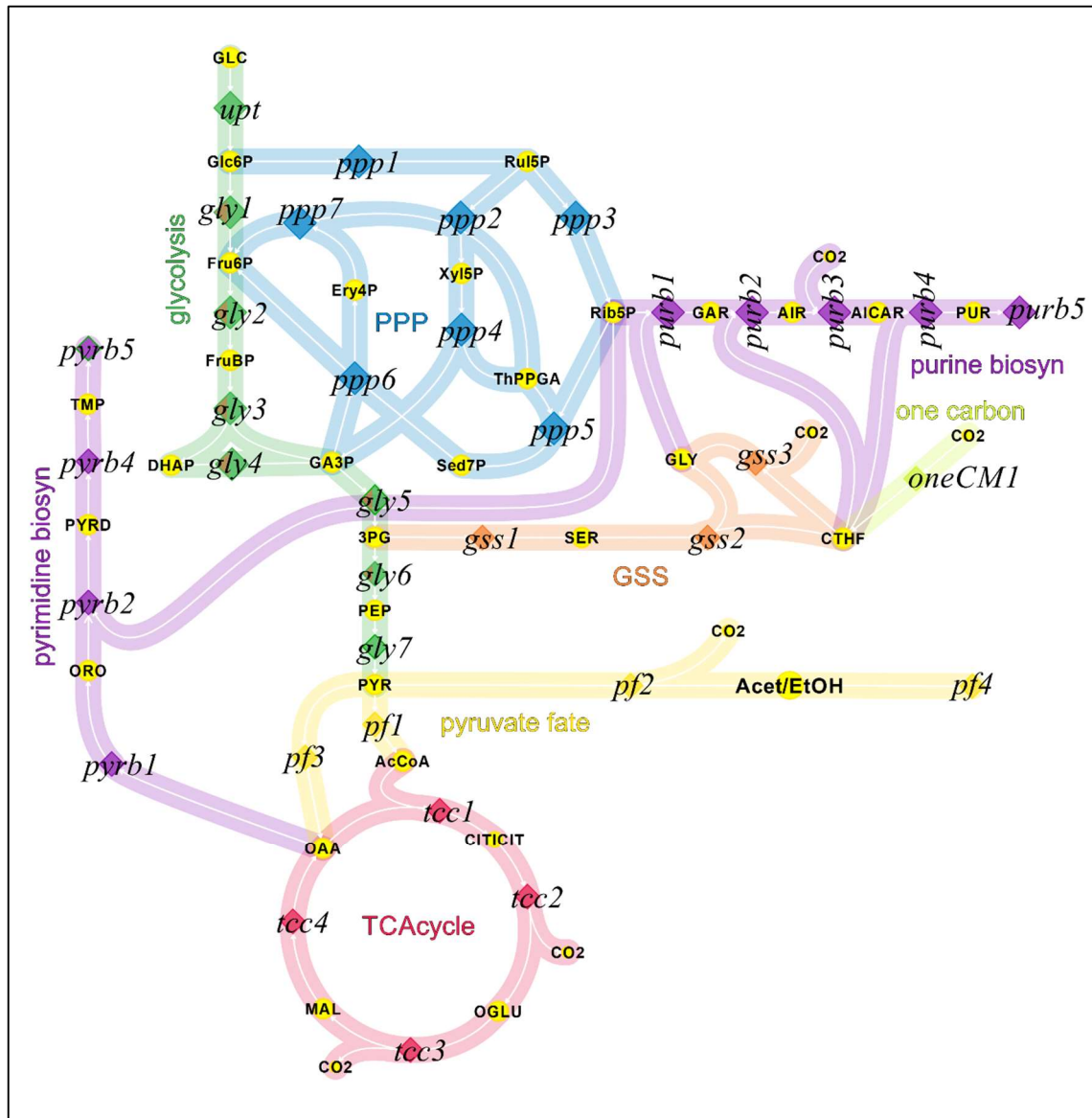
Figure 3.8 – Reduced genome-scale metabolic model of proliferating *S. cerevisiae*. Pathways included in the model: glycolysis, PPP – pentose phosphate pathway, pyruvate fate, TCA cycle, GSS – glycine/serine system, purine biosynthesis, pyrimidine biosynthesis. Metabolic fluxes and metabolite pools (single and clusters) as per Figure 3.4.

The independent flux sets for forward simulation comprise the scanned fluxes, those that vary over a range of values, and the fluxes which values are kept constant. We configured combinations of ranges of flux rates for glycolysis (*gly1*), the oxidative branch of PPP (*ppp_{ox}*), citrate synthase (*tcc1*) and PC (*pf3*) (Table 3.10). All flux values were normalized for a *upt* flux of 10 fmol/h.cell.

Table 3.10 – Sets of independent fluxes and respective rates used in the forward simulations.

Set	constant flux rate (fmol/h.cell)		scanned flux rates (fmol/h.cell)						
Glycolysis *vs* PPP			***gly1***						
	upt	10	0	1	2				
	pf4	0	3	4	5				
	tcc1	15	6	7	8				
	purb5	0.13	9	10					
	pyrb3	0.14							
TCA cycle *vs* Pyruvate carboxyalse			***gly1; tcc1***						
			0;0	2;0	3;0	4;0	6;0	8;0	10;0
			0;1	2;1	3;1	4;1	6;1		10;1
			0;2	2;2	3;2	4;2	6;2	8;2	10;2
			0;3	2;3	3;3	4;3	6;3		10;3
	upt	10	0;4	2;4	3;4	4;4	6;4		10;4
	pf4	0	0;5	2;5	3;5	4;5	6;5	8;5	10;5
	purb5	0.13	0;7	2;7		4;8	6;8		10;8
	pyrb3	0.14	0;10	2;10	3;10	4;10	6;10		10;10
			0;12	2;12			6;12		
			0;15	2;15	3;15	4;15	6;15	8;15	10;15
					3;17	4;17		8;16	10;17
							6;18	8;18	10;18
									10;19

3.2.3| *In silico* mass isotopomer distribution of deoxynucleosides and nucleosides.

The forward simulation provides the *in silico* MID of deoxynucleosides and nucleosides (Figures 3.9 and 3.10). The analysis of the MID for a range of metabolic fluxes let us examine the sensitivity of the deoxynucleosides and nucleosides MID to these flux rates. The rationalization on the MID trend of deoxynucleosides and nucleosides as metabolic flux rates change within the range let us infer on the relative activity of the metabolic pathways by comparing MID of deoxynucleosides with MID of nucleosides (Tables 3.11 and 3.12).
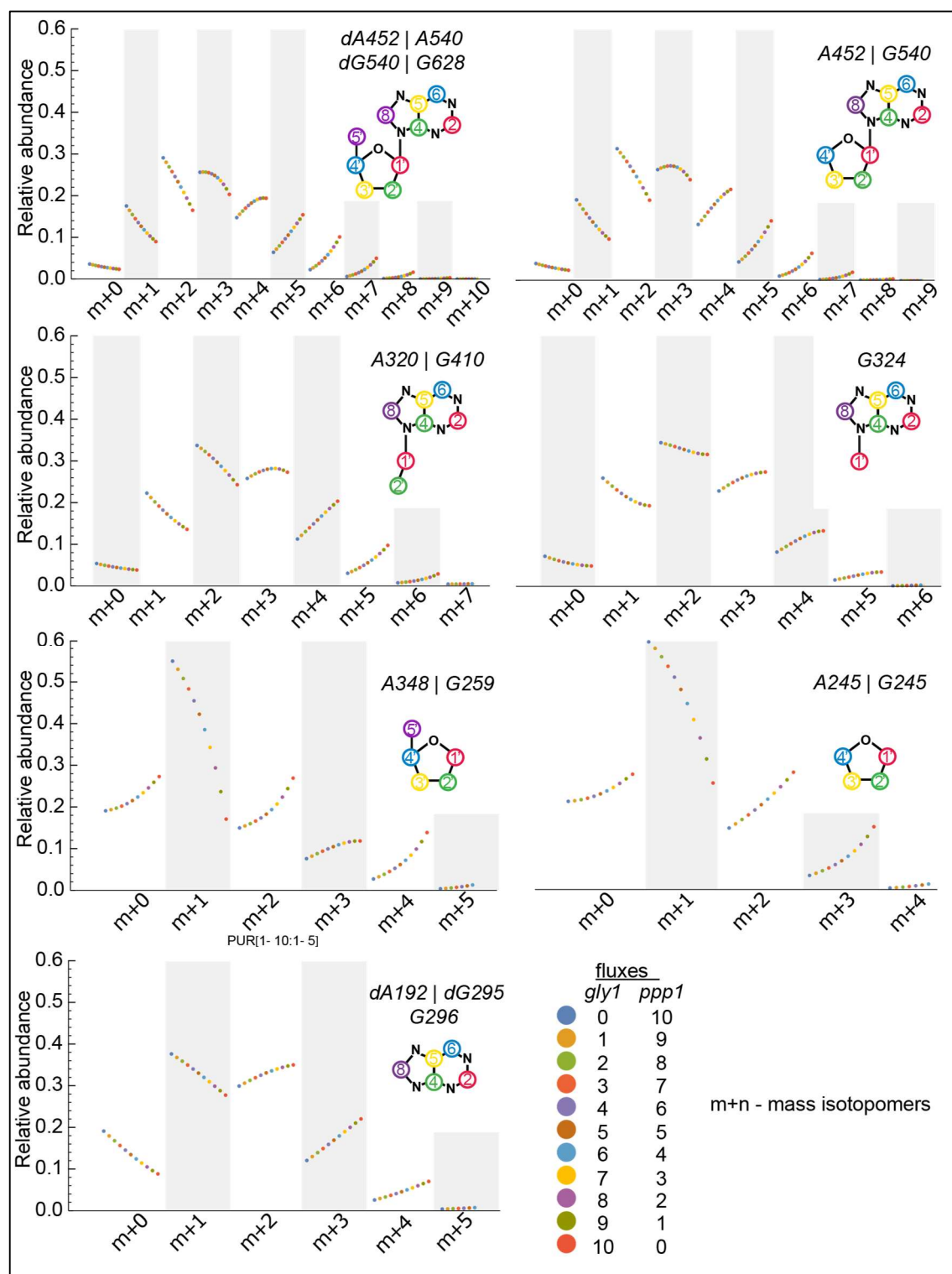
Figure 3.9 – *in silico* simulated MID of purine for sets of fluxes. Evaluation of the impact of scanning of *gly1* fluxes in the abundance of mass isotopomer populations. Metabolic flux rates used are presented in Table 3.10.
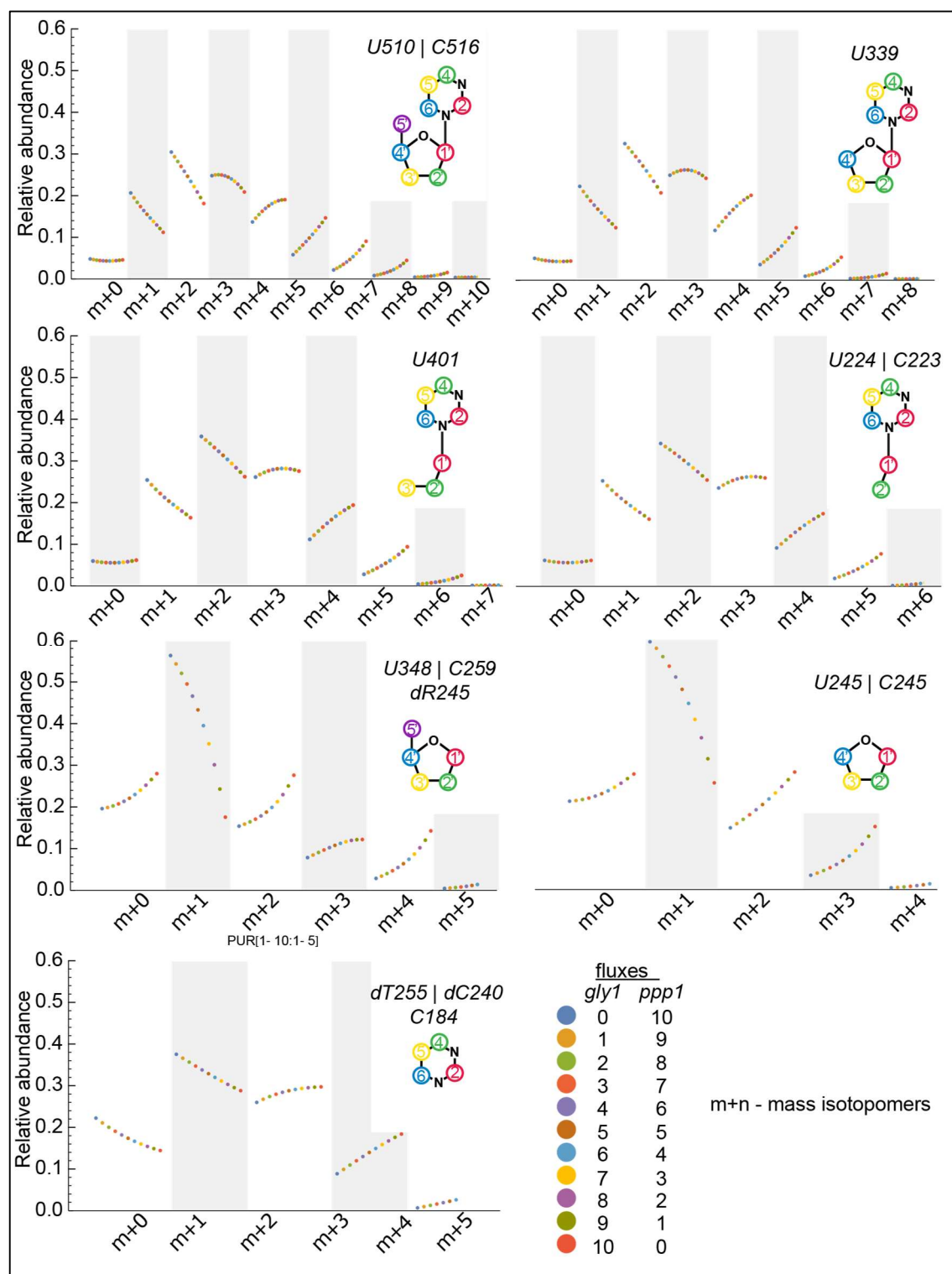
Figure 3.10 – *in silico* simulated MID of pyrimidine for sets of fluxes. Evaluation of the impact of scanning of *gly1* in the abundance of mass isotopomer populations.

As the flux through glycolysis (*gly1*) increases (0 – 10 fmol/h.cell, normalized for glucose uptake flux), with concomitant decreasing of PPP$_{ox}$ (*ppp1*), the ribose moiety mass isotopomers *(m+0)*, *(m+2)*, *(m+4)* and *(m+5)* increase, *(m+3)* increases until *gly1* flux of 5, then it stays constant and *(m+1)* decreases.

According to the stoichiometric matrix, *pf3* depends only on *pyrb3* and not on *tcc4*. Therefore, the OAA and, thus, ASP pools were dependent on the rate ratio $\frac{tcc4}{pf3}$; knowing that *pyrb3*, and thus *pf3*, are constant, then, the larger the *tcc1* the greater the contribution of TCA cycle flux to OAA and ASP ^{13}C isotopomer pools.

Table 3.11 – Trending of mass isotopomer abundance of purine and pyrimidines for scanning of *gly1* flux rates.

purine

ppp1	10	9	8	7	6	5	4	3	2	1	0
gly1	0	1	2	3	4	5	6	7	8	9	10
m+1, m+2	↓	↓	↓	↓	↓	↓	↓	↓	↓	↓	↓
m+3 (tcc1 = 15)	↔	↔	↔	↔	↓	↓	↓	↓	↓	↓	↓
m+4 (pf3 = 0.14)	↑	↑	↑	↑	↔	↔	↔	↔	↔	↔	↔
m+5, m+6	↑	↑	↑	↑	↑	↑	↑	↑	↑	↑	↑

pyrimidine

ppp1	10	9	8	7	6	5	4	3	2	1	0
gly1	0	1	2	3	4	5	6	7	8	9	10
m+1, m+2	↓	↓	↓	↓	↓	↓	↓	↓	↓	↓	↓
m+3 (tcc1 = 15)	↔	↔	↔	↔	↔	↔	↔	↓	↓	↓	↓
m+4 (pf3 = 0.14)	↑	↑	↑	↑	↑	↑	↑	↔	↔	↔	↔
m+5, m+6	↑	↑	↑	↑	↑	↑	↑	↑	↑	↑	↑

ribose moiety

ppp1	10	9	8	7	6	5	4	3	2	1	0
gly1	0	1	2	3	4	5	6	7	8	9	10
m+0	↑	↑	↑	↑	↑	↑	↑	↑	↑	↑	↑
m+1	↓	↓	↓	↓	↓	↓	↓	↓	↓	↓	↓
m+2 (tcc1 = 15)	↑	↑	↑	↑	↑	↑	↑	↑	↑	↑	↑
m+3 (pf3 = 0.14)	↑	↑	↑	↑	↑	↑	↔	↔	↔	↔	↔
m+4	↑	↑	↑	↑	↑	↑	↑	↑	↑	↑	↑
m+5	↑	↑	↑	↑	↑	↑	↑	↑	↑	↑	↑

pyrimidine nucleobase moiety

ppp1	10	9	8	7	6	5	4	3	2	1	0
gly1	0	1	2	3	4	5	6	7	8	9	10
m+0	↓	↓	↓	↓	↓	↓	↓	↓	↓	↓	↓
m+1	↓	↓	↓	↓	↓	↓	↓	↓	↓	↓	↓
m+2 (tcc1 = 15)	↑	↑	↑	↑	↑	↑	↑	↑	↔	↔	↔
m+3 (pf3 = 0.14)	↑	↑	↑	↑	↑	↑	↑	↑	↑	↑	↑
m+4	↑	↑	↑	↑	↑	↑	↑	↑	↑	↑	↑
m+5	↑	↑	↑	↑	↑	↑	↑	↑	↑	↑	↑

The lower the *gly1*, the least impact of *tcc1 vs pf3* branching point scan on MID of nucleobase pyrimidine. For higher range of *tcc1*, the contribution of *pf3* becomes negligible. For sake of simplicity, we chose to not display any figure presenting the MID of the forward simulations of TCA cycle *vs* PC. However we systematize the trending in the Table 3.12.

Table 3.12 – Trending of mass isotopomer abundance of purine and pyrimidines for scanning of *tcc1* flux rates at different flux values of *gly1*.

purine	*tcc1*	0	1	2	3	4	5	7	8	10	12	15	16	17	18	19
m+1		↔	↔	↔	↔	↔	↔	↓	↓	↓	↓	↓	↓	↓	↓	↓
m+2	*gly1 < 3*	↔	↔	↔	↔	↔	↔	↓	↓	↓	↓	↓				
	gly1 > 4	↔	↔	↔	↔	↔	↔	↔	↔	↓	↓	↓	↓	↓	↓	↓
m+3	*gly1 < 6*	↔	↔	↔	↔	↔	↔	↑	↑	↑	↑	↑	↑	↑	↑	
	6 < gly1 < 8	↔	↔	↔	↔	↔	↔	↔	↔	↔	↔	↔	↔	↔	↔	↔
	gly1 > 8	↔	↔	↔	↔	↔	↔	↔	↔	↔	↓	↓	↓	↓	↓	↓
m+4	*gly1 < 4*	↔	↔	↔	↔	↔	↔	↑	↑	↑	↑	↑	↑	↑		
	gly1 > 6	↔	↔	↔	↔	↔	↔	↔	↔	↑	↑	↑	↑	↑	↑	↑
m+5	*gly1 < 4*	↔	↔	↔	↔	↔	↔	↑	↑	↑	↑	↑	↑	↑		
	gly1 > 6	↔	↔	↔	↔	↔	↔	↔	↔	↑	↑	↑	↑	↑	↑	↑

pyrimidines	*tcc1*	0	1	2	3	4	5	7	8	10	12	15	16	17	18	19
m+1	*gly1 < 1*	↑	↑	↑	↑	↔	↔	↔	↔	↔	↔	↔	↔	↔	↔	↔
	1 < gly1 < 3	↑	↔	↔	↔	↔	↔	↓	↓	↓	↔	↔				
	3 < gly1 < 6	↓	↓	↓	↓	↓	↓	↓	↔	↔	↔	↔	↔	↔		
	gly1 > 8	↓	↓	↓	↓	↓	↓	↓	↓	↔	↔	↔	↔	↔	↔	↔
m+2	*gly1 < 1*	↔	↔	↔	↔	↔	↔	↔	↔	↔	↔	↔	↔	↔		
	1 < gly1 < 4	↓	↓	↓	↓	↓	↓	↔	↔	↔	↔	↔	↔	↔	↔	↔
	4 < gly1 < 8	↓	↓	↓	↓	↓	↓	↓	↓	↔	↔	↔	↔	↔	↔	
	gly1 > 8	↓	↓	↓	↓	↓	↓	↓	↓	↓	↓	↔	↔	↔	↔	↔
m+3	*gly1 < 1*	↓	↓	↓	↓	↓	↔	↔	↔	↔	↔	↔	↔			
	1 < gly1 < 4	↓	↓	↓	↓	↔	↔	↔	↔	↔	↔	↔	↔	↔		
	gly1 > 6	↔	↔	↔	↔	↔	↔	↔	↔	↔	↔	↔	↔	↔	↔	↔
m+4	*1 < gly1 < 4*	↓	↓	↔	↔	↔	↔	↔	↔	↔	↔	↔				
	1 < gly1 < 3	↔	↔	↔	↔	↔	↔	↔	↔	↔	↔	↔	↔	↔		
	3 < gly1 < 8	↑	↑	↑	↑	↑	↑	↑	↑	↑	↔	↔	↔	↔		
	gly1 > 8	↑	↑	↑	↑	↑	↑	↑	↑	↑	↑	↑	↔	↔	↔	↔
m+5	*gly1 < 3*	↔	↔	↔	↔	↔	↔	↔	↔	↔	↔	↔				
	3 < gly1 < 8	↑	↑	↑	↑	↑	↑	↑	↔	↔	↔	↔	↔	↔	↔	↔
	gly1 < 8	↑	↑	↑	↑	↑	↑	↔	↔	↔	↔	↔	↔	↔	↔	↔

Table 3.12 (continued)

pyrimidine nucleobase	*tcc1*	0	1	2	3	4	5	7	8	10	12	15	16	17	18	19
m+0	*gly1 < 2*	↑	↑	↑	↔	↔	↔	↔	↔	↔	↔	↔				
	2 < gly1 < 3	↑	↑	↔	↔	↔	↔	↔	↔	↔	↔	↔	↔	↔		
	3 < gly1 < 6	↔	↔	↔	↔	↔	↔	↔	↔	↔	↔	↔	↔	↔	↔	↔
	6 < gly1 < 8	↓	↓	↓	↔	↔	↔	↔	↔	↔	↔	↔	↔	↔		
	gly1 > 8	↓	↓	↔	↔	↔	↔	↔	↔	↔	↔	↔	↔	↔	↔	↔
m+1	*gly1 < 2*	↓	↓	↓	↔	↔	↔	↔	↔	↔	↔	↔				
	3 < gly1 < 4	↓	↓	↓	↓	↔	↔	↔	↔	↔	↔	↔	↔	↔		
	gly1 > 6	↓	↓	↓	↔	↔	↔	↔	↔	↔	↔	↔	↔	↔	↔	↔
m+2	*gly1 < 2*	↓	↓	↓	↔	↔	↔	↔	↔	↔	↔	↔				
	3 < gly1 < 4	↓	↓	↔	↔	↔	↔	↔	↔	↔	↔	↔	↔	↔		
	4 < gly1 < 6	↔	↔	↔	↔	↔	↔	↔	↔	↔	↔	↔	↔	↔	↔	↔
	gly1 > 6	↑	↑	↑	↔	↔	↔	↔	↔	↔	↔	↔	↔	↔	↔	↔
m+3	*gly1 < 2*	↓	↓	↔	↔	↔	↔	↔	↔	↔	↔	↔				
	2 < gly1 < 4	↑	↑	↑	↔	↔	↔	↔	↔	↔	↔	↔	↔	↔		
	4 < gly1 < 6	↑	↑	↑	↑	↔	↔	↔	↔	↔	↔	↔	↔	↔		
	gly1 > 8	↑	↑	↑	↑	↑	↑	↑	↔	↔	↔	↔	↔	↔	↔	↔
m+4	*gly1 < 4*	↔	↔	↔	↔	↔	↔	↔	↔	↔	↔	↔				
	4 < gly1 < 6	↑	↑	↑	↑	↔	↔	↔	↔	↔	↔	↔	↔	↔		
	gly1 > 6	↑	↑	↑	↑	↑	↔	↔	↔	↔	↔	↔	↔	↔	↔	↔

With the forward simulations we gathered in silico evidence that MID of deoxynucleosides and nucleosides respond to the relative metabolic flux rates; and thus, we can determine metabolic flux rates from MID of deoxynucleosides and nucleosides. Moreover, the MID of the different fragments are specifically sensitive to metabolic pathways yielded the precursor of that fragment moiety. For instance, consistently, the MID of the fragments composed of ribose moiety does not change with changes in flux of TCA cycle. The most informative fragments are those composed of nucleobase of pyrimidine since its ^{13}C labeling depends directly on the TCA cycle and PC activity and indirectly on the glycolysis and PPP activity, which influence the ^{13}C labeling in pyruvate.

4| Results

4.1| CARBON COMPOSITION OF NUCLEOSIDE FRAGMENT MOIETIES

4.1.1| Identification and assignment of derivatized nucleosides and deoxynucleosides.

For the identification and assignment of the derivatized compounds in the GC-MS, a range of concentrations from 40 – 800 µM of each pure, naturally labeled nucleoside and deoxynucleoside was independently measured in scan mode. The RT of each derivatized compound was, at first, guessed from the increasing signal area for increasing concentrations of compound (Figure 4.1, top panel). At this chromatographic RT the spectrum was inspected and the presence of the molecular ion, identified by the corresponding *m/z*, confirmed the assignment of the compound to that RT. The molecular ions are the derivatization products of the respective nucleosides and deoxynucleosides. Their molecular structures are shown in Figure 4.2. The measurement of such range of concentrations served the dual purpose of i) determining the sensitivity range for each derivative of nucleoside and deoxynucleoside and ii) establishing the amount of analyte required to be isolated from cells to guarantee a chromatographic abundance above 1×10^6 for every analyte, and thus a confident determination of the mass isotopomers. We established the concentration of 20 µM per deoxynucleoside or nucleoside in every preparation and a sample volume of 50 µL. The used injection volume was 1 µL, thus 20 mmol deoxynucleoside or nucleoside for each measurement.

Next, a mixture of the 4 derivatized nucleosides and of the 4 derivatized deoxynucleosides was measured in scan mode. The chromatogram and spectra of the mixture of nucleosides and of deoxynucleosides are presented in *Gas chromatogram* and *Mass spectrum* panels of Figure 4.3 and Figure 4.4, respectively. The applied mixture of standard compounds contained 80 µM uridine and guanosine, 60 µM adenosine, 720 µM cytidine, 160 µM thymidine, 80 µM deoxycytidine and 60 µM deoxyadenosine and deoxyguanosine, such that the chromatographic signal abundances were above 1×10^6 for every derivative. The derivatization process resulted in complete trimethylsilylation of all the purine and pyrimidine nucleosides as well as of the purine deoxynucleosides. In the derivatization of deoxythymidine and deoxycytidine, the pyridine ring promoted the cleavage of the *N*-glycosidic bond. Subsequently, the nucleobases reacted with MSTFA, resulting in the respective *N*-trimethylsilyl derivative of thymine and cytosine.

In Figure 4.5 we present a mechanistic proposal (Brook, 1974) for the above mentioned cleavage of the *N*-glycosidic bond. In the basic medium used for derivatization, deoxyribose and the pyrimidine ring suffered base catalyzed elimination.
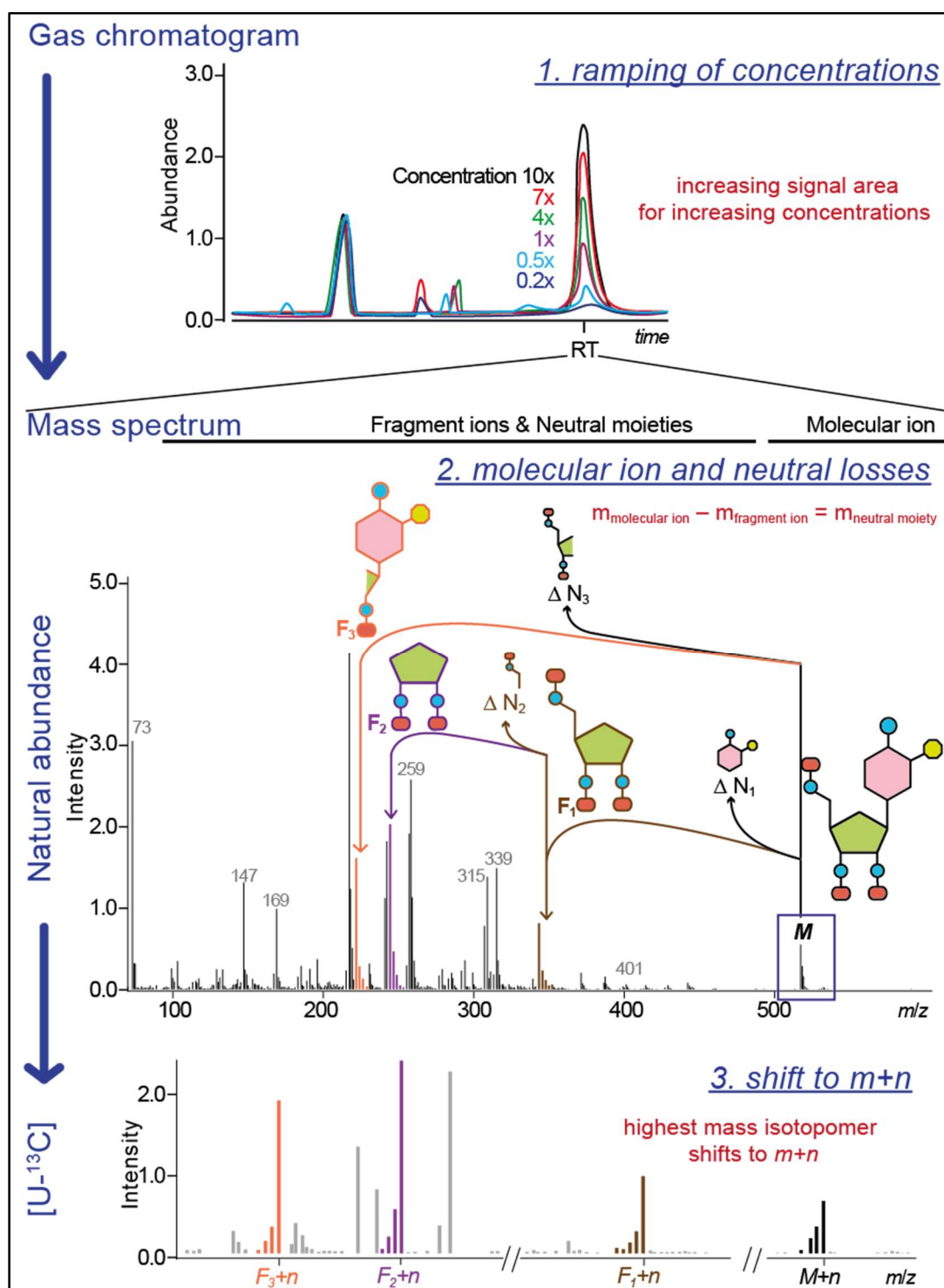
Figure 4.1 – Schematic representation of the GC-MS procedure to identify the derivatives of nucleosides and of deoxynucleosides and to assign the carbon compositions of their fragments. 1 – ramping of concentrations: the RT of each derivative of (deoxy)nucleoside is identified by the increasing chromatographic signal area for increased concentrations of analyte. 2 – molecular ion and neutral losses: spectral assignment of the molecular ion (M) and of the respective fragments (F_i). ΔN_i represents the molecule moieties that are lost because they become neutral upon fragmentation. 3 – shift to $m+n$: verification of the number of fragment's carbon. The number of carbons of the fragment is well assigned if the most abundant m/z corresponds to $m+n$, n the putative number of carbons of the fragment.
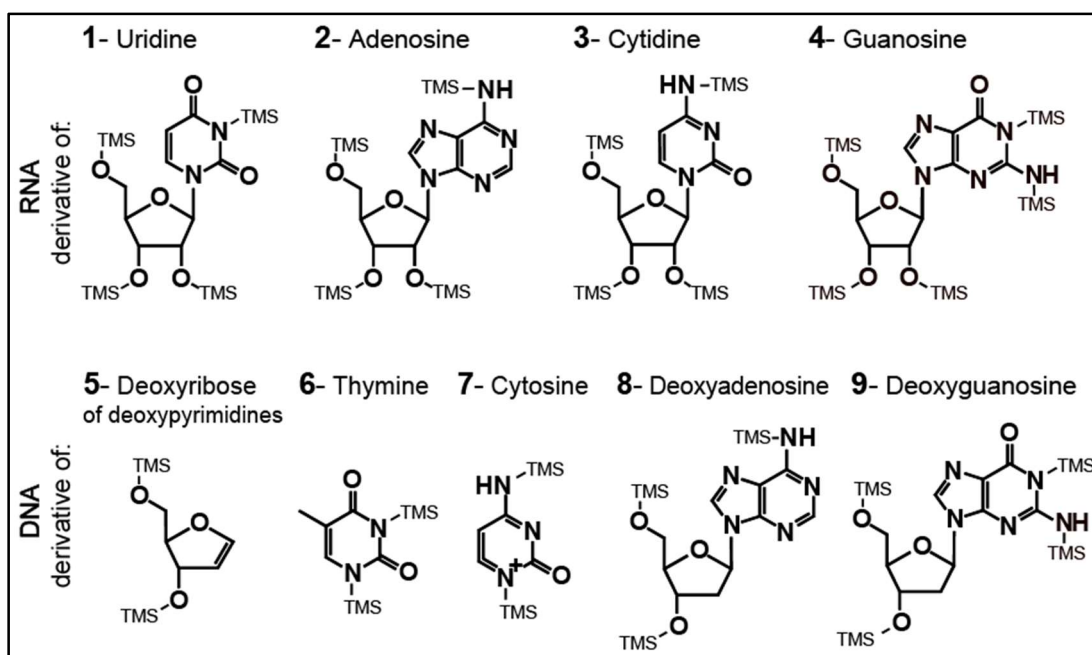
Figure 4.2 – Trimethylsilyl derivatives of nucleosides of RNA (1 – 4) and deoxynucleosides of DNA (5 – 9). 1 – tetrakis-trimethylsilyl derivative of <u>uridine</u>; 2 – tetrakis-trimethylsilyl derivative of <u>adenosine</u>; 3 – tetrakis-trimethylsilyl derivative of <u>cytidine</u>; 4 – pentakis-trimethylsilyl derivative of <u>guanosine</u>; 5 – bis-trimethylsilyl derivative of <u>deoxyribose</u>; 6 – bis-trimethylsilyl derivative of <u>thymine</u>; 7 – bis-trimethylsilyl derivative of <u>cytosine</u>; 8 – tris-trimethylsilyl derivative of <u>deoxyadenosine</u>; 9 – tretrakis-trimethylsilyl derivative of <u>deoxyguanosine</u>. *m/z* of the cationic form (M^+) of the respective structure: $M^+(1) = 532$; $M^+(2) = 531$; $M^+(3) = 555$; $M^+(4) = 644$; $M^+(5) = 270$; $M^+(6) = 260$; $M^+(7) = 254$; $M^+(8) = 467$; $M^+(9) = 555$.

The results are two different trimethylsilylated species in the chromatogram, trimethylsilyl-deoxyribose (5) and trimethylsilylpyrimidines (6) and (7). The molecular ions are observable for all the derivatized products, although at low intensity (Figure 4.3 and 4.4). The fragment resulting from the loss of a methyl group of the trimethylsilyl substituent yields a peak approximately as intense as that of the molecular ion, which, thus, can also be used for the identification of the compound. Table 4.1 presents the RT and respective *m/z* values for the nucleosides and for the deoxynucleosides. We chose to present the RT relative to the compound eluted first (Table 4.1) because the absolute RT is dependent on the current length of the gas chromatographic column.
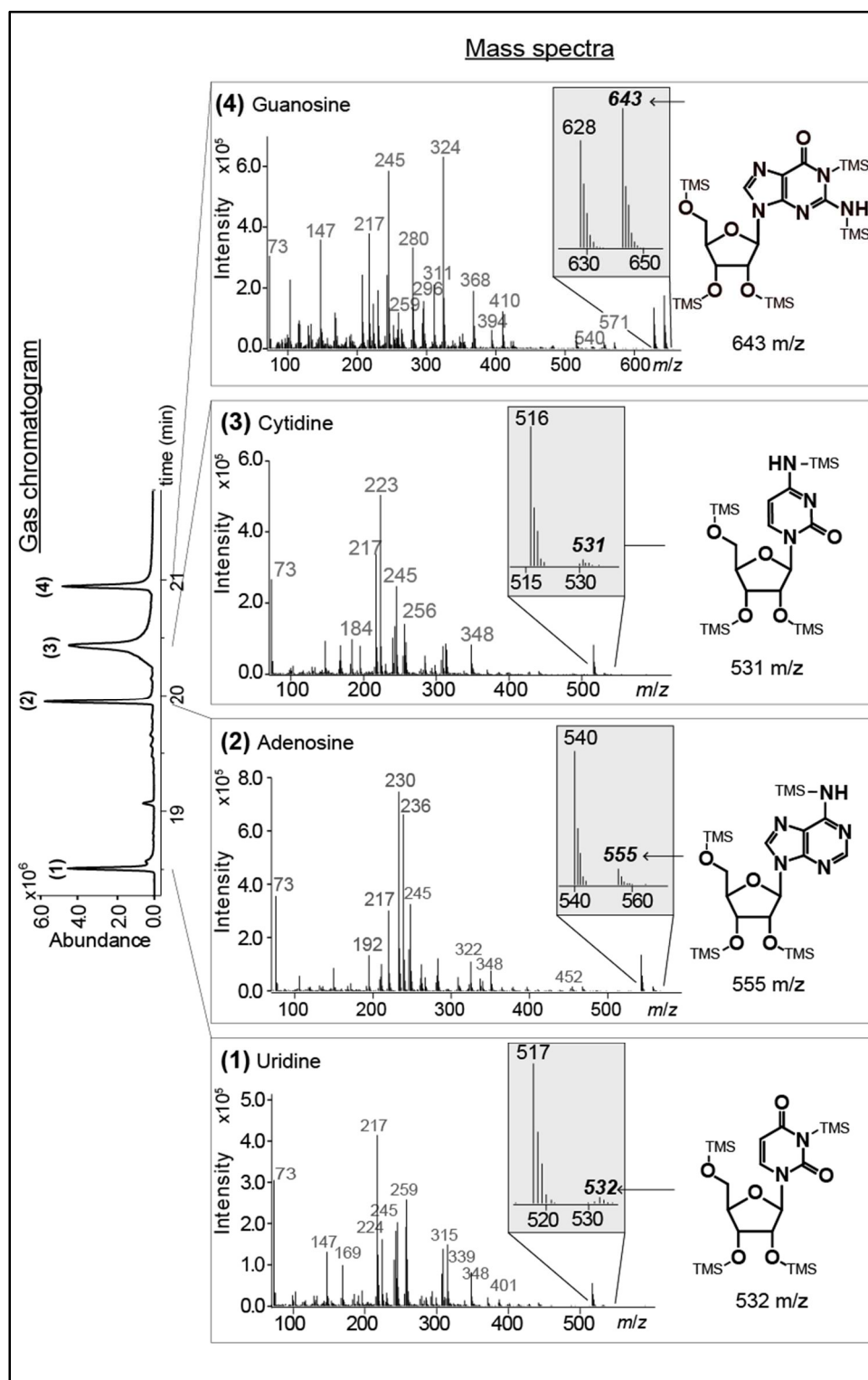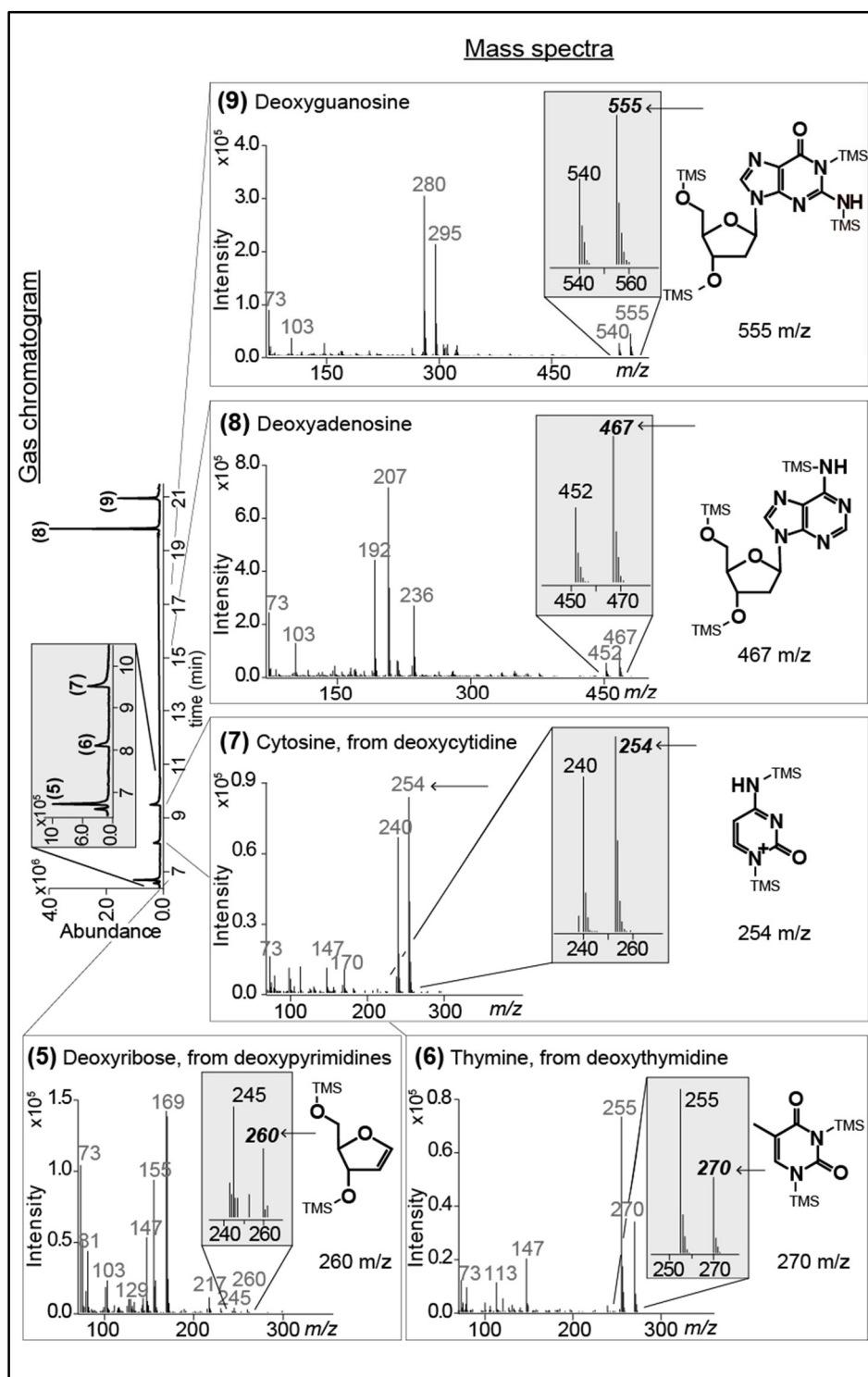
Figure 4.3 – GC-MS chromatogram and spectra at the respective RT of the trimethylsilyl derivatives of nucleosides. The number in between brackets by each chromatographic signal (Gas Chromatogram panel) and by each spectrum panel corresponds to the respective structure presented in there. The solid arrows (→) in Mass Spectra (1) - (4) point out the *m/z* corresponding to the molecular ions of the parent molecules whose structures are presented. Nucleoside-(TMS)$_n$ identified in Gas Chromatogram by (1) - (4) were prepared from standard compounds at the following concentrations: [uridine] = 0.08   mM,   [adenosine] = 0.06   mM,   [cytidine] = 0.36   mM, [guanosine] = 0.08 mM.

Figure 4.4 – GC-MS chromatogram and spectra at the respective RT of the trimethylsilyl derivatives of deoxynucleosides. The number in between brackets by each chromatographic signal (Gas Chromatogram panel and its insert) and by each spectrum panel corresponds to the respective structure presented. The solid arrows (→) in Mass Spectra (5) - (9) point out the *m/z* corresponding to the molecular ions of the parent molecules whose structures are presented. Deoxynucleoside-(TMS)$_n$ identified in Gas Chromatogram by (5) - (9) were prepared from standard compounds at the following concentrations: [Thymidine] = 0.16 mM, [deoxycytidine] = 0.08 mM, [deoxyadenosine] = 0.06 mM, [deoxyguanosine] = 0.06 mM.

Table 4.1 – Relative RT and respective *m/z* of the molecular ions of each compound.

Nucleosides of RNA			deoxynucleosides of DNA		
Compound	Relative RT*	Molecular ion *m/z*	Compound	Relative RT*	Molecular ion *m/z*
1 – tetrakis-trimethylsilyl derivative of **uridine**	1	532	5 – bis-trimethylsilyl derivative of **deoxyribose**	1	250
2 – tetrakis-trimethylsilyl derivative of **adenosine**	1.44	555	6 – bis-trimethylsilyl derivative of **thymine**	1.4	270
3 – tetrakis-trimethylsilyl derivative of **cytidine**	1.94	531	7 – bis-trimethylsilyl derivative of **cytosine**	2.85	254
4 – pentakis-trimethylsilyl derivative of **guanosine**	2.44	643	8 – tris-trimethylsilyl derivative of **deoxyadenosine**	13.13	467
			9 – tretrakis-trimethylsilyl derivative of **deoxyguanosine**	14.28	555

*RT relative to the RT of the compound eluted first.
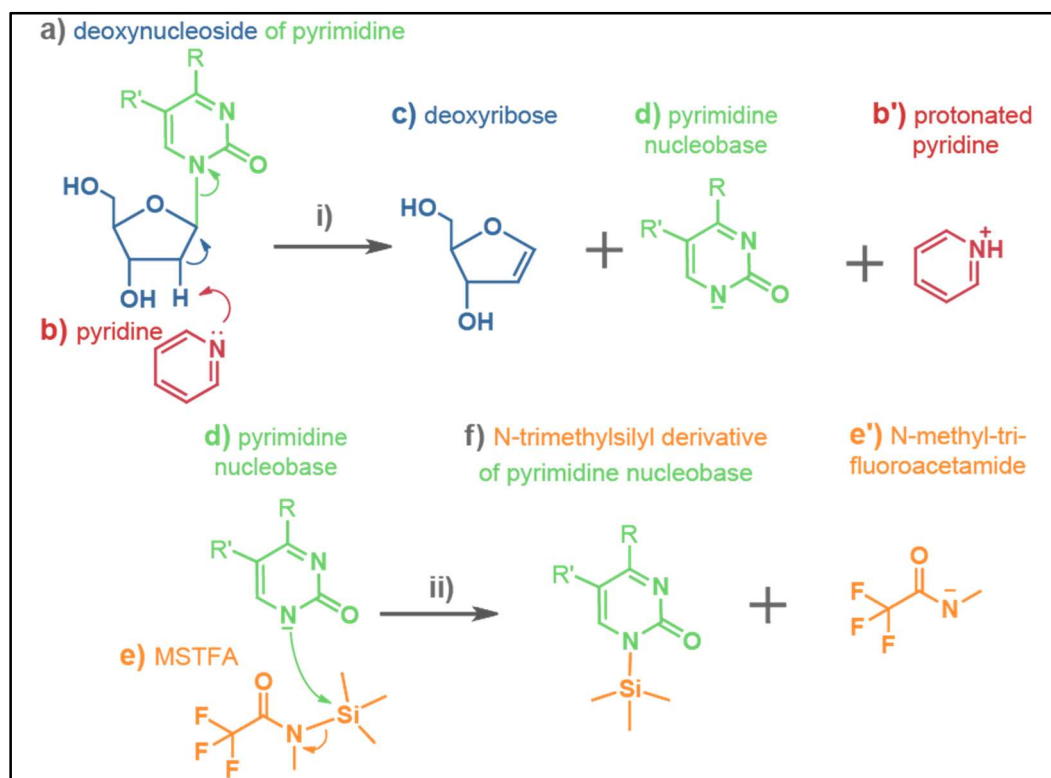
Figure 4.5 – Proposed mechanism for the cleavage of the *N*-glycosidic bond of deoxynucleosides of pyrimidine in the presence of pyridine. a) deoxynucleoside of pyrimidine; b) pyridine, the solvent; c) deoxyribose; d) pyrimidine nucleobase; b') protonated pyridine; e) MSTFA; f) N-trimethylsilyl derivative of pyrimidine nucleobase; e') *N*-methyl-trifluoroacetamide. *R* = OH in thymidine and thymine; NH_2 in deoxycytidine. *R'* = CH3 in thymidine and thymine; H in deoxycytidine.

4.1.2| Tracing of nucleic acids with ^{13}C labeled glucose.

In order to ascertain that the nucleic acid monomers would become enriched by the supplied ^{13}C traced substrate, we grew *S. cerevisiae* CEN.PK113-7D in batch culture fed with [U-^{13}C] glucose. We harvested RNA and DNA at mid-exponential phase of culture growth and digested them into their respective nucleosides and deoxynucleosides. Upon derivatization with MSTFA, RNA and DNA samples were measured in GC-MS in scan mode. The MID of nucleosides, [U-^{13}C] nucleosides, deoxynucleosides and [U-^{13}C] deoxynucleosides are presented in Figure 4.6 and 4.7, respectively.
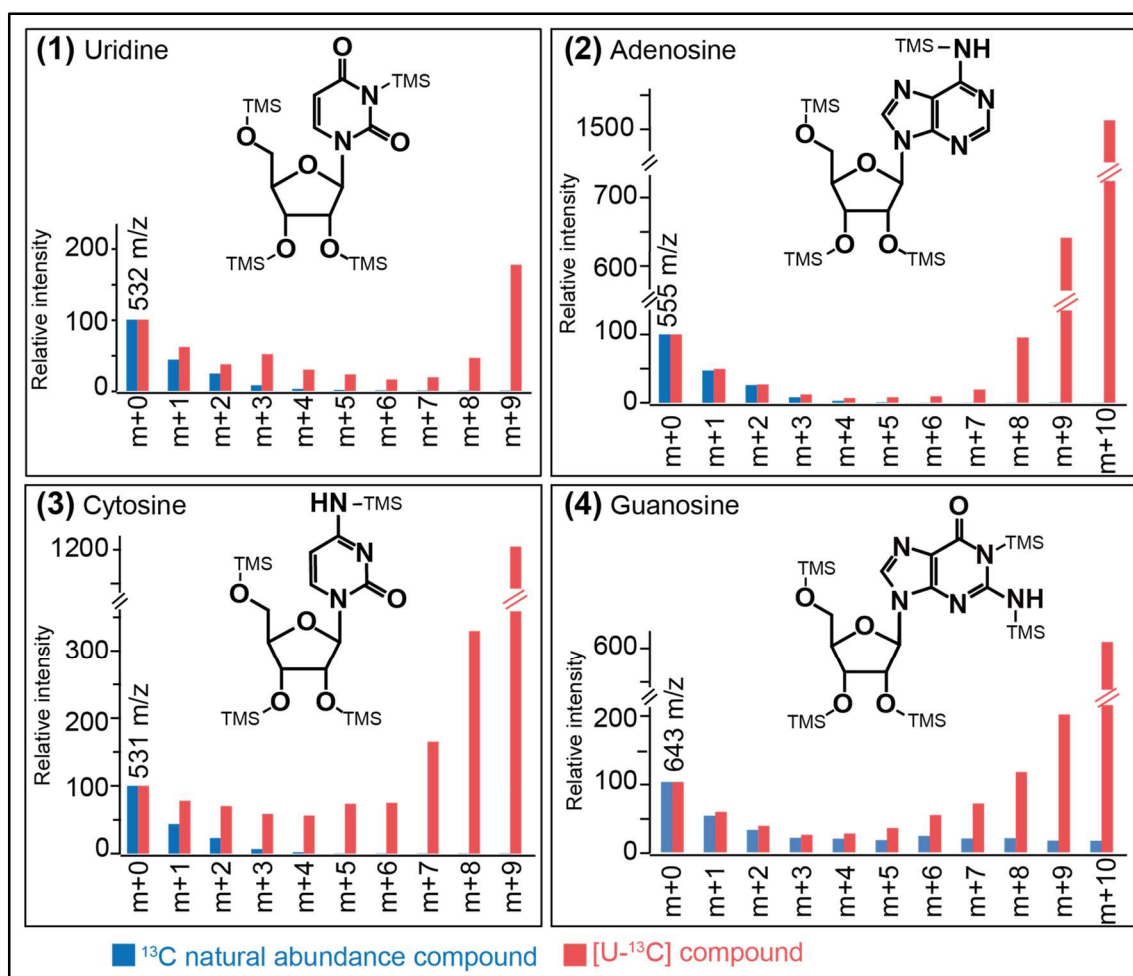
Figure 4.6 – Mass isotopomer relative abundance of the molecular ions of nucleosides. (blue) ^{13}C natural abundance nucleosides; (red) [U-^{13}C] glucose-derived nucleosides. (1) molecular ion of uridine; (2) molecular ion of adenosine; (3) molecular ion of cytosine; (4) molecular ion of guanosine.

Chromatographic abundances below 1×10^6 were not considered for spectral analysis. It was possible to identify the four derivatives of nucleosides and the five derivatives of deoxynucleosides. The most abundant mass isotopomer of every molecular ion was the *(m+n)*, except for the nucleobase derivative of deoxythymidine, meaning that

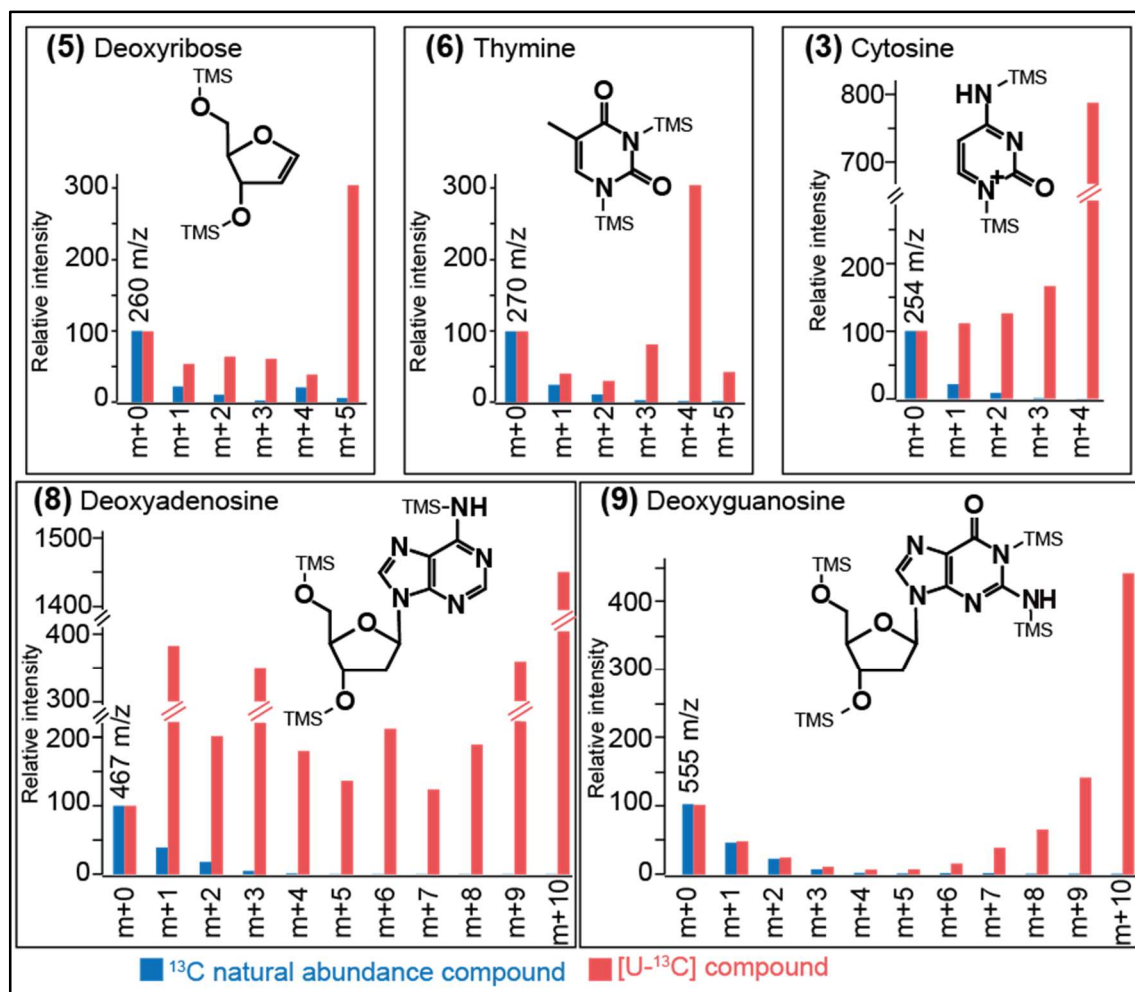the nucleosides and deoxynucleosides became mostly uniformly enriched upon feeding with [U-^{13}C] glucose.

Figure 4.7 – Mass isotopomer relative abundance of the molecular ions of deoxynucleosides. (blue) ^{13}C natural abundance nucleosides; (red) [U-^{13}C] glucose derived nucleosides. (5) molecular ion of deoxyribose moiety from deoxypyrimidines; (6) molecular ion of thymine moiety from deoxythymidine; (7) molecular ion of cytosine moiety from deoxycytidine; (8) molecular ion of deoxyadenosine; (9) molecular ion of deoxyguanosine.

4.1.3| Mass spectra analysis and fragment assignment.

To assign carbon composition of fragments, three criteria were used: (i) matching of the *m/z* of fragment ions to plausible structures (neutral loses), (ii) mismatch between the experimental and the theoretical natural isotopic distribution of each proposed fragment ion, and (iii) shifting to (*m+n*)/*z* (*n* equals the number of carbons) of the most intense mass isotopomer of the fragment ions in [U-^{13}C] nucleosides and [U-^{13}C] deoxynucleosides. The spectra at the corresponding RT of each compound were analyzed in detail, seeking for ions that could result from fragmentation of the molecular ion. The complete spectra of the derivatized nucleosides and deoxynucleosides are

presented in the *Mass spectrum* panels (top most panel) of Figures 4.8 to 4.12 and 4.13 to 4.14, respectively.
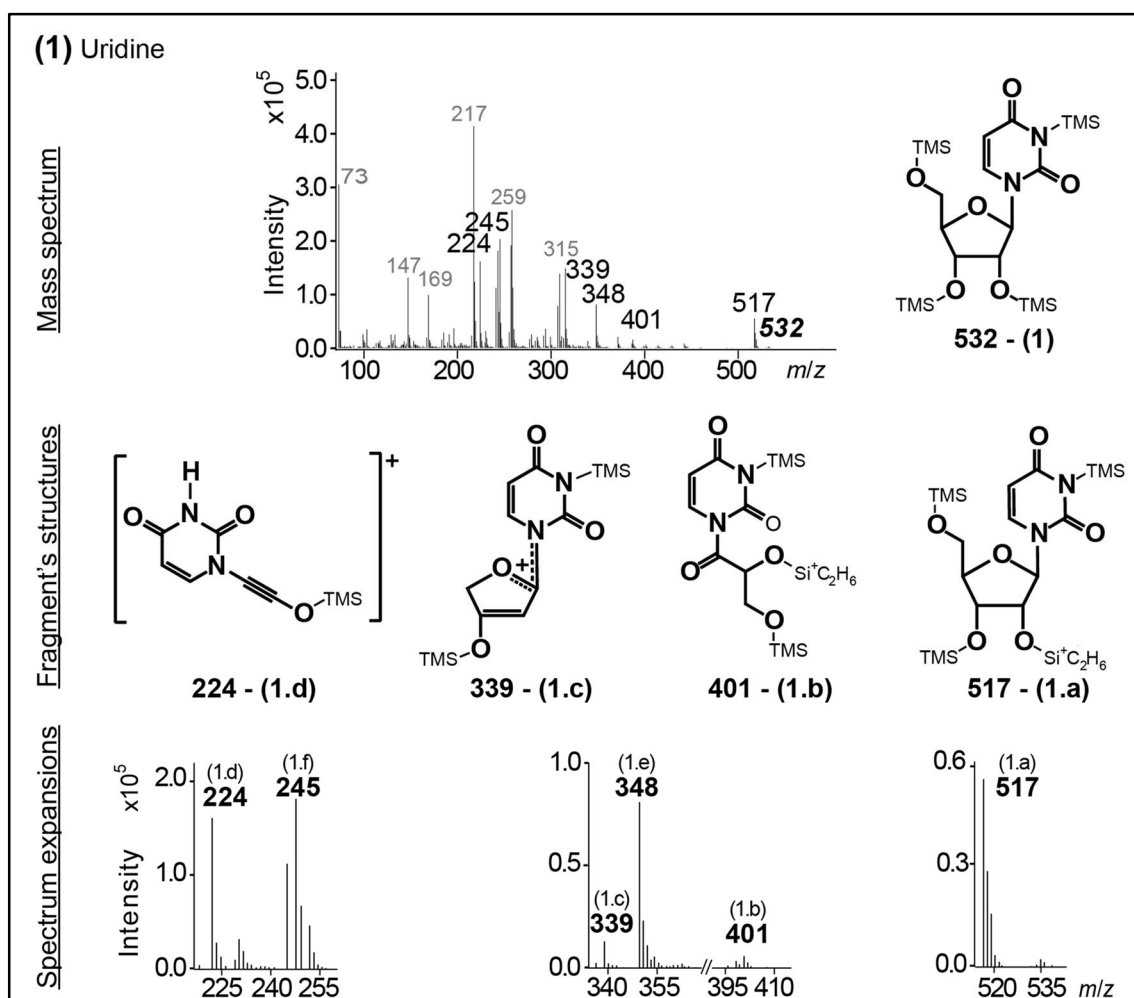

Figure 4.8 – Fragments of Uridine, naturally labelled standard compound. Mass spectrum at the RT correspondent to the trimethylsilyl uridine derivative, which structure (1) is presented to the right of the spectrum. The *m/z* values in black note the assigned fragments generated from the molecular ion of the trimethylsilyl uridine derivative; the corresponding fragment's structures ((1.a) - (1.d)) are depicted below the spectrum; the structures of fragments 348 and 245 *m/z* are common to derivative of all nucleosides and are presented in Figure 4.12; spectrum expansions at the regions of the assigned fragments are shown in the bottom of this figure.
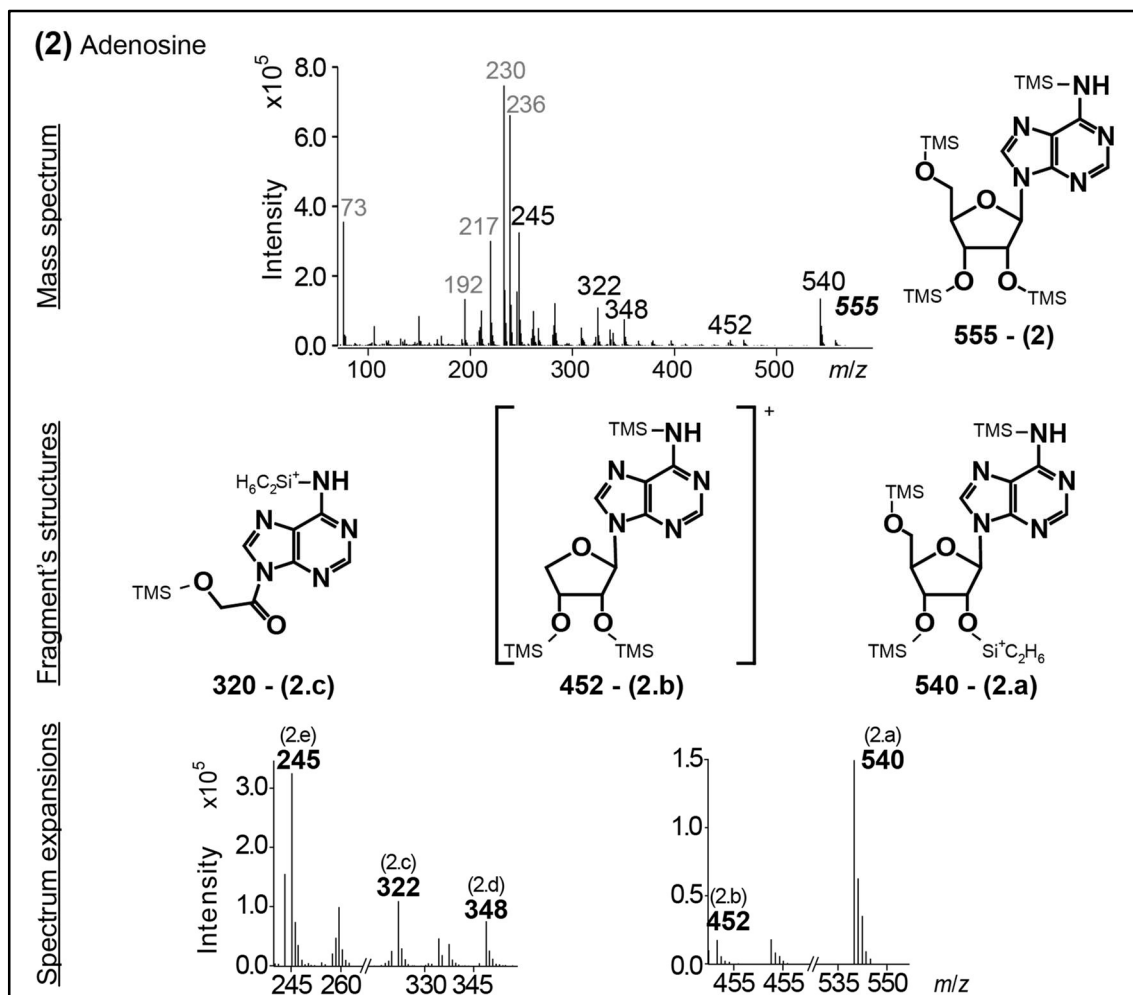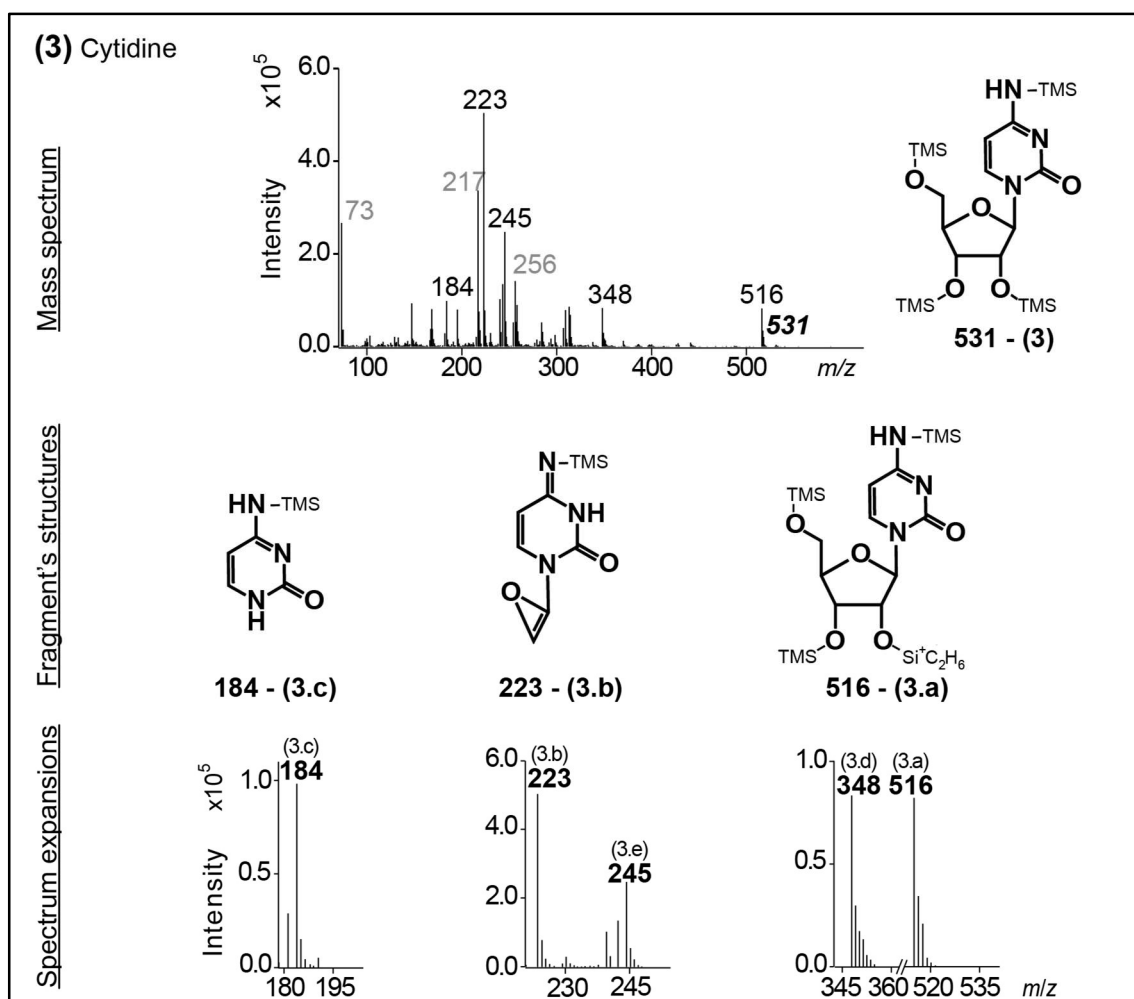
Figure 4.9 – Fragments of Adenosine, naturally labelled standard compound. Mass spectrum at the RT correspondent to the trimethylsilyl adenosine derivative, which structure (2) is presented to the right of the spectrum. The *m/z* values in black note the assigned fragments generated from the molecular ion of the trimethylsilyl adenosine derivative; the corresponding fragment's structures ((2.a) - (2.c)) are depicted below the spectrum; the structures of fragments 348 and 245 *m/z* are common to derivative of all nucleosides and are presented in Figure 4.12; spectrum expansions at the regions of the assigned fragments are shown in the bottom of this figure.

Figure 4.10 – Fragments of cytidine, naturally labelled standard compound. Mass spectrum at the RT correspondent to the trimethylsilyl cytidine derivative, which structure (3) is presented to the right of the spectrum. The *m/z* values in black note the assigned fragments generated from the molecular ion of the trimethylsilyl cytidine derivative; the corresponding fragment's structures ((3.a) - (3.c)) are depicted below the spectrum; the structures of fragments 348 and 245 *m/z* are common to derivative of all nucleosides and are presented in Figure 4.12; spectrum expansions at the regions of the assigned fragments are shown in the bottom of this figure.

Following the classical rules of fragmentation, we calculated the neutral loss (Figure 4.1, central panel) which is the mass difference between the molecular ion and every plausible fragment ion ($m_{molecular\ ion} - m_{fragment\ ion} = m_{neutral\ moiety}$).

We began with 102 plausible fragments. Knowing that, under the conditions applied, fragment ions carry only one charge allowed us to exclude 28 out of the 102 plausible fragment ions that did not fulfill this difference between $m_{molecular\ ion}$ and $m_{fragment\ ion}$.
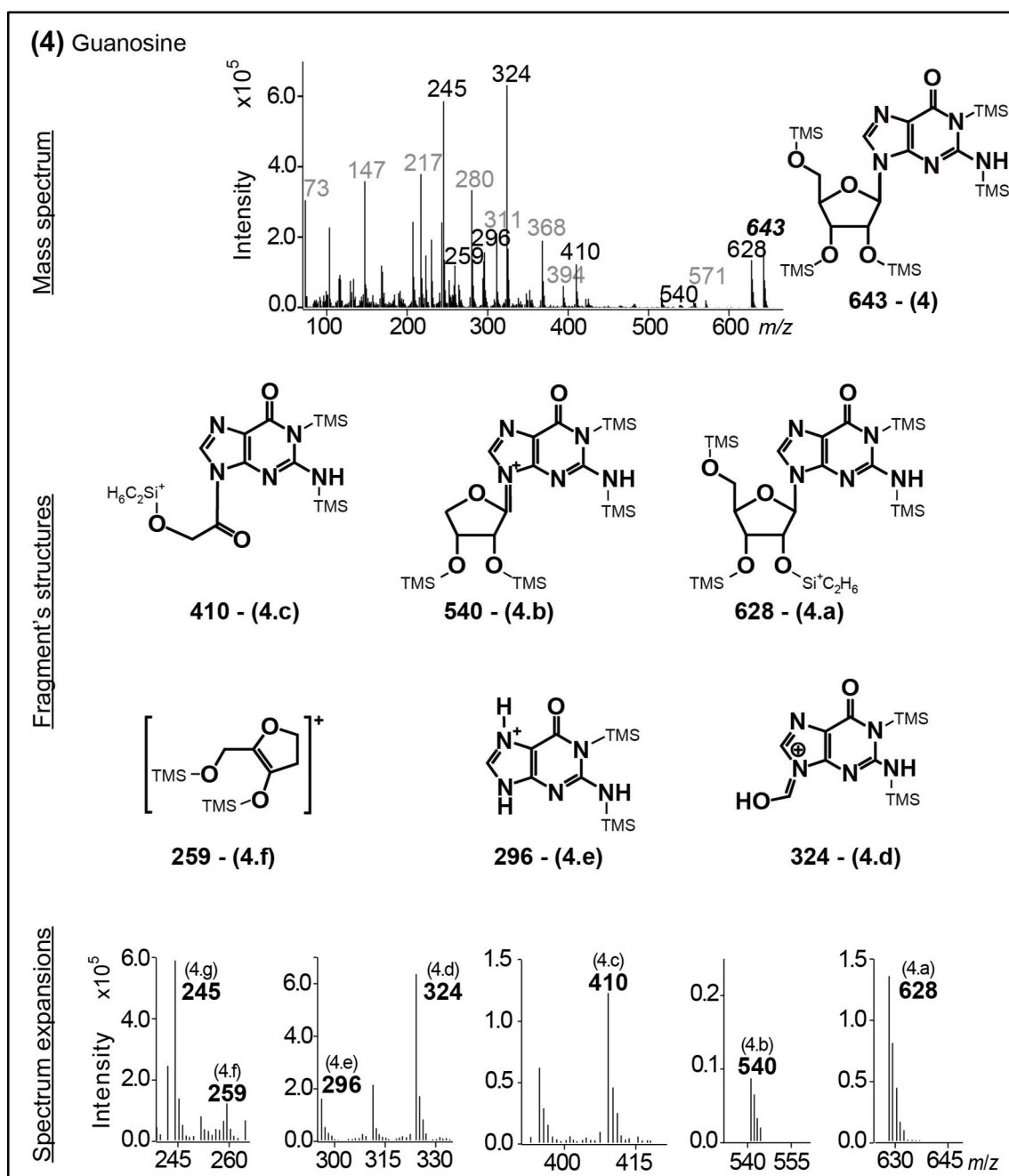
Figure 4.11 – Fragments of Guanosine, naturally labelled standard compound. Mass spectrum at the RT correspondent to the trimethylsilyl guanosine derivative, which structure (4) is presented to the right of the spectrum. The *m/z* values in black note the assigned fragments generated from the molecular ion of the trimethylsilyl guanosine derivative; the corresponding fragment's structures ((4.a) - (4.f)) are depicted below the spectrum; the structures of fragments 348 and 245 *m/z* are common to derivative of all nucleosides and are presented in Figure 4.12; spectrum expansions at the regions of the assigned fragments are shown in the bottom of this figure.

In the second criterion we intended to verify the molecular formula of the plausible fragment ions that passed the first criterion. SIM mode measurement of the remaining 74 selected fragment ions allowed the assessment of the mismatch between their experimentally measured isotopic distribution and the known (calculated) natural

one of such ion formula (Table 4.2). A mismatch larger than 15% led to exclusion (Lai, Kind and Fiehn, 2017) of further 37 fragments.
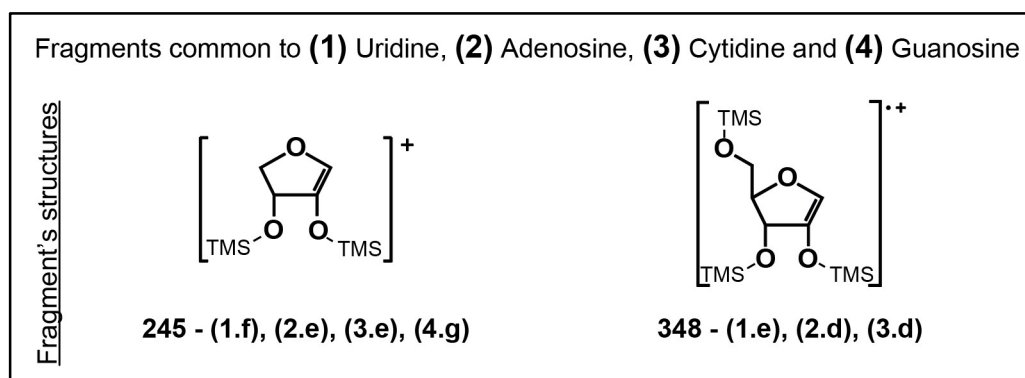

Figure 4.12 – Fragments common to uridine, adenosine, cytidine and guanosine. Structures and respective *m/z* of the fragments ((1.e), (2.d), (3.d) and (1.f), (2.e), (3.e), (4.g)) of the trimethylsilyl uridine, adenosine, cytidine and guanosine derivatives.

For the third criterion, we used [U-^{13}C] nucleosides and [U-^{13}C] deoxynucleosides to assess the number of carbons in the predicted fragments (Figure 4.1, bottom panel). [U-^{13}C] nucleosides and [U-^{13}C] deoxynucleosides had been obtained from RNA and DNA, respectively, after cultivation of yeast on [U-^{13}C] glucose, from the experiment of tracing nucleic acids with ^{13}C. These samples were measured in SIM mode for the mass isotopomers of the 37 ions that had passed the second criterion. The ions selectively measured in SIM mode corresponded to the mass isotopomers from *(m+0)* to *(m+n)* (where n is the total number of carbons in the carbon backbone of the molecular ion) for every molecular ion of derivatized nucleosides and deoxynucleosides. The fragments whose *m/z* of the most intense mass isotopomer did not shift to $(m+n)/z$ (where n is the total number of carbons in the carbon backbone of the fragment) were discarded. The fragments that, in addition to $(m+n)/z$, presented also a high intensity mass isotopomer $(m+x)/z$ (where x is any number of carbons in the carbon backbone), were also discarded because they may be two different fragment ions with the same mass but different total number of carbons of the backbone. The proposed structures and the respective detailed spectra of the 30 fragments that passed the three above-mentioned criteria are shown in *Fragment's structures* and *Spectrum expansions* panels of Figures 4.8 to 4.12 for nucleosides and 4.13 to 4.14 for deoxynucleosides.
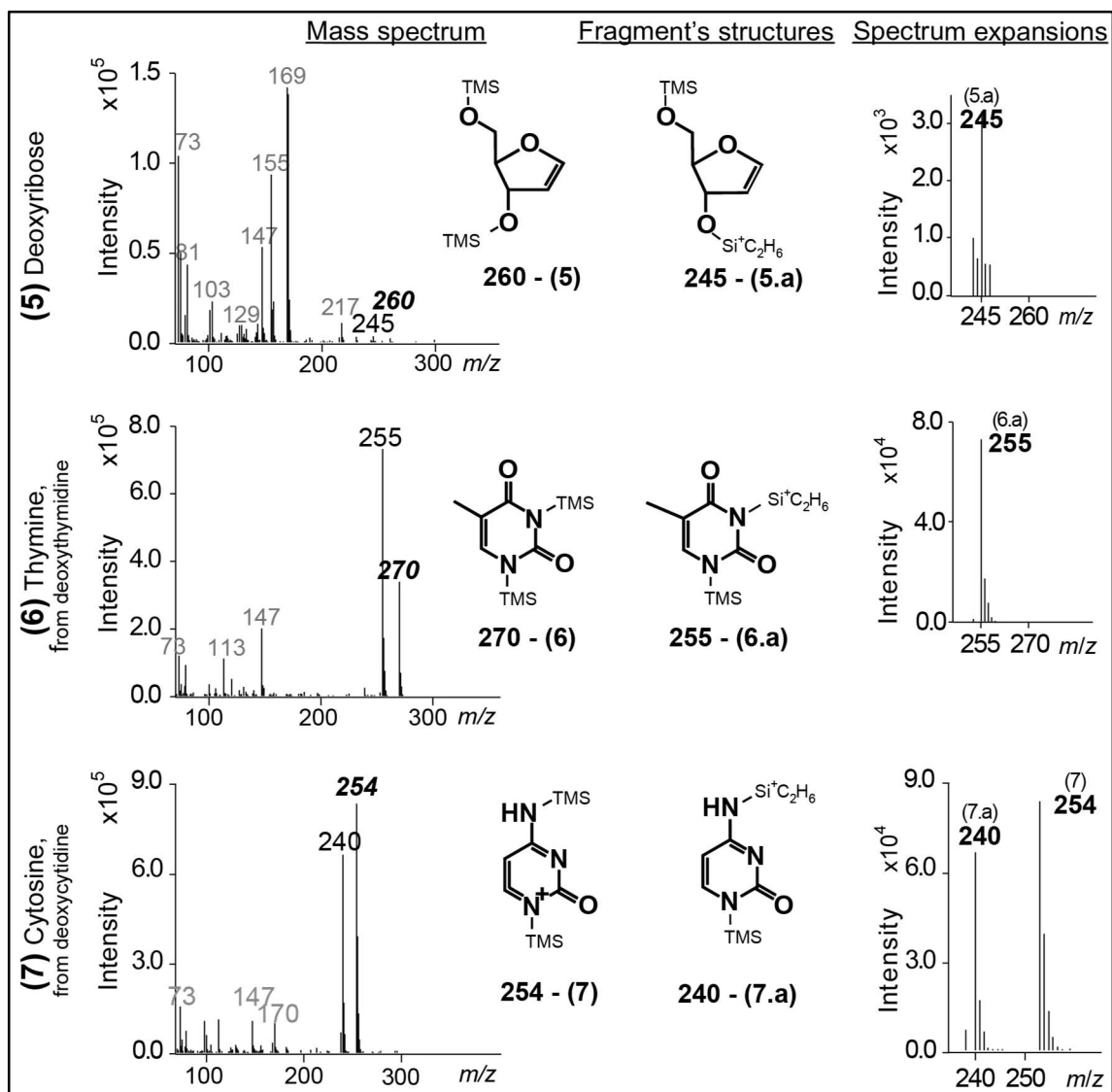
Figure 4.13 – Fragments of deoxypyrimidines, naturally labelled standard compound. Mass spectrum at the RT correspondent to the trimethylsilyl derivatives of deoxycytidine and deoxythymidine, which structures (5) - (7) are presented to the right of the spectrum. The *m/z* values in black note the assigned fragments generated from the molecular ion of the trimethylsilyl derivatives of deoxypyrimidines; spectrum expansions at the regions of the assigned fragments are shown at the right side of this figure and the corresponding fragment's structures ((5.a) - (7.a)) are depicted by the expansion of spectra.
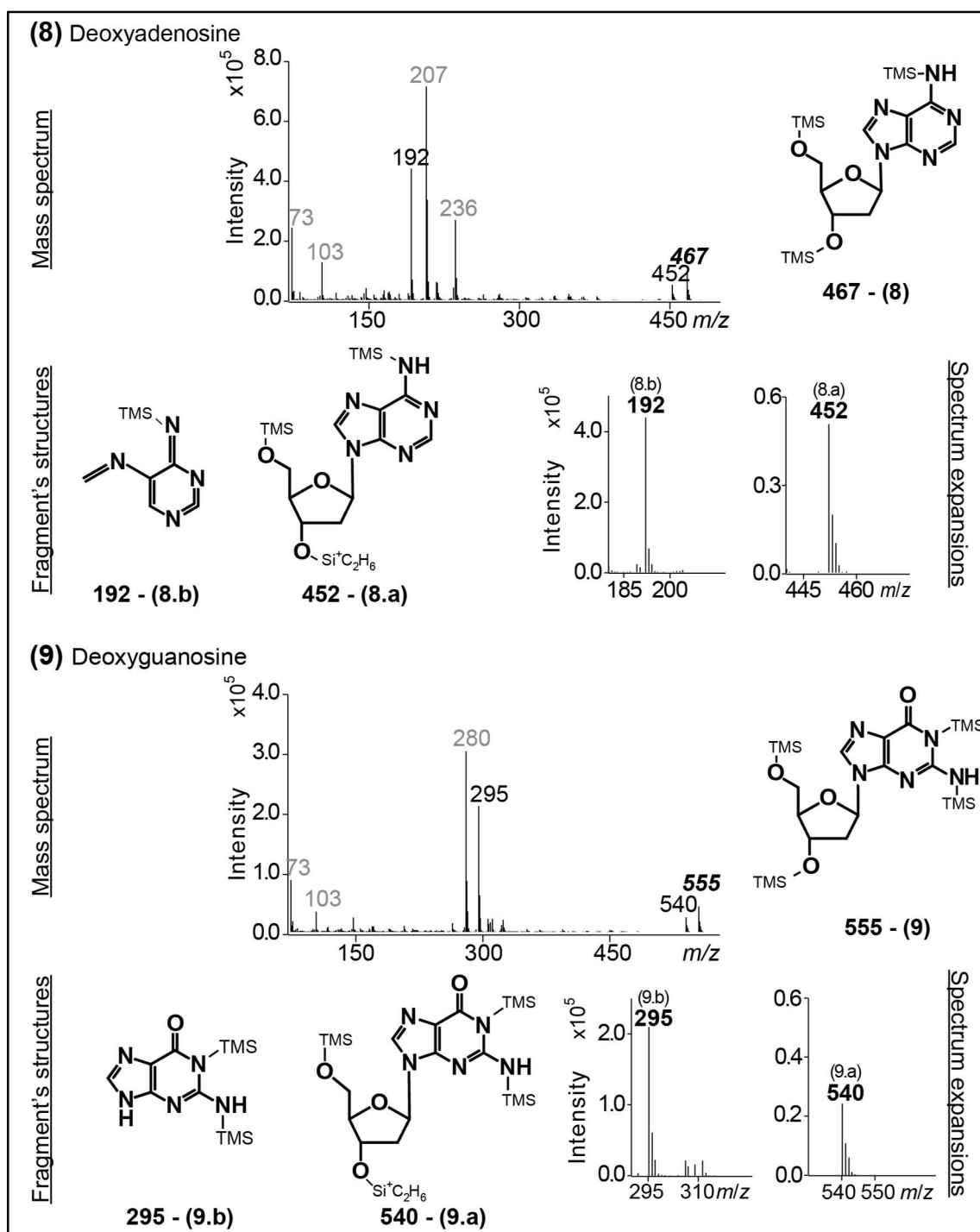
Figure 4.14 – Fragments of deoxypurines, naturally labelled standard compound. Mass spectrum at the RT correspondent to the trimethylsilyl derivatives of deoxyadenosine and deoxyguanosine, which structures (8) - (9) are presented to the right of the spectrum. The *m/z* values in black note the assigned fragments generated from the molecular ion of the trimethylsilyl derivatives of deoxypyrimidines; spectrum expansions at the regions of the assigned fragments are shown at the right side of this figure and the corresponding fragment's structures ((8.a) - (9.b)) are depicted by the expansion of spectra.

Table 4.2 - Mass isotopomer ratios of the identified fragments of the natural abundant trimethylsilyl derivatives of nucleosides and deoxynucleosides. exp: experimental; calc: calculated.

Fragment ions		Mass isotopomers			Fragment ions		Mass isotopomers		
		I M+1/M	I M+2/M	I M+3/M			I M+1/M	I M+2/M	I M+3/M
(1) Uridine					**(4) Guanosine**				
(1.a)	exp	0.438	0.242	0.076	**(4.a)**	exp	0.523	0.319	0.207
	calc	*0.439*	*0.236*	*0.069*		*calc*	*0.472*	*0.249*	*0.076*
(1.b)	exp	0.359	0.183	0.056	**(4.b)**	exp	0.433	0.218	0.065
	calc	*0.331*	*0.161*	*0.036*		*calc*	*0.460*	*0.242*	*0.072*
(1.c)	exp	0.277	0.228	0.080	**(4.c)**	exp	0.355	0.160	0.037
	calc	*0.268*	*0.108*	*0.019*		*calc*	*0.341*	*0.160*	*0.036*
(1.d)	exp	0.171	0.053	0.016	**(4.d)**	exp	0.252	0.098	0.020
	calc	*0.161*	*0.051*	*--*		*calc*	*0.256*	*0.101*	*0.017*
(1.e)	exp	0.326	0.161	0.048	**(4.e)**	exp	0.268	0.106	0.022
	calc	*0.312*	*0.153*	*0.033*		*calc*	*0.245*	*0.096*	*0.015*
(1.f)	exp	0.205	0.086	0.014	**(4.f)**	exp	0.259	0.110	0.062
	calc	*0.216*	*0.093*	*0.013*		*calc*	*0.227*	*0.096*	*0.015*
					(4.g)	exp	0.223	0.101	0.024
						calc	*0.216*	*0.093*	*0.013*
(2) Adenosine					**(5) deoxyribose**				
(2.a)	exp	0.473	0.259	0.081	**(5.a)**	exp	0.219	0.106	0.024
	calc	*0.460*	*0.242*	*0.072*		*calc*	*0.216*	*0.093*	*0.013*
(2.b)	exp	0.349	0.159	0.050	**(6) Thymine**				
	calc	*0.375*	*0.172*	*0.042*	**(6.a)**	exp	0.220	0.092	0.018
(2.c)	exp	0.259	0.095	0.027		*calc*	*0.223*	*0.093*	*0.014*
	calc	*0.256*	*0.101*	*0.017*					
(2.d)	exp	0.304	0.157	0.043	**(7) Cytosine**				
	calc	*0.312*	*0.153*	*0.033*	**(7.a)**	exp	0.213	0.088	0.013
(2.e)	exp	0.211	0.092	0.023		*calc*	*0.222*	*0.091*	*0.013*
	calc	*0.216*	*0.093*	*0.013*					
(3) cytidine					**(8) deoxyadenosine**				
(3.a)	exp	0.436	0.230	0.067	**(8.a)**	exp	0.392	0.180	0.047
	calc	*0.442*	*0.236*	*0.069*		*calc*	*0.387*	*0.177*	*0.044*
(3.b)	exp	0.169	0.051	0.013	**(8.b)**	exp	0.157	0.473	--
	calc	*0.164*	*0.049*	*0.000*		*calc*	*0.156*	*0.044*	*--*
(3.c)	exp	0.154	0.051	0.016	**(9) deoxyguanosine**				
	calc	*0.141*	*0.044*	*--*	**(9.a)**	exp	0.452	0.224	0.072
(3.d)	exp	0.314	0.158	0.143		*calc*	*0.472*	*0.247*	*0.075*
	calc	*0.312*	*0.153*	*0.033*	**(9.b)**	exp	0.2447	0.096	0.015
(3.e)	exp	0.213	0.092	0.015		*calc*	*0.2561*	*0.093*	*0.017*
	calc	*0.216*	*0.093*	*0.013*					

Altogether, of the 30 assigned fragments, 12 present distinct carbon composition. In Figure 4.15 are shown the 12 distinct fragments and those from nucleosides and deoxynucleosides that are equivalent.
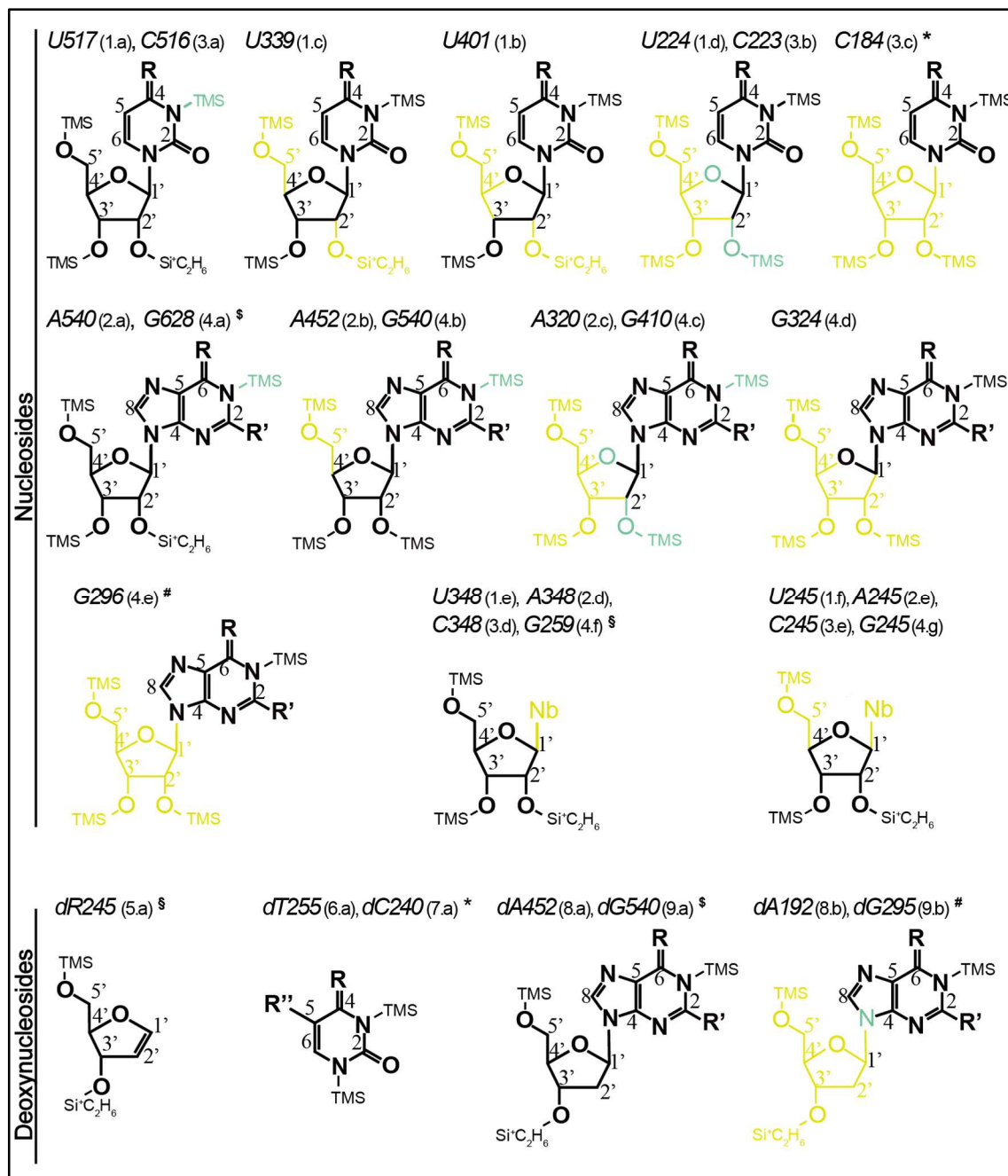

Figure 4.15 – Fragments presenting distinct carbon composition. R = O in thymidine, uracil and ; NH_2 in deoxycytidine. R' = H in deoxy adenosine; NH2 in deoxyguanosine; R'' = H in cytidine; CH3 in thymidine. Fragments from nucleosides and deoxynucleosides and having the same C composition are noted with *, §, $, and #. R – O or NH. R' – NH_2 or H. R'' – H or CH3. Nb – nucleobase or pyrimidine or purine. NH groups are usually derivatized.

4.2| QUALITATIVE ANALYSIS OF THE METABOLIC PHENOTYPE IN S-PHASE

The metabolic phenotype of S-phase was investigated by qualitative analysis of the MID of fragments and of the respective ^{13}C positional isotopomers of deoxynucleosides obtained from nDNA. Furthermore, the comparison of these MID with those of nucleosides obtained from RNA allows us to inspect differences between the metabolic phenotype of S-phase and the average of the metabolic states over the entire CDC. The isotopic distribution of the deoxynucleosides and nucleosides gets imprinted from that of their precursors, which, in turn, reflects the corresponding MFD at the moment of their biosynthesis. DNA replication is confined to the S-phase of CDC whereas RNA biosynthesis occurs at the other phases, predominantly during G1 and G2 (ref). The respectively required deoxynucleosides and nucleosides are biosynthesized prior to their immediate demand for nucleic acid biosynthesis (Cohen *et al.*, 1983). Thus, deoxynucleosides are biosynthesized at the onset and during S-phase whereas nucleosides are biosynthesized mostly in G1 and G2 phases of CDC.

Given the reported metabolic heterogeneity along the phases of CDC, we anticipate the ^{13}C tracer distribution in deoxynucleosides of nDNA to be different from that of nucleosides of cRNA (Figure 4.16).
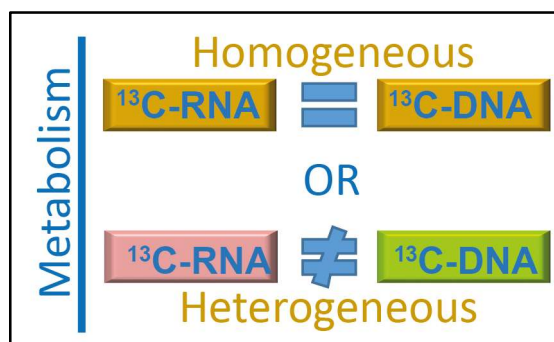

Figure 4.16 – Schematic representation of the qualitative analysis of metabolic phenotype heterogeneity over CDC. If the ^{13}C isotopic distribution of deoxynucleosides from DNA equals that of RNA, then metabolic phenotype is the same over CDC. If the ^{13}C isotopic distribution of deoxynucleosides from DNA differs from that of RNA, then the metabolic phenotype of S-phase differs from that of the other phase.

4.2.1| Extraction and digestion of cellular DNA and RNA

We grew *S. cerevisiae* in continuous culture fed with [1,2-^{13}C] glucose 5 mM and subjected to a flow rate of 0.1 h^{-1}. Cells of *S. cerevisiae* were cultivated as described in the chapter 2.2.2 and ice-cold harvested from the outlet. We isolated cRNA, nDNA, mtRNA and mtDNA separately and promoted their digestion to the respective nucleosides. For all extractions of both RNA and DNA, the A$_{260/280}$ ratios were in the

range of 1.8 - 2.0 and the $A_{260/230}$ ratios ranged between 2.0 - 2.3, indicating a high degree of nucleic acid purity. On average, we obtained 180 µg of cRNA per extraction of 100×10^6 cells, which represents approximately 4.5% of the biomass. On average, we extracted 130 µg of nDNA per extraction of 7×10^9 cells, corresponding to 0.075% of the biomass. The digestion, performed as described in 2.3.5 yielded above 50%, resulting in a minimum of 50 nmol of each nucleoside and of each deoxynucleoside per digestion. Nucleosides and deoxynucleosides were derivatized 2.3.6 and measured in GC-MS in scan and SIM mode 2.4.1. Mass spectral analysis of the fragments measured in the SIM mode was performed as described in Methods 2.4.2. The contributions of the natural isotopic abundance of all atoms other than those belonging to the carbon backbones of interest were subtracted (van Winden *et al.*, 2002). The mass isotopomer abundances, $r\ (m+n_i)$, presented are relative to the total abundance of all mass isotopomers of each molecular ion and fragment, equation (4.1), where m is the m/z of the molecular ion or fragment, n is the number of carbon atoms belonging to the carbon backbone.

$$r\ (m + n_i) = \frac{m + n_i}{\sum_{i=0}^{n}(m + n_i)} \quad (4.1)$$

Analysis of MID of the measured fragments was performed in order to infer positional isotopomers of the parent ions. From now on, fragments of (deoxy)nucleosides will be identified by the initials of the nucleoside followed by the m/z value of the respective fragment, e. g., uridine derivative fragment of m/z equal to 224 m/z: *U224*; in order to mention mass isotopomers, we will refer to $m+n$, where n is the number of ^{13}C isotopes in the fragment, *e. g.,* by *U224 m+3* we mean the mass isotopomer 227 m/z of *U224*. In the elucidation of the positional isotopomers, we will mean: *1C_Nb*, one labeled but unidentified carbon in the nucleobase; *2C_Nb*, two labeled but unidentified carbons in the nucleobase; *3C_Nb*, three labeled but unidentified carbons in the nucleobase; *C?*, labeled carbon either in nucleobase or ribose moiety; *C?'*, labeled but unidentified carbon in the ribose moiety.

4.2.2| Qualitative analysis of ^{13}C isotopomers of nucleosides of nDNA and cRNA.

We measured the following fragments of nucleoside derivatives in SIM mode: uridine derivative, 517 m/z, 401 m/z, 348 m/z, 339 m/z, 245 m/z and 224m/z; adenosine derivative, 541 m/z, 453 m/z, 348 m/z, 323 m/z and 245 m/z; cytidine derivative, 516 m/z, 348 m/z, 245 m/z, 223 m/z and 184 m/z; guanosine derivative, 643 m/z, 410 m/z, 324 m/z, 296 m/z, 259 m/z and 245 m/z. Not all the fragment ions of adenosine and guanosine derivatives were detected in the spectra and those that could be observed presented signal intensities three times below the noise. The signal intensities of uridine and cytidine derivatives, though above three times the noise, were also below what had been obtained in previous experiments. This was due to the unexpected low yield obtained in nucleic

acid digestion (nucleosides were quantified by HPLC, data not shown). The low yield of nucleosides is likely due to an enzymatic activity lower than before, given that we followed the previously optimized digestion protocol (Miranda-Santos *et al.*, 2015).

4.2.2.1| ^{13}C isotopomers of nucleosides of cRNA

The assigned fragments of uridine derivative are composed of the ribose moiety *U348* and its fragment *U245,* and of the nucleobase plus some ribose's carbons, *U401*, *U339 and U224*. The analysis of their mass isotopomers elucidates whether the labeling is predominantly in nucleobase or in ribose and within ribose in C1'- C2', C1'- C3', C4' or C5'. Inspecting the MID of the fragments of the uridine derivative (Figure 4.17), we highlight the following:

i) The fragments composed of nucleobase and ribose moieties – namely *U517*, *U401*, *U339* and *U224* – are considerably enriched in multi-labeled isotopomers. This multi-labelling is mainly contributed by the nucleobase moiety. This is inferred from the observation that fragments composed only of ribose moiety, namely *U348* and *U245,* are predominantly labeled in one carbon (m+1) or non-labeled (m+0).
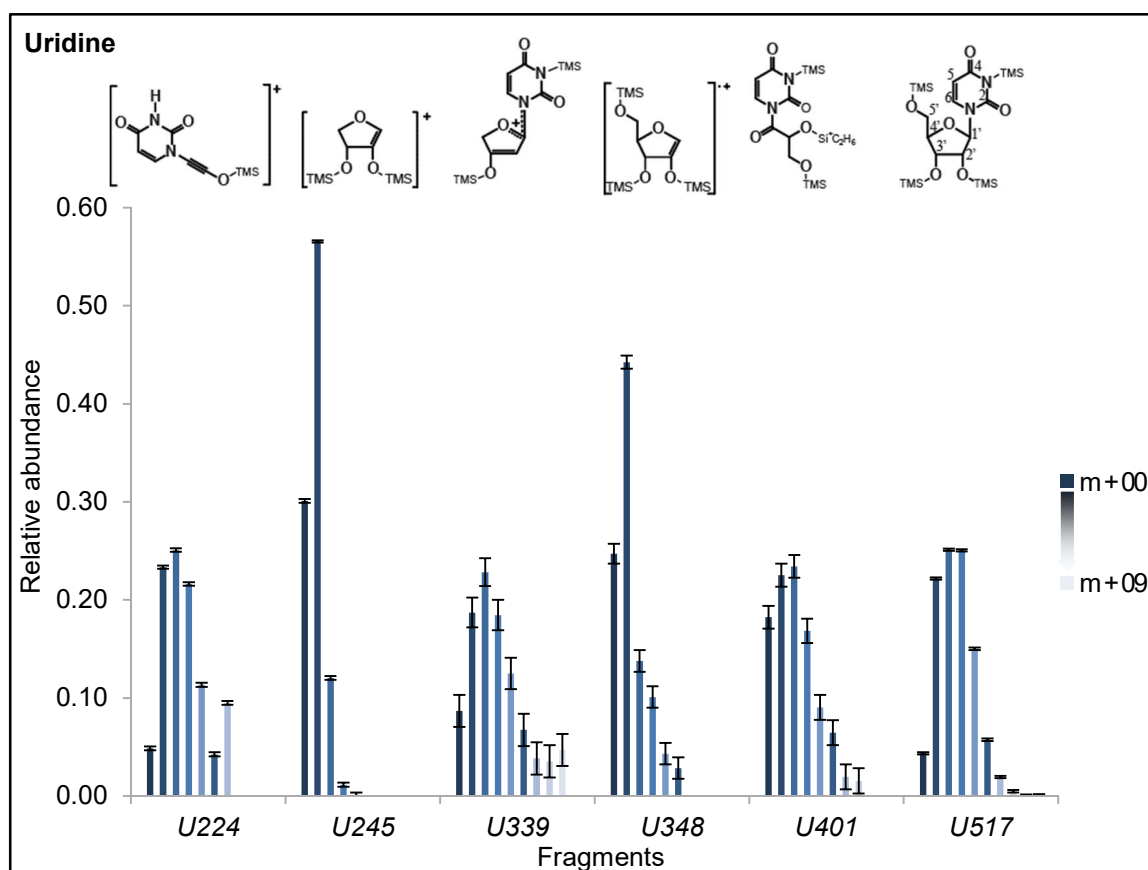

Figure 4.17 – MID of fragments of uridine derivative.

ii) The comparison of the labelling of *U348* with that of *U245* indicates that C5', carbon 5 of ribose ring, is labeled. Because the difference between *U348* and *U245* is the loss of C5', when missing ^{13}C5' the MID will exhibit a lower abundance of multi-labeled mass isotopomers. Indeed, the relative abundance of *U245 m+0* is higher than that of *U348 m+0*, which indicates that when losing C5' the mass isotopomer *U348 m+1* becomes *U245 m+0*. This observation suggests that *U348 m+1* is composed of the isotopomer [C5'-^{13}C] U348, which corresponds to [U-^{12}C] U245, thus *U245 m+0*. C5' is also one of the two labeled carbons in some of the mass isotopomers *U348 m+2* because *U245 m+1* is more abundant than *U348 m+1*, suggesting that *U348 m+2* is composed of [C?',C5'-^{13}C] U348 and corresponds to [C?'-^{13}C] U245, thus *U245 m+1*. Lastly, C5' is one of the 3 labeled carbons in *U348 m+3* because *U245 m+3* is negligible and *U245 m+2* is as abundant as *U348 m+3*, suggesting that [C?',C?',C5'-^{13}C] U348 gives rise to *U348 m+3* and corresponds to [C?',C?'-^{13}C] U245.

iii) C3' is the carbon missing in *U224* comparing to *U401*. The analysis of the MID of these two fragments reveals that C3' is one of the two, three or four labeled carbons of the mass isotopomers *U401 m+2, m+3* and *m+4*, respectively, because *U224 m+1, m+2* and *m+3* are more abundant than *U401 m+2, m+3* and *m+4*, respectively. This suggests that *U401 m+2, m+3* and *m+4* are made of [C3',C?-^{13}C] U401, [C3',C?,C?-^{13}C] U401 and [C3',C?,C?,C?-^{13}C] U401 respectively, corresponding to [C?-^{13}C] U224 (*U224 m+1)*, [C?,C?-^{13}C] U224 (*U224 m+2)* and [C?,C?,C?-^{13}C] U224 (*U224 m+3)*.

vii) *U401* lacks C4' and C5' in comparison with *U517. m+1, m+2* and *m+3* are the most abundant mass isotopomers in both *U401* and *U517*, whereas *U401 m+0* is much more abundant than *U517 m+0*. This indicates that C5' or/and C4' of *U517* are substantially labeled. The abundances of *U517 m+1* and *U517 m+2* are similar to those of *U401 m+1* and *U401 m+2*, respectively, but *U401 m+4* is less abundant than *U517 m+4*. This overall pattern of abundances might be explained in the following two different ways. Either (i) *U517 m+1* and *U517 m+2* are not labeled in C5' and/or C4', or (ii) in *U517 m+3, U517 m+4, U517 m+5*, C4' and/or C5' are one or two of the three, four and five labeled carbons, respectively. Hypothesis (ii) is supported by the fact that *U401 m+3* and *U401 m+4* are less abundant than *U517 m+3* and *U517 m+4*. Altogether, the comparison between *U401* and *U517* indicates that [C?,C?,C5'-^{13}C] U517, [C?,C?,C4'-^{13}C] U517 or [C?,C?,C4',C5'-^{13}C] U517 correspond to [C?,C?-^{13}C] U401, [C?,C4',C5'-^{13}C] U517 corresponds to [C?-^{13}C] U401 and that [C?,C?,C?,C5'-^{13}C] U517, [C?,C?,C?,C4'-^{13}C] U517 correspond to [C?,C?,C?-^{13}C] U401.

iv) The following comparison of *U517* with *U224* reinforces the evidence that in *U517* carbons C3', C4' and C5' are substantially labeled. *U224 m+3, U224 m+4* and *U224 m+5* are less abundant than *U517 m+3, U517 m+4* and *U517 m+5* respectively.This suggests that [C?,C?,C5'-^{13}C] U517, [C?,C?,C4'-^{13}C] U517, [C?,C?,C3'-^{13}C] U517, [C?,C?,C4',C5'-^{13}C] U517, [C?,C?,C3',C4'-^{13}C] U517 and

[C?,C?,C3',C5'-^{13}C] U517 correspond to [C?,C?-^{13}C] U224; and [C?,C4',C5'-^{13}C] U517, [C?,C3',C4'-^{13}C] U517 and [C?,C3',C5'-^{13}C] U517corresponds to [C?-^{13}C] U224.

The assigned fragments of cytidine derivative are composed of the nucleobase moiety, *C184*, of the ribose moiety *C348* and its fragment *C245* and of the nucleobase plus C1' and C2' of ribose, C*223*. The analysis of their mass isotopomers elucidates whether the labeling is either in nucleobase or in ribose and within ribose either in C1'-C2', C3'-C5' or in C4'-C5'. From the observation of the MID of the fragments of cytidine derivative (Figure 4.18) we notice the following:

i) In *C516* and *C223* the mass isotopomer abundances are approximately evenly distributed among *m+1*, *m+2* and *m+3*. *C348* and *C245* are predominantly labeled in one carbon. The next most abundant mass isotopomers are *m+0* and *m+2* in the case of *C245*, and *m+2* and *m+3* in the case of *C348*. In the fragment *C184,* the *C184 m+0* is the most abundant mass isotopomer being followed gradually and slightly by *C184 m+1, C184 m+2*. *C184 m+3* and *C184 m+0*4 are significantly less abundant.

ii) The similarity of the abundances of *C245 m+0* and *C348 m+0* indicates that in *C348 m+1,* C5' is not labeled. However, the higher abundances of *C245 m+1* and *C245 m+2* relative to *C348 m+1* and *C348 m+2* indicate that C5' is one of the two and three labeled carbons of *C348 m+2* and *C348 m+3,* respectively. This suggests that *C348 m+2* and *C348 m+3* are composed of [C?',C5'-^{13}C] C348 and of [C?',C?',C5'-^{13}C] C348, respectively, thus corresponding to [C?'-^{13}C] C245 and to [C?',C?'-^{13}C] C245.

iii) The comparison of *C223* with *C184* yields insight on the discrimination of labelling between C1' and C2' and in the nucleobase, as explained below:

a) The most abundant *C223* mass isotopomers are *C223 m+1, C223 m+2* and *C223 m+3*, whereas *C223 m+0* has a low abundance. However, *C184 m+0* is very abundant and slightly more abundant than *C184 m+1*. Therefore, *C223 m+1* and *C223 m+2* are labeled in C1' or/and C2'. That is, they are constituted by [C1'-^{13}C] C223, *or* [C2'-^{13}C] C223 and [C1',C2'-^{13}C] C223, respectively, all of which can only yield *C182 m+0*.

b) *C184 m+1* is the second most abundant mass isotopomer and slightly more abundant than *C223 m+1, C223 m+2* and *C223 m+3*. This supports the following two inferences. First, *C184 m+1* corresponds to C223 *m+2* and/or C223 *m+3*: if C223 *m+2* is labeled in either C1' or C2' and one C of the nucleobase moiety (*i.e.*, [1C_Nb, C1'-^{13}C] C223 or [1C_Nb, C2'-^{13}C] C223), it yields *C184 m+1* when missing C1' and C2'. Second, *C223 m+3* is labeled in C1', C2' and in one carbon of the nucleobase, (*i.e.,* [1C_Nb,C1',C2'] C223). *C184 m+2* is as abundant as *C223 m+3*. Therefore, *C223 m+3* may also be labeled in two carbons

of the nucleobase moiety and either in C1' or C2' (*i.e.,* [2C_Nb,C1'-^{13}C] C223 or [2C_Nb,C2'-^{13}C] C223), which yields *C184 m+ 2* (*i.e,* [2C_Nb-^{13}C] C184). Alternatively, *C184 m+2* may correspond to [2C_Nb,C1',C2'-^{13}C] C223 (*C223 m+4*). *C184 m+3* is approximately as abundant as *C223 m+4*. This indicates that *C223 m+4* may also be labeled in three carbons of the nucleobase moiety and either C1' or C2' (*i.e.,* [3C_Nb,C1'-^{13}C] C223).
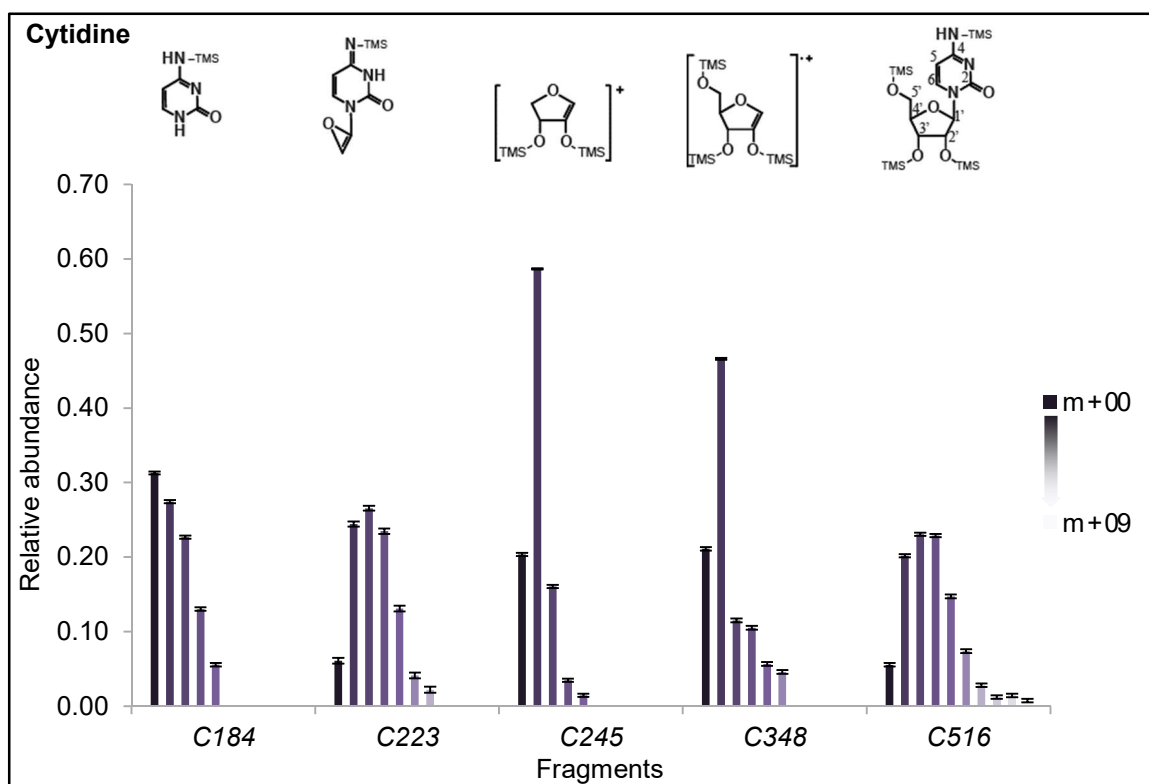

Figure 4.18 – MID of fragments of cytidine derivative.

iv) The MID of fragments *C516* and *C223* present a very similar profile. Namely, a) *m+2* is the most abundant mass isotopomer, followed by *m+3* and *m+1* in case of *C517* but by *m+1* and *m+3* in case of *C223*, b) the fourth most abundant mass isotopomer is *m+4* and then *m+0* and *m+5*. This similarity indicates that either the MID of *C516* is determined by the ^{13}C enrichment in carbons retained in the fragment *C223* (nucleobase carbons and C1' and C2') or the ^{13}C enrichment is evenly distributed in the ribose moiety of *C516*. The slight inversion of relative abundances between *C223 m+1*, *C223 m+3*, *vs. C516 m+1*, *C516 m+3*, indicates that there is a substantial ^{13}C enrichment in C3' to C5'.

Both the *C348 m+4* ribose moiety fragment and the *C184 m+4* nucleobase moiety are present in low abundances. This indicates that *C516 m+4* is predominantly labeled in three carbons of the nucleobase and in either C1' or C2', *i.e,* [3C_Nb, C1'] C516 or [3C_Nb,C2'] C516. However, because *C223 m+4* is slightly less abundant than *C516 m+4* and *C223 m+3* is slightly more abundant than *C516 m+4*, the *C516 m+4* mass isotopomer may also contain labeling in two carbons of nucleobase, one carbon of the

C3'-C5' moiety and either C1' or C2' (*i.e.*, [2C_Nb,C1',C?'-^{13}C] C516 or [2C_Nb,C2',C?'-^{13}C] C516).

In Table 4.3 we present the plausible positional isotopomers that can be elucidated from the analysis of the MID of uridine and cytidine derivative fragments. In uridine, single labeled ribose moiety is either labeled in C5' or in other ribose carbon (C?') whereas single labeled cytidine is either labeled in C1' or C2'. In cytidine, labeling in C5' coexists with labeling in C1' or C2'. It was not possible to elucidate any labeling position in the nucleobase moieties of uridine and cytidine because these moieties did not fragment.

Table 4.3 - Plausible ^{13}C isotopomers of uridine and cytidine of cRNA. #C_Nb, total number of ^{13}C in the nucleobase moiety.

| | nucleoside | Mass isotopomers | | | |
		m+1	*m+2*	*m+3*	*m+4*
Positional isotopomers	**Uridine**		[1C_Nb,C5'] [1C_Nb,C?']	[1C_Nb,C?',C5'] 2C_Nb, C5'	[1C_Nb,C?',C?',C5'] [2C_Nb,C?',C5']
	Cytidine	[C1'] [C2'] [1C_Nb]	[1C_Nb,C1'] [1C_Nb,C2'] [C1',C5'] [C2',C5']	[2C_Nb,C1'] [2C_Nb,C2'] [1C_Nb,C1',C5'] [1C_Nb,C2',C5']	[3C_Nb,C1'] [3C_Nb,C2'] [2C_Nb,C1',C5'] [2C_Nb,C2',C5']

4.2.2.2| ^{13}C isotopomers of deoxynucleosides of nDNA

The fragments of deoxynucleoside derivatives measured in SIM mode were the following: derivative of the deoxyribose moiety of deoxycytidine and thymidine, 245 *m/z*; thymidine nucleobase moiety derivative, 255 *m/z*; cytidine nucleobase moiety derivative, 240 *m/z*; deoxyadenosine derivative, 468 *m/z*, 453 *m/z* and 193 *m/z*; deoxyguanosine derivative, 555 *m/z* and 295 *m/z*.

The assigned fragments of deoxypyrimidine derivatives are composed of the deoxyribose moiety *dR245* and of the respective nucleobases moieties *T255* and *dC240*. The analysis of their mass isotopomers elucidates the distribution of labeling among the deoxyribose or nucleobase moieties. In Figure 4.19 and 4.20 we present the MID of the fragments of deoxynucleosides of nDNA. The vast majority of deoxyribose moiety of thymidine and deoxycytidine is non-labeled, *dR245 m+0*. However, around 10% is labeled in two carbons, *dR245 m+2*. The position of these two labeled carbons cannot be elucidated due to the lack of fragments splitting the deoxyribose moiety. The mass isotopomer abundances of the nucleobase moieties of thymidine and deoxycytidine are evenly distributed among *m+0*, *m+1* and *m+2*. *NbdT255 m+1* is as abundant as *NbdT255 m+0*, whereas *NbdC240 m+1* is less abundant than *NbdC240 m+0* possibly due to the presence of ^{13}C labeling in the methyl group of thymidine.
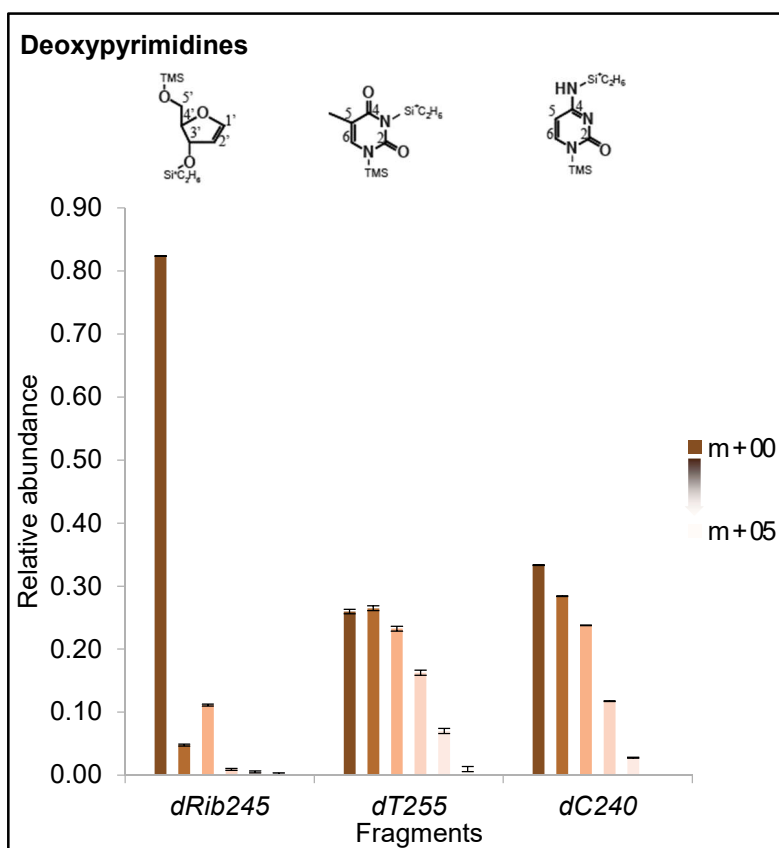
Figure 4.19 – MID of fragments of deoxypyrimidines derivatives, deoxyribose, thymine and cytosine.

The assigned fragments of deoxypurines derivatives are composed of nucleobase moieties *dA192* and *dG295*. From the observation of the relative MIDs of the fragments of deoxyadenosine derivative (Figure 4.20) we notice the following:

i) *dA468* is predominantly and equally labeled in two (*dA468 m+2*) or three carbons (*dA468 m+3*), followed by labeling in four (*dA468 m+4*) and in one carbons (*dA468 m+1*).

ii) *dA193* is predominately labeled in one (*dA193 m+1*) or two carbons (*dA193 m+2*), followed by non-labeled (*dA193 m+0*) and labeled in three carbons (*dA193 m+3*).

iii) The comparison of the intensities of the different mass isotopomers of *dA468* and *dA193* suggests that the deoxyribose moiety is labeled in one and two carbons because the MID of *dA193* resembles that of *dA468* but shifted to *m+(n-1)* mass isotopomers.

iv) Unlike *dA468 m+4*, *dA193 m+4* has a very low abundance, *dA193 m+3* is approximately as abundant as *dA468 m+4,* and *dA193 m+2*lightly more abundant than *dA468 m+3*. This suggests that the molecules contributing to *dA468 m+4* either have two labeled carbons in the nucleobase and two in the deoxyribose moiety, i.e.

[C?,C?,C?',C?'-^{13}C] dA468, resulting in *dA193 m+2*, or three labeled carbons in the nucleobase and one in the deoxyribose moiety, i.e. [C?,C?,C?,C?'-^{13}C] dA468, resulting in *dA193 m+3*.

v) *dA193 m+3* is less abundant than *dA468 m+3* but *dA193 m+2* is slightly more abundant than *dA468 m+2*. This suggests that molecules contributing to *dA468 m+3* are labeled in two carbons of the nucleobase moiety and in one carbon of the deoxyribose moiety, i.e. [C?, C?, C?'-^{13}C] dA468 because.

vi) Similarly to v), molecules contributing to *dA468 m+2* and to *dA468 m+1* should be labeled, respectively in one carbon in the nucleobase and one carbon in the deoxyribose, i.e. [C?,C?'-^{13}C] dA468, and non-labeled in the nucleobase and labeled in one carbon of the deoxyribose moiety, i.e. [C?'-^{13}C] dA468.
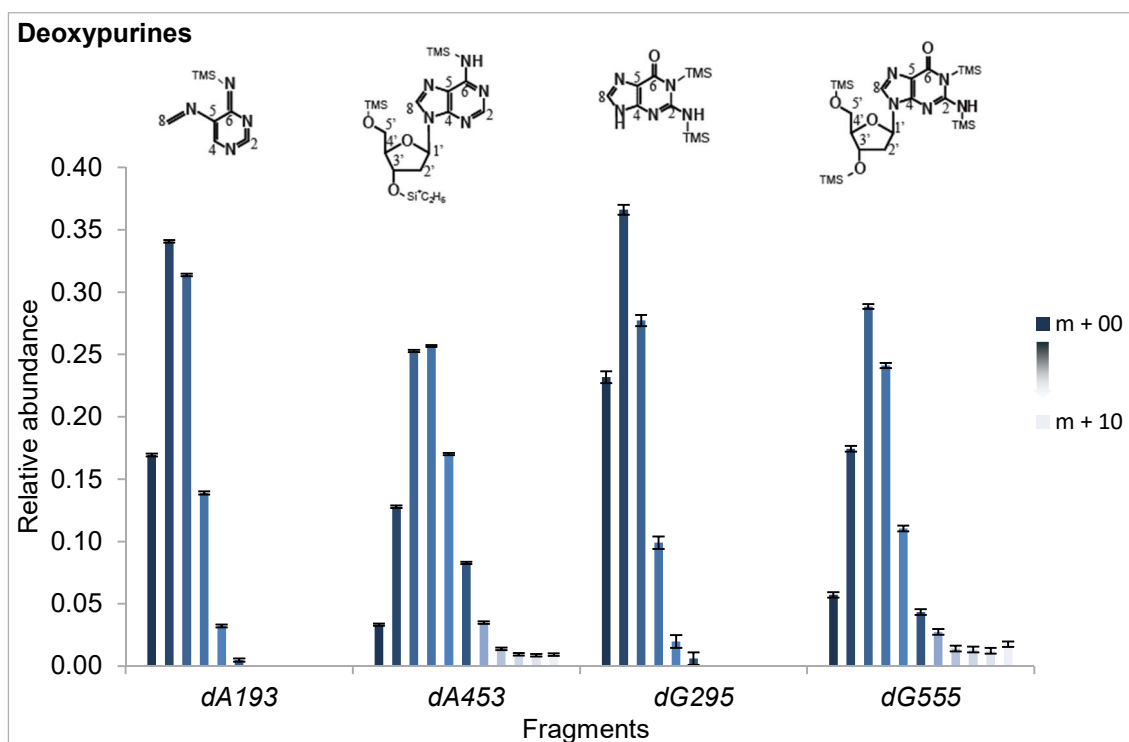
Figure 4.20 – MID of fragments of deoxyadenosine and deoxyguanosine derivatives.

From the observation of the relative MIDs of the fragments of deoxyguanosine derivative (Figure 4.20) we notice the following:

i) *dG555* is predominantly labeled in two carbons (*dG555 m+2*), followed by labeling in three (*dG555 m+3*) carbons and in one carbon (*dG555 m+1*).

ii) *dG295* is predominantly labeled in one carbon (*dG295 m+1*), followed by labeling in two carbons (*dG295 m+2*) and non-labeled (*dG295 m+0*).

iii) The MID of *dG295* is similar to that of *dG555* but shifted to m+(n-1) mass isotopomers. Therefore, and similarly to deoxyadenosine, we can anticipate the deoxyribose moiety to be labeled in one carbon or in two carbons, in the case of *dG555 m+4* and *m+5*.

Table 4.4 - Plausible ^{13}C isotopomers of deoxyadenosine and deoxyguanosine of nDNA.

	deoxynucleoside	*m+1*	*m+2*	*m+3*	*m+4*
				Mass isotopomers	
Positional isotopomers	**deoxyadenosine**	[C?']	[1C_Nb,C?']	[2C_Nb,C?']	[2C_Nb,C?',C?'] [3C_Nb,C?']
	deoxyguanosine	[C?']	[1C_Nb,C?']	[2C_Nb,C?'] [1C_Nb,C?',C?']	[3C_Nb,C?']

iv) The abundance of *dG295 m+4* is very low, *dG295 m+3* is approximately as abundant as *dG555 m+4,* and *dG295 m+2* is approximately as abundant as *dG555 m+3*. Therefore, molecules contributing to *dG555 m+4* should be predominantly labeled in three carbons in the nucleobase moiety and in one carbon in the deoxyribose moiety, i.e. [C?,C?,C?,C?'-^{13}C] dG555 (Figure 4.20).

v) *dG555 m+3* results of the presence of both molecules labeled in two carbons in the nucleobase and one in the deoxyribose, i.e. [C?,C?,C?'-^{13}C] dG555, and molecules labeled in one carbon in the nucleobase and two carbons in the deoxyribose, i.e. [C?,C?',C?'-^{13}C] dG555, because *m+1* (*dG295 m+2)* increases considerably more than *m+2* (*dG295 m+2)* from *dG555* to *dG295*.

vi) Molecules labeled only in one carbon in the nucleobase moiety and one carbon in the deoxyribose moiety, i.e. [C?, C?'-^{13}C] dG555*,* contribute to *dG555 m+2* (Figure 4.20).

vi) *dG555 m+1* results of the contribution of molecules labeled only in one carbon of deoxyribose, *i. e.* [C?'-^{13}C] dG555.

vii) It is worth to highlighting that the *dG555 m+0* mass isotopomer is slightly more abundant than those of other nucleosides, which contributes also to a more abundant *dG295 m+0, i. e. dG555 m+0* comes from [^{12}C] dG555 yielding [^{12}C] dG295, which gives raise to mass isotopomer *dG295 m+0*.

In Table 4.4 we present the plausible positional isotopomers that can be elucidated from the analysis of the MID of deoxyadenosine and deoxyguanosine derivative fragments. These are not the unique positional isotopomers but those that can be inferred from the MID of the present fragments. For deoxycytidine and thymidine it was not possible to propose plausible positional isotopomers because there is no fragmentation of these ions. #C_Nb, total number of 13C in the nucleobase moiety.

Deoxypyrimidine nucleobases are predominantly non-labeled, labeled in one and in two carbons, whereas deoxypurines nucleobases are predominantly labeled in one and two carbons. This is not a surprise as their carbon backbones originate from different precursors: ASP and glycine, respectively. The observation that m+0 of deoxypurinic nucleobases is much more abundant than that of the whole deoxypurines shows that deoxyribose of purines has to be predominantly labeled in some carbons, unlike the deoxyribose moiety of deoxypyrimidines that is 90% non-labeled.

4.2.2.3| Qualitative analysis of ^{13}C isotope tracing of nucleosides of nDNA and cRNA

The analysis of the plausible ^{13}C isotopomers of deoxynucleosides and nucleosides led us to a first approximation of the metabolic profile of proliferating cell.

The most abundant mass isotopomers of uridine and cytidine are *(m+1)*, *(m+2)* and *(m+3)*, being *(m+4)* also quite abundant (Figure 4.17 and 4.18). Comparing *U348*, *C348* and *U245*, *C245*, we noticed that they are mostly labeled in one carbon *(m+1)*, followed by non-labeled *(m+0)* and labeled in two carbons *(m+2)*. This indicates that C5' is not contributing to *U348* or *C348 (m+1)*. This indicates preferential activity of PPP$_{ox}$, which yields [1-^{13}C] R5P. On the other hand, *U245*, *C245 (m+3)* is much less abundant than that of *U348*, *C348* what suggests that C5' is one of three labeled carbons in the *(m+3)* mass isotopomer of these fragments. This is only possible when there is activity of the PPP$_{non-ox}$ towards R5P (PPP$_{non-ox}$ backw) and shunting back and forward, resulting in [1,4,5-^{13}C] R5P and [2,4,5-^{13}C] R5P (Table 3.11 and 3.12). *U224*, *C223* keep only C1' and C2' of the ribose moiety, thus, *(m+3)* has to have the contribution of labeling in the nucleobase. Hence, *U517, C516 (m+3)* and *(m+4)* must be labeled both in ribose and nucleobase moieties. Altogether these evidences indicate that shunting through the PPP [PPP$_{ox}$ → PPP$_{non-ox}$ fwd ←→ PPP$_{non-ox}$ bckw] should be the predominantly active pathway series and that there is also some glycolytic activity generating the F6P and GA3P isotopomers that result in some labeling in C5' (Table 3.13).

The MID of *C184* and *dC240* suggest that pyrimidine nucleobases are simultaneously non-labeled, labeled in one and in two carbons because *(m+0)*, *(m+1)* and *(m+2)* are the most abundant mass isotopomers. This gives evidence that the metabolic series that preceded cytidine nucleobase biosynthesis was PPP$_{ox}$ and both PC and TCA cycle (Table 3.15).

The *dT255* presents *(m+1)* as intense as *(m+0) of dC240,* and *(m+3)* more abundant than d*C240*. Hence, the methyl substituent should be ^{13}C traced. This gives evidence of the presence of H$^{13}CO_3^-$, thus the one carbon pool is ^{13}C traced.

The most abundant mass isotopomer of *dR245* is *(m+0)*, followed by *(m+2)* low abundant, though. The activity of the series glycolysis followed by PPP$_{non-ox}$ bckw

[glycolysis → PPP$_{non-ox}$ bckw] results in non-labeled R5P but also [1,2-^{13}C] R5P isotopomer, to some extent. [1,2-^{13}C] R5P gives rise to *dR245 (m+2)* (Table 3.13).

In deoxypurines the most abundant mass isotopomers are *(m+2)* and *(m+3)*, followed by *(m+1)* and *(m+4)*. Their nucleobases are predominately labeled in one or two carbons, *(m+1)* and *(m+2)*. The *(m+1)* mass isotopomer was biosynthesized either from [1-^{13}C] or [2-^{13}C] glycine; whereas *(m+2)* was biosynthesized either from [1,2-^{13}C] glycine or from [1-^{13}C] or [2-^{13}C] glycine and [1-^{13}C] FTHF. The mass isotopomers *(m+0)* and *(m+3)* are also of relevance. The activity of the series glycolysis, PPP$_{non-ox}$ shunting back and forward yields approximately the same abundance of [U-^{12}C], [2-^{13}C] and [1,2-^{13}C] glycine. Together with [^{12}C] or [1-^{13}C] FTHF will result in the observed deoxypurine MID: *(m+1) > (m+2) > (m+0) > (m+3)*.

4.2.3| Analysis of the mass isotopomer distribution of equivalent fragments of deoxynucleosides and nucleosides.

4.2.3.1| Comparison of mass isotopomer distribution of equivalent fragments of deoxynucleosides from nDNA with nucleosides from cRNA

We compared the pairs dR245/C348 and dC240/C184 (Figure 4.21). We also compared the MID of equivalent fragments from the same nucleic acid to serve as negative control. We compared the pairs U348/C348, U245/C245, U517/C516 (Figure 4.17 and 4.18), dA295/dG555 (Figure 4.20), which present the same MID among each other. If the equivalent fragments from the same nucleic acid, either cDNA or cRNA, present the same MID profile, then any difference between the MID of equivalent fragments of deoxynucleosides and nucleosides concern metabolic differences between S-phase and the other phases. Indeed, dR245/C348 pair presents a distinct MID indicating that the MFD of the biosynthesis of either nDNA deoxynucleosides or cRNA nucleosides are distinct. The analysis of the *in silico* MID of the same fragments of deoxynucleosides and nucleosides obtained from the forward simulations permits comparing the relative activity of metabolic pathways. The *(m+0)* of dRib245 (nDNA) is much more abundant than that of C348 (cRNA), and the *(m+1)* of dRib245 is much less abundant than that of C348. According to the results of forward simulation (Table 3.11 and Figure 3.8), *(m+0)* of ribose increases and *(m+2)* decreases for higher rates of *gly1*. Therefore, in S-phase, glycolysis flux rate is much higher than that of PPP$_{ox}$, whereas out of S-phase PPP$_{ox}$ flux rate is higher than that of glycolysis. The cytidine nucleobase fragments of nDNA, dC240, and cRNA, C184, present an alike MID profile. This suggests that i) MFD of their biosynthesis is not distinct; ii) the ^{13}C labelling pattern used ([1,2-^{13}C] glucose) does not lead to distinguishable MID in these fragments; iii) or that the turnover of ASP pool (the pyrimidine nucleobase precursor) is slow. Cytidine and deoxycytidine pools exhibited a slow turnover. This is noticeable from the relative abundance of *(m+n)* of [U-^{13}C] molecules. Cytosine nucleosides and deoxynucleosides present an evenly distributed

MID, unlike, uridine and thymine that present a *(m+9)* mass isotopomer much more abundant than any other. This means that deoxycytidine and cytidine takes much longer to achieved the isotopic steady state than other nucleosides. This might explain the similarities between MID of cytidine and deoxycytidine nucleobases.
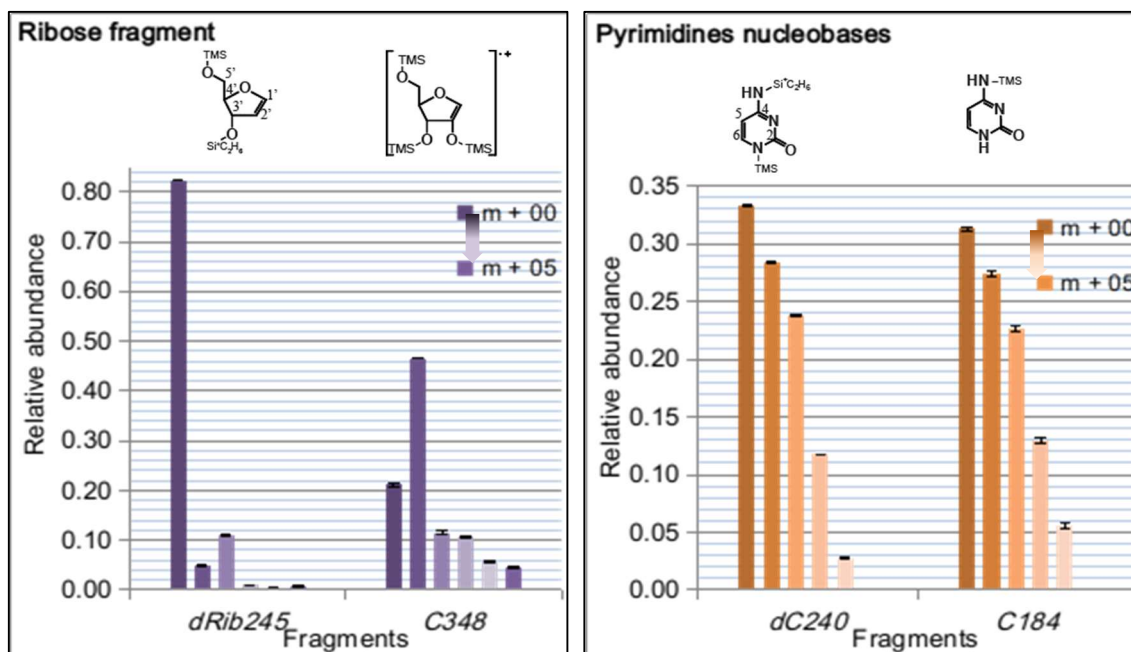

Figure 4.21 – MID of equivalent fragments from deoxynucleosides and nucleosides. dRib245, deoxyribose moiety of deoxypyrimidines (DNA); C348, ribose moiety of cytidine (RNA); dC240, nucleobase moiety of deoxycytidine (DNA); C184, nucleobase moiety of cytidine (RNA).

The analysis of the *in silico* MID could not help much in elucidating the lack of discrimination in the pyrimidine nucleobases. The isotopomer population of the ASP pool depends on the relative flux of [glycolysis *vs* PPP_{ox}], [TCA cycle vs PC] and [PC *vs* glyoxylate cycle]. The impact of relative fluxes of one branching point on the MID of pyrimidinic nucleobases can be neutralized by the impact of the others. The forward simulations of the branching point [TCA cycle *vs* PC] were clamped by the technical limitation of maneuvering the *pf3* flux. Yet, looking at the *in silico* MID of forward simulation of [TCA cycle *vs* PC], we notice that MID are multi-phasic with respect to *tcc1* and *gly1* flux values, which limits the confidence of a qualitative comparison.

Nonetheless, observing the relative abundances of the mass isotopomers of the pair dC240/C184 it is noticeable that C184 *(m+4)* and *(m+3)* are more abundant than those of dC240, and that C184 *(m+0)* is less abundant that dC240 *(m+0)*. This means that although the MID of the pair show the same order of relative abundances, i.e., *(m+0) > (m+1) > (m+2) > (m+3)*, the relative abundances of each mass isotopomer of dC240 are not equal to those of C184. It is noticeable that between *(m+0)* and *(m+3)* the gap of relative abundances in dC240 is bigger that in C184. Therefore, and acknowledging the mentioned caveats, results suggests that the ratio PC/TCAcycle is lower in S-phase than out of S-phase, consistent with higher activity of TCA cycle.

4.2.3.1| Comparison of mass isotopomer distribution of equivalent fragments of (deoxy)nucleosides from nDNA and cRNA with mtDNA and RNA.

The rationale of tracing back the MFD from the MID of deoxynucleosides and nucleosides can also be applied to the mitochondrial nucleic acids. Mitochondrial nucleic acid biosynthesis does not relate to any particular phase of CDC, unlike nDNA. Since mtDNA is biosynthesized over the CDC, we anticipated to not notice any difference in the MID of nucleosides from mtDNA and mtRNA.

Due to the low yield of the mitochondrial nucleic acid digestion, we obtained very low amounts of mitochondrial deoxynucleosides and nucleosides, which left very few fragments to be analyzed. Under these conditions we got restricted to the only analyzable fragment in common to the four different nucleosides, the ribose moiety. In Figure 4.22 we present the MID of the ribose moieties of cRNA, nDNA and mtRNA and mtDNA.
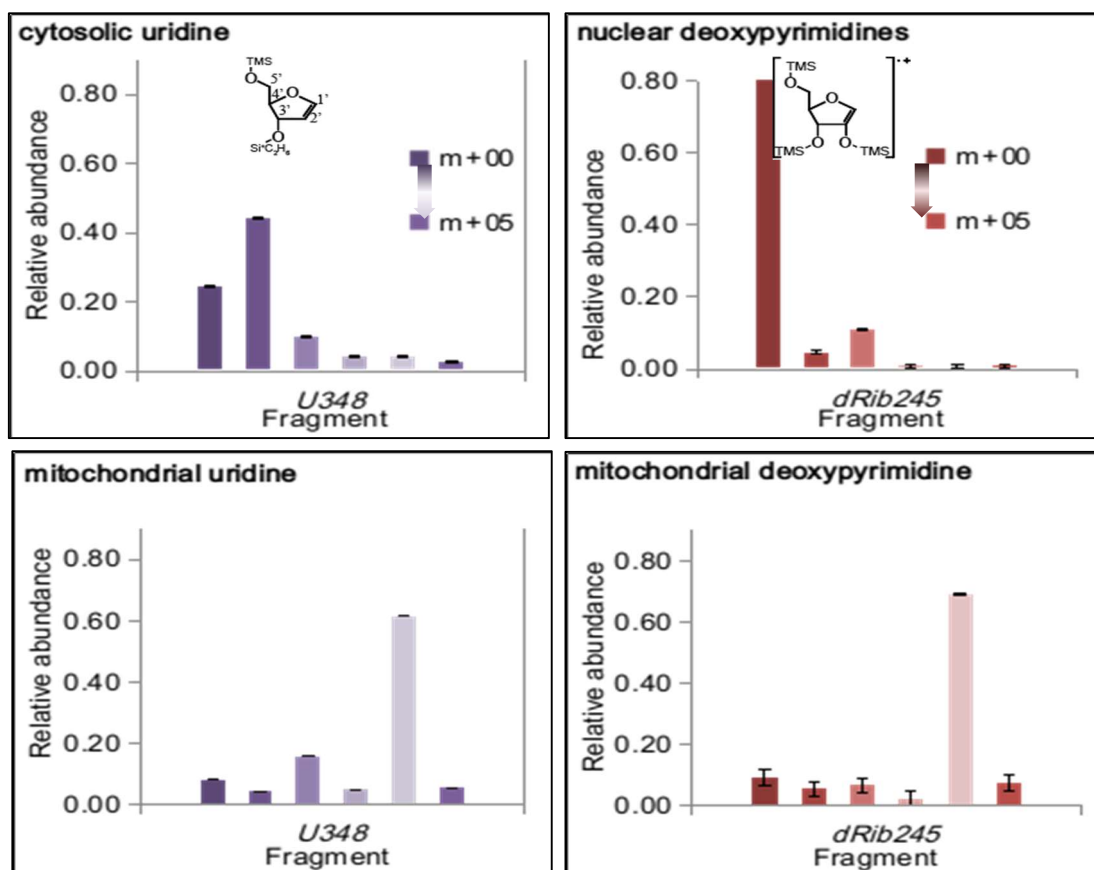

Figure 4.22 – MID of the ribose and deoxyribose fragments of derivatives of uridine and thymidine obtained from cRNA (cytosolic U348), nDNA (nuclear dR245), mtRNA (mt U348) and mtDNA (mt dR245).

Importantly, whereas the MID of the ribose moiety from cytosolic *U348* strongly differs from that of the deoxyribose moiety from nuclear *dR245* (Figure 4.22 upper

panels), the MID of the ribose moiety from mitochondrial *U348* is very similar to that of the deoxyribose moiety from mitochondrial *dR245* (Figure 4.22 lower panels). Furthermore, we can also observe dramatic differences between the MIDs of mitochondrial and cytosolic *U348*, and between the MIDs of mitochondrial and nuclear dR245. Mitochondrial ribose moiety is highly enriched in ^{13}C, presenting in a mass isotopomer *(m+4)* abundance of around 60% whereas the other mass isotopomers are below 20% each.

4.2.4| Numerical exploration of the relationship between mass isotopomer distribution and the metabolic flux distribution.

The deoxynucleosides and nucleosides' MID obtained from the forward simulations (*cf.* chapter 3.2.2 and 3.2.3) were organized emulating the experimental GC-MS spectra. Hence, for each set of MFD used in the forward simulation we have *in silico* spectra of deoxynucleosides and nucleosides.

The numerical exploration of these MID and respective MFD aimed at acquiring insight on the correlation between them and preceded the ^{13}C-MFA. The ^{13}C-MFA requires a set of starting flux rates (*cf.* Chapter 1.4.1), which revealed not straightforward to guess; not even using the sampling algorithms implemented in ^{13}C-Flux2. Acknowledging these difficulties, we used the numerical exploration of the relationship between MID and MFD to eventually find a feasible set of starting flux rates for the fitting towards flux rate estimation.

We approximated the *in silico* to the experimentally acquired spectra in order to guess a plausible set of starting flux rates. We performed a first approximation of the *in silico* MID from the forward simulation sets of [glycolysis *vs* PPP$_{ox}$], which indicated a reasonable range of glycolysis flux rates. Secondly, we took the *in silico* MID from the forward simulation sets of [TCA cycle (*tcc1*) *vs* pyruvate carboxylase (PC) (*pf3*)], for the just guessed glycolysis flux rate. The flux values used in the forward simulations are relative to a glucose uptake rate (*upt*) of 10 fmol/h·cell.

4.2.4.1| **Mass isotopomer distribution of deoxynucleosides from nDNA and metabolic flux distribution in S-phase.**

The *in silico* spectra in better agreement with the experimental spectra of deoxynucleosides (Figures 4.19 and 4.20) were obtained from forward simulations (Table 3.10) in which *gly1* flux rate is around 4 fmol/h·cell and *tcc1* flux rate is around 10 fmol/h·cell.

The evidence for this matching comes from the high abundance of *(m+2)* and *(m+3)* followed by *(m+4)*, *(m+1)* and *(m+5)* of deoxypurine molecular ions dA453 and

dG555. This evidence is supported by the high abundance of mass isotopomers (m+0), (m+1 and (m+2) of fragments dA193 and dG295, dRib245, dC240 and dT255.

Figure 4.22 – MFD set yielding the MID in best agreement with experimental spectra of deoxynucleosides. Flux rates relative to *upt* of 10 fmol/h·cell.

4.2.4.1| Mass isotopomer distribution of nucleosides from cRNA and metabolic flux distribution out of S-phase.

The *in silico* spectra in best agreement with the experimental spectra of uridine and citidine (Figure 4.17 and 4.18) result from the forward simulation set of fluxes (Table 3.1) in which *gly1* and *tcc1* flux rates are around 2 fmol/h·cell.

The evidence for this matching comes from the MID profile of fragment U517 and C516 showing that the abundances of the mass isotopomers *(m+2)* and *(m+3)* are equal and the most abundant, and *(m+1)* is much more abundant than *(m+4)*. The MID

profile of other fragments reiterate the guessed MFD, namely, fragments U348, C348 and U245, C245 presenting high abundant mass isotopomer *(m+1)* and the *(m+0)* considerably more abundant than *(m+2)*; and fragments U339 and U224, C223 exhibiting the mass isotopomers *(m+1)*, *(m+2)* and *(m+3)* much more abundant than any others and *(m+4)* more abundant than *(m+0)*.
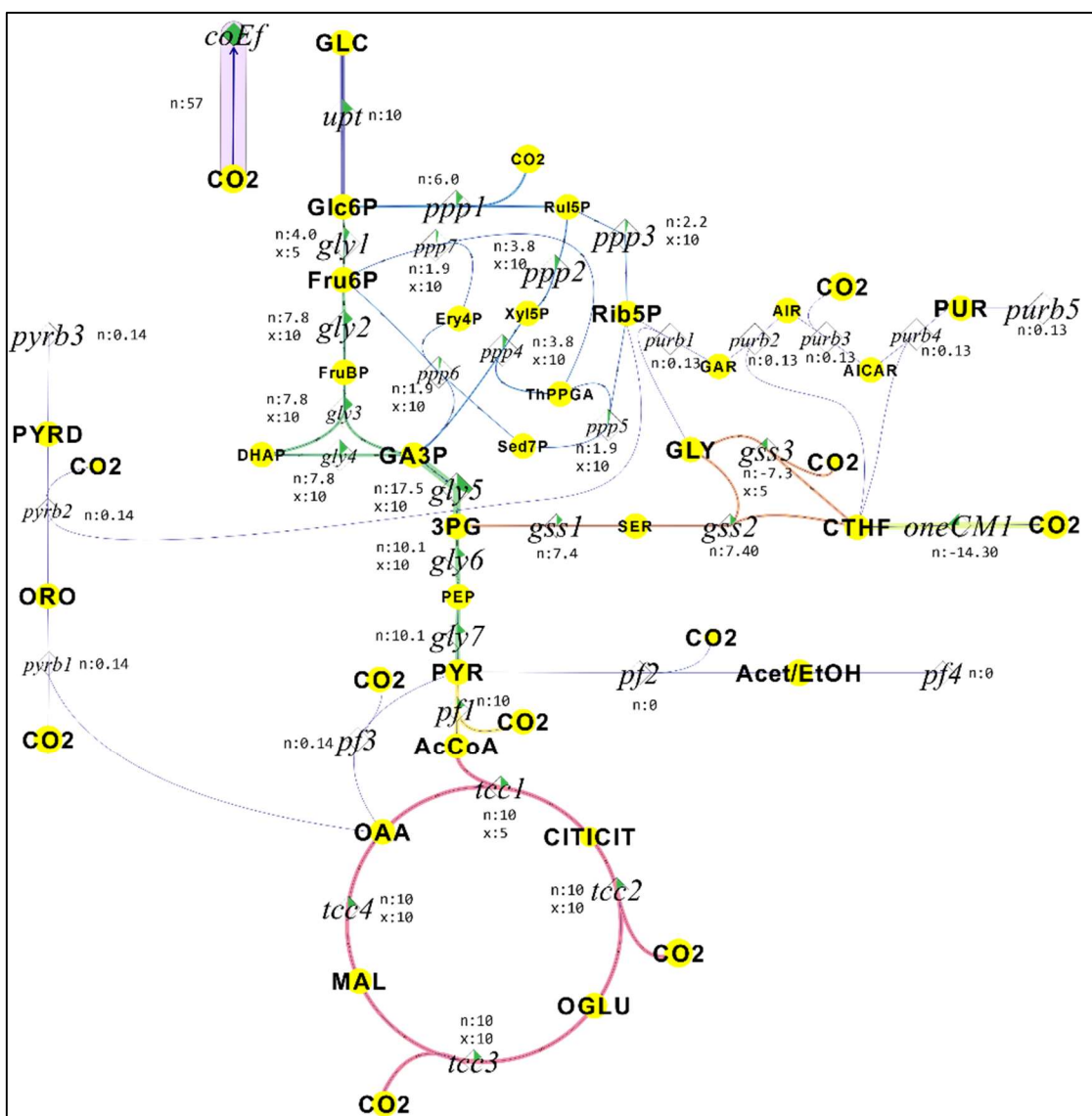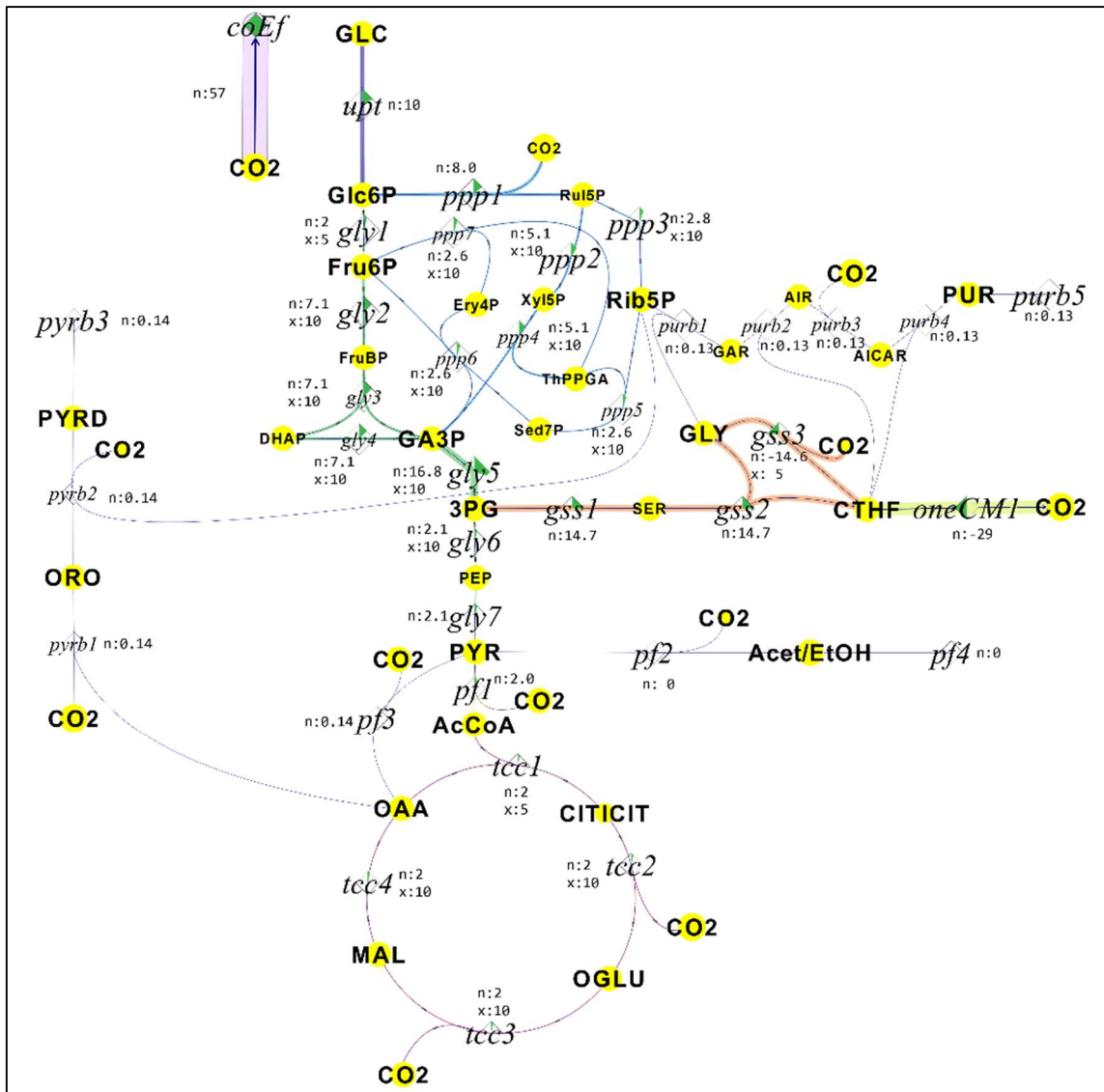

Figure 4.23 – MFD set yielding the MID in best agreement with experimental spectra of nucleosides. Flux rates relative to *upt* of 10 fmol/h·cell.

4.3| ESTIMATION OF METABOLIC FLUX DISTRIBUTION IN S-PHASE

The analysis of the MID of deoxynucleosides (s-phase) based on the MID and MFA provided initial guesses for quantitative flux estimation. Using these initial guesess we could fit the proposed model (Figure 3.4 and appendix) to the experimental data of MID of deoxynucleosides. Metabolic fluxes in S-phase could be successufully estimated using least square minimization (Figure 4.23), which improved residual was 306862.
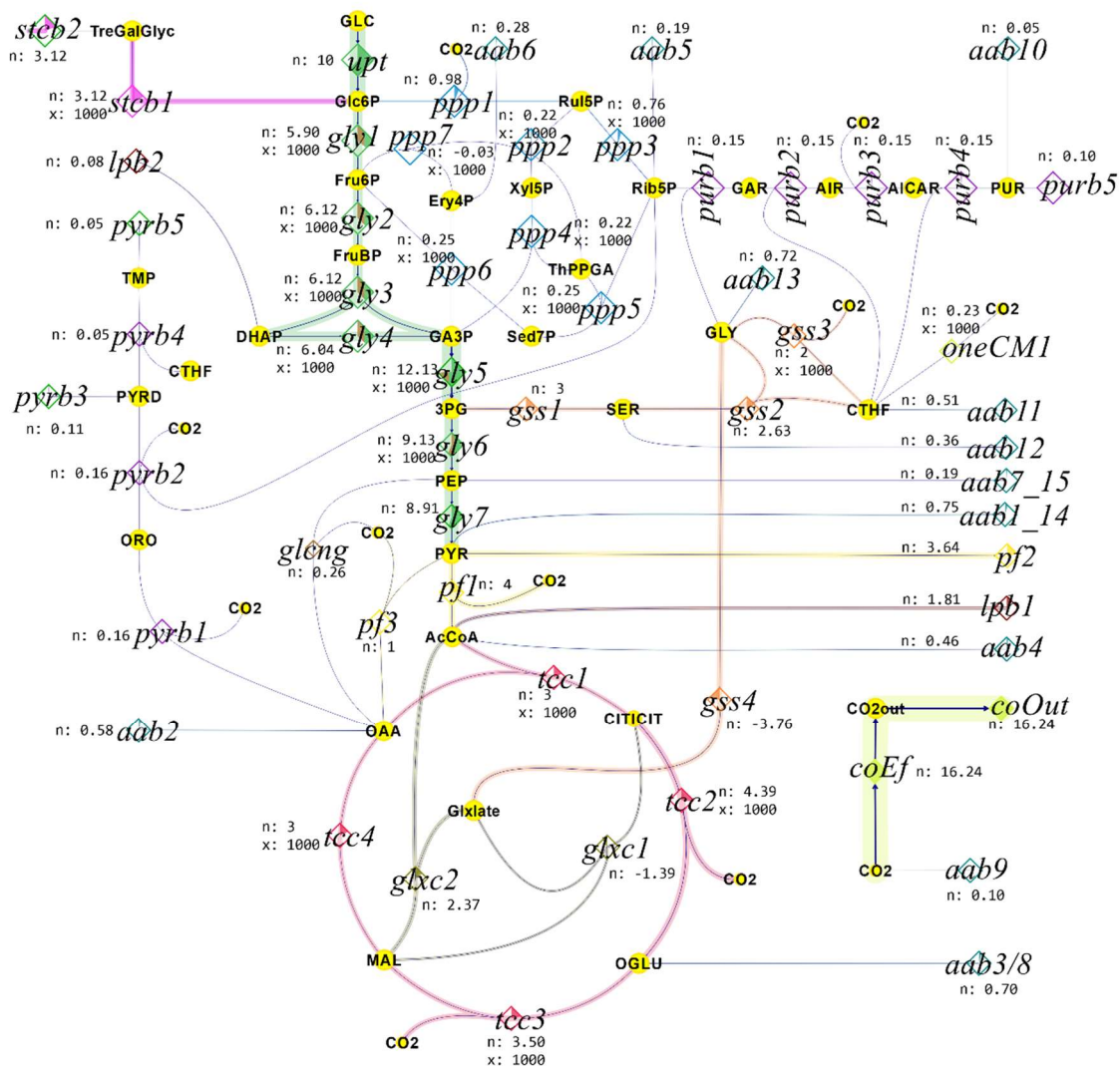
Figure 4.23 – MFD in S-phase estimated by fitting to experimental MID of deoxynucleosides isolated from nDNA.

However, the MFD of the remaining phases of CDC could not be successfully estimated, despite using as initial guesses the fluxes values surveyed with the numerical exploration. This is an indication of further metabolic heterogeneity over G2, M and G1 phases of CDC, such that it is not possible to fit a single model to the experimental data.

5| Discussion

We aimed at clarifying whether and how the MFD of the intermediary metabolism differs among the phases of the CDC. We hypothesized that each phase of the CDC has a characteristic metabolic phenotype. Furthermore, we also hypothesized that the metabolic differences between quiescent and proliferating cells is due, at least in part, to such metabolic heterogeneity over the CDC phases.

This hypothesis came from the evidence of metabolic oscillations coupled to the phases of the CDC in synchronized proliferating budding yeast (Tu et al., 2005). These oscillations in pO$_2$ and NADH (Furukawa, Heinzle and Dunn, 1983) are accompanied by oscillations in metabolic transcriptome and in metabolome (Tu et al., 2005). Such evidence triggered the formulation of the constitutive oscillation hypothesis (*cf.* Chapter 1.3.2). It postulates that the metabolic oscillations observed in synchronized proliferating cells also occur at the individual cell level in asynchronous proliferating populations.

In this viewpoint, the proliferating cell population is metabolically heterogeneous due to the coexistence of cells in each phase of the CDC at each time.

Metabolic oscillations that may be related to the CDC have been characterized so far at the level of gene transcription and metabolite concentrations in synchronized cell populations. However, whether and how the MFD changes over the CDC in unsynchronized cell populations had never been studied before this work.

The investigation of the constitutive oscillation hypothesis demanded a methodology that would simultaneously allow the study of CDC phase-specific metabolism without cell synchronization or sorting (*cf.* Chapter 1.2.2), and be suitable for CLE. We devised and implemented a ^{13}C tracer-GC-MS based methodology using DNA and RNA as intrinsic biological reporters for S-phase metabolism (DNA) and for metabolism in the other phases (RNA) (*cf.* Chapter 1.2.2). The rationale behind this methodology is that the ^{13}C isotopic distribution in the building blocks of biopolymers gets imprinted from that of their precursors, hence, reflects the MFD at the moment of monomer biosynthesis. In this way, we overcame the limitations and drawbacks of the state-of-the-art methods for CDC related metabolic studies. In proliferating cells deoxynucleosides and nucleosides are biosynthesized by the *de novo* pathway and are readily incorporated in DNA and RNA, respectively. Therefore, a significant difference between the 13C isotopomer distribution of the deoxynucleosides from nuclear DNA and that of the nucleosides from cytoplasmic RNA will reveal that the MFD is heterogeneous over the CDC.

Moreover, the ^{13}C isotopomer abundances in deoxynucleosides constitute an asset of quantitative data useful for determination of the MFD in S-phase. Therefore, we developed a ^{13}C-MFA computational model and used it perform *in silico* CLE under a

range of MFD. We rationalized the effect of MFD in the MID of deoxynucleosides and nucleosides based on the series of *in silico* MID obtained from the forward simulations. Based on this knowledge and on the experimental MID of deoxynucleosides and nucleosides we compared and inferred the relative activity of the pathways of the intermediary metabolism in S-phase and in the other phases of CDC. Furthermore, the 13C-MFA can be used to quantitatively determine the MFD in S-phase.

5.1| CARBON COMPOSITION OF NUCLEOSIDE FRAGMENT MOIETIES

^{13}C labeling of DNA and RNA with stable isotopes has been used before to determine cell proliferation rates in tumor (Defoiche *et al.*, 2009) and infected cells, like lymphocytes (Ho *et al.*, 1995; Wei *et al.*, 1995; Asquith *et al.*, 2009). In such studies cell proliferation was determined only from the total ^{13}C enrichment in nucleosides. Most commonly, ^{13}C-glucose, ^{2}H-glucose (Macallan *et al.*, 2009) and ^{13}C-dNTP have been used allowing also to distinguish the contribution of the *de novo* synthesis and salvage pathways to the biosynthesis of DNA. However, these studies did not exploit the selective ^{13}C enrichment of deoxynucleosides and nucleosides incorporated in DNA and RNA to eventually obtain information about the MFD in proliferating cells. Furthermore, the analysis of the ^{13}C isotopomers of (deoxy)nucleosides will reflect the MFD at the moment of their respective biosynthesis. Hence, ^{13}C isotopomers of deoxynucleosides from nDNA and nucleosides from cRNA are reportes of the MFD during S- and out of S-phase, respectively.

The determination of positional isotopomers improves the accuracy and precision of ^{13}C-MFA calculations (Choi and Antoniewicz, 2011). Previous work has elucidated the fragmentation of amino acids (Antoniewicz, Kelleher and Stephanopoulos, 2007; Choi, Grossbach and Antoniewicz, 2012) and of metabolic intermediates (Rühl *et al.*, 2012), but not that of deoxynucleosides and nucleosides. Here we assigned the fragment formula of nucleosides leading to a partial determination of ^{13}C positional isotopomers. We unequivocally assigned 30 fragments from the analysis of the fragmentation spectra and of the isotopic abundances of naturally and uniformly ^{13}C labeled nucleosides.

The chromatographic sequence allowed the complete separation of the five derivatives of deoxynucleosides and of the four derivatives of nucleosides. Not surprisingly, the equivalent derivatives of nucleosides and deoxynucleosides, namely adenosine and deoxyadenosine, guanosine and deoxyguanosine, presented approximately the same RT. This fact reinforced the option of measuring deoxynucleosides and nucleosides separately.

When feeding cells in batch culture with [U-^{13}C] glucose, the deoxynucleosides and nucleosides isolated from their respective nucleic acids became enriched in ^{13}C, as expected (Figures 4.6 and 4.7). The most abundant mass isotopomer of all deoxynucleoside and nucleoside derivatives, except the nucleobase of deoxythymidine, was the *(m+n)* mass isotopomer. This observation corroborates the knowledge that in proliferating cells deoxynucleosides and nucleosides are biosynthesized *via* the *de novo* pathway. We harvested DNA and RNA at mid-exponential phase to guarantee that culture was growing at its specific growth rate (μ) and that substrate was not limiting.

Moreover, the relative abundances of the mass isotopomers *(m+0)* to *(m+n)* of [¹³C] deoxynucleosides and [¹³C] nucleosides indicate the distinct turnover rates of their pools and/or of the pools of their precursors. The higher the relative abundances of the multi-labelled mass isotopomers, the higher the turnover rate of that pool. Among deoxynucleosides, deoxyadenosine presents the highest turnover rate, followed by deoxycytidine nucleobase moiety, by deoxyguanosine. Deoxythymidine nucleobase moiety and deoxyribose moiety have the slowest turnover rates. The *(m+5)* mass isotopomer of the nucleobase moiety of [¹³C] deoxythymidine, which is its *(m+n)*, has a much lower relative abundance than that of the *(m+4)*. One of the carbons of the nucleobase of deoxythymidine is the methyl substituent provided by one-carbon unit pools, which have a rather low turnover rate. Therefore, we hypothesize that at mid-exponential phase these pools were not fully enriched in ¹³C.

In uridine, adenosine and guanosine we observed fragments corresponding to the loss of the single carbon C5' (Figure 4.8 (1.c), 4.9 (2.b) and 4.11 (4.b)). In all the nucleosides we observed fragments corresponding to fragmentation of part of the ribose ring, keeping the *N*-glycosidic bond intact (Figure 4.8 (1.b) and (1.d), 4.9 (2.c), 4.10 (3.b), and 4.11 (4.c) and (4.d)). The fragmentation at the *N*-glycosidic bond is common to nucleosides and to the purine deoxynucleosides originating different fragments. We observed fragments retaining the whole ribose moiety (Figure 4.12 (1.e), (2.d), (3.d) and 4.11 (4.f)), fragments formed by the loss of C5' of the ribose moiety (Figure 4.12 (1.f), (2.e), (3.e) and (4.g)) and fragments keeping the nucleobase moiety (Figure 4.10 (3.c), 4.5 (4.e), and 4.14 (8.b) and (9.b)).

Though ions of the ribose and deoxyribose moieties smaller than 245 *m/z* and 157 *m/z* could be observed in the spectra, fragments could not be unequivocally assigned to them. This is a common difficulty when a fragment ion can be assigned distinct moieties of the molecule but having the same atom composition, thus the same chemical formula (Wegner *et al.*, 2014) and *m/z*. Hence, a high resolution accurate-mass MS system could not decipher it either. This difficulty can be overcome using selectively labeled molecules or using a MS/MS system. We also could not assign any fragment to nucleobase moieties, which prevented elucidation of their positional isotopomers.

The limited positional isotopomer resolution is overcome by the adequate choice of the ¹³C labelling pattern of the feeding substrate. Given a set of labelling and of metabolic fluxes for the involved pathways, the *in silico* simulations done with the metabolic computational model assist the choice of the ¹³C labelling pattern. Therefore, despite the incomplete resolution of positional isotopomers, the mass isotopomers of the assigned fragment ions[20] (Figure 4.15) provide rich information for qualitative appreciation of metabolic fluxes and for quantitative flux estimation.

---

[20] Fragment ions of nucleobase, ribose and deoxyribose moieties, and of moieties retaining the complete nucleobase and some ribose carbons.

5.2| METABOLIC PROFILES OF PROLIFERATING *S. CEREVISIAE*

We studied the metabolic profiles over the CDC of proliferating *S. cerevisiae* from the analysis of the ^{13}C isotopomers of deoxynucleosides and nucleosides of nDNA and cRNA, respectively. The ^{13}C tracer labelling pattern of the metabolites reflects the MFD at a given moment and it is passed to the deoxynucleosides and nucleosides. Therefore, the ^{13}C isotope tracing of deoxynucleosides and nucleosides becomes imprinted from that of their precursors at the moment of their biosynthesis. Acknowledging that nDNA is biosynthesized during S-phase of the CDC and RNA is biosynthesized during the other phases, the labelling pattern of deoxynucleosides report the MFD of S-phase and that of nucleosides report the MFD of the other phases. Moreover, the analysis of the ^{13}C tracing in the deoxynucleosides and nucleosides report back the activity of glycolysis, PPP, TCA cycle, PC, glyoxylate cycle and GSS. PPP fluxes, both the oxidative and the non-oxidative branch, are tracked in the isotopomers of the nucleoside fragments retaining ribose and deoxyribose moieties. The isotopomers of the nucleobase fragments of purines report the glycine-serine metabolic system (GSS). The GSS feeds purine nucleobase biosynthesis both directly *via* glycine and indirectly via FTHF. FTHF belongs to the one-carbon metabolism system and is in exchange with methyl tetrahydrofolate which is a product of serine conversion to glycine. The flux distribution between glycolysis and PPP, and between TCA cycle and pyruvate carboxylase (and glyoxylate cycle when present) is tracked in the MID of pyrimidine nucleobases.

The clearly different MID of deoxynucleosides and nucleosides from nDNA and cRNA, respectively, is evidence of the distinct MFD in S- and out of S-phase of the CDC.

We analyzed in detail the MID of deoxynucleosides, nucleosides and respective fragments, and inferred the ^{13}C isotopomers (*cf.* Chapter 4.2.2). In order to investigate how distinct are the MFD in S- and out of S-phases we followed three complementary approaches: i) ^{13}C isotopomer analysis to identify unique fingerprints; ii) comparative analysis of MID of equivalent fragments; iii) numeric exploration of forward simulation spectra. We predicted the ^{13}C isotopomer populations of extreme scenarios of MFD in order to identify unique fingerprints resulting from [1,2-^{13}C] glucose and the different arrays of such flux rates. This permitted univocally determine whether or not a pathway or a series of fluxes presented activity (*cf.* Chapter 3.2.1). The presence of [U-^{12}C] R5P and [1,2-^{13}C] R5P in deoxynucleosides and *(m+1)* and *(m+2)* in nucleobases of deoxypurines was evidence of activity of glycolysis and PPP$_{non-ox}$ backward during S-phase. The presence of $^{13}C1'$ in the R5P moiety of nucleosides gives evidence of activity of PPP$_{ox}$ out of S-phase. Furthermore, the presence of [1,4,5-^{13}C] R5P and [2,4,5-^{13}C] R5P in nucleosides, namely the $^{13}C5'$ is fingerprint for activity of shunting forward and backward in the PPP$_{non-ox}$ branch upon a partial feeding of the GA3P pool via glycolysis.

Furthermore, the comparison of the MID of equivalent fragments from deoxynucleosides and nucleosides was then confronted with the *in silico* MID trending from the forwards simulations. We found evidence supporting that in S-phase glycolysis rate is higher than the activity of PPP_{ox} whereas in the other phases PPP_{ox} activity is greater than that of glycolysis. The comparative activity of [TCA cycle vs PC] was not clear but there are evidences that TCA cycle flux rate is greater in S-phase than in the other phases.

From the numerical exploration of the forward simulations we found the *in silico* spectra in best agreement with the experimental MID. The set of fluxes originating the best agreement spectra reinforced the so far inferred metabolic profiles of S- and non-S-phase. Namely, the S-phase best agreeing spectra was obtained from a *gly1* flux rate of 4 fmol/h·cell and *ppp1* of 6 fmol/h·cell, the *tcc1* flux rate was 10 fmol/h·cell and that of *pf3* was 0.14 fmol/h·cell. In the other phases, the set of fluxes was *gly1* equal to 2 fmol/h·cell and *ppp1* equal to 8 fmol/h·cell, *tcc1* flux rate of 2 fmol/h·cell and *pf3* of 0.14 fmol/h·cell.

Lastly, we took those MFD as a feasible set of starting flux rates with which we proceeded to the flux estimation.

As an internal negative control for our approach to unveil metabolic heterogeneity over the CDC, we analyzed the MID of ribose moieties of mitochondrial nucleic acids. The biosynthesis of mtDNA and mtRNA is not specific of any phase of the CDC and occurs simultaneously. As expected, and validating our approach, the mtDNA deoxynucleosides and mtRNA nucleosides present the same MID. These results reinforce the notion that the observed labeling differences between deoxynucleosides obtained from nDNA and nucleosides obtained from cRNA are due to metabolic heterogeneity over the CDC.

The MID of the ribose moiety of mitochondrial nucleic acids is surprisingly different from that of the cRNA (Figure 4.21). This stark difference in MID is unexpected because mitochondrial biogenesis is assumed to be independent of CDC phases. The former MID shows a very high *(m+4)* fraction (>60%). Such high enrichment given a partially labeled substrate ([1,2-^{13}C] glucose) suggests that mitochondrial ribose may be formed *via* non-oxidative branch of PPP preceding from gluconeogenic precursors, e.g. pyruvate originated either from decarboxylation of malate and OAA pool of TCA cycle or secreted and taken up acetate. In fact, there are results showing that in asynchronous population there is no accumulation of acetate or ethanol in the extracellular milieus. Moreover, metabolomics studies in synchronized populations show cyclic oscillation of the extracellular concentration of acetate/ethanol (Murray, Beckmann and Kitano, 2007).

We show that in asynchronous proliferating *S. cerevisiae* culture during S-phase the highest fluxes were glycolysis, PPP_{non-ox} backward branch and TCA cycle flux. In the other phases the fluxes presenting greater activity were PPP_{ox} branch, shunting forward and backward in PPP_{non-ox} branch, whereas the flux though TCA cycle was reduced.

Proliferating cell metabolism is commonly known to be highly glycolytic towards production of ethanol or lactate (depending on the cell) and to have flux through the PPP_{ox} branch to support biosynthesis. The novelty we show here is that glycoysis and PPPox are indeed active but each presenting higher relative rates at distinct phases of the CDC. Moreover, we show evidence of considerable activity of TCA cycle rather than only fermentative metabolism. The results from mitochondrial nucleic acids suggest activity of gluconeogenesis from the precursors ^{13}C ethanol or ^{13}C acetate.

5.3| ANALYSIS OF THE METABOLIC HETEROGENEITY OVER THE CELL DIVISION CYCLE

The characterization of proliferating cell metabolism, namely of the MFD, is our leading scientific interest. This motivation frames the present work, which was triggered by the evidence of coupling between YMC and CDC. More precisely, there is accumulated knowledge that proliferating cells, particularly yeast, present cyclic oscillation in gene transcription and metabolome (YMC) which are also coupled to the CDC phases. Hence, we postulated that the metabolic oscillations observed in synchronized proliferating yeast cultures occur in individual, single cell in asynchronous proliferating cultures (*cf.* Chapter 1.3.2) – *constitutive oscillation hypothesis*.

With the methodology we developed and could address this hypothesis directly and without disturbing the MFD during S-phase and during the other phases of the CDC. The clear difference in the MID of deoxynucleosides and nucleosides in our results confirms the constitutive oscillation hypothesis, namely that the periodic oscilations occur at the single cell level in proliferation cell population despite no population level oscillations are observable. This is also consistent with the hypothesis (Tu *et al.*, 2005) that the CDC correlates in time with YMC. That is, there is a MFD characteristic and specific of certain phases of CDC. Namely, the synthesis of DNA occurs only when the MFD profile is high flux rate of glycolysis and TCA cycle and activity of the PPP_{non-ox} bckw branch.

G2 and G1 are phases described to be devoted to cell growth, therefore biomass biosynthesis. Biosynthesis activity during S phase is just ~1% of that in G1/G2 (Table 3.4 – 3.7). This justifies the observed anabolic MFD out of S-phase. The vast majority of biosynthetic precursors derive from metabolite pools of PPP and TCA cycle. Hence, the predominant activity of PPP, both oxidative and non-oxidative branch, forward and backward, and of PC observed during G2, M and G1 phases warrants the required precursors and reducing equivalents and energy.

Conversely, our results show that metabolism during S-phase is more oxidative-like, therefore more energetic. Glycolysis and TCA cycle present higher relative flux rates during biosynthesis of DNA. During replication DNA is especially prone to damage, particularly oxidative damage, thus, preventing DNA damage during replication is a leading concern. Therefore, we would expect DNA biosynthesis to require a non-oxidative environment. Nonetheless, cell counts with machinery to keep redox environment at the desirable equilibrium and to correct eventual damage. This machinery is highly demanding on ATP and reducing equivalents. Hence, our results show evidence that during S-phase and DNA replication the production of ATP for a readily and efficient redox control is privileged.

6| Outlook

A high priority to complete this work is to quantitatively estimate the fluxes by fitting the two-populations model to the experimental MIDs, which has so far proven difficult to achieve.

The accuracy of flux rate estimation can be improved by the following procedures. To perform ^{13}C tracing analyis of the extracellular metabolites in order to determine evaluate whether there is interchange between the extracellular and intracellular pools. To measure MID using a LC-MSMS system which will detect (deoxy)nucleosides fragments different from those detected by GC-MS. Furthermore it will also allow the univocal assignment of smaller fragments. To use the building blocks of other molecules such as histone amino acids for S-phase, amino acids from cyclins and lipids from membranes.

The problem of heterogeneity over the CDC and the metabolic profile in S-phase are particularly relevant for tumor biology. Proliferating human tumor cells spend a very large fraction of their CDC in S phase (Baserga R, 1965), and therefore a better understanding of the MFD in this phase may inform therapeutic approaches. Extension of the methodology presented in this thesis to mammalian cells is thus an enticing perspective.

7|References

Agrawal, P. *et al.* (1982) 'Theoretical investigations of dynamic behavior of isothermal continuous stirred tank biological reactors', *Chemical Engineering Science*. Pergamon, 37(3), pp. 453–462. doi: 10.1016/0009-2509(82)80098-5.

Ahmed, Z. *et al.* (2013) 'Software LS-MIDA for efficient mass isotopomer distribution analysis in metabolic modelling.', *BMC bioinformatics*, 14, p. 218. doi: 10.1186/1471-2105-14-218.

Antoniewicz, M. R., Kelleher, J. K. and Stephanopoulos, G. (2007) 'Accurate assessment of amino acid mass isotopomer distributions for metabolic flux analysis.', *Analytical chemistry*, 79(19), pp. 7554–9. doi: 10.1021/ac0708893.

Aon, M. A. *et al.* (2019) 'Synchrony and mutual stimulation of yeast cells during fast glycolytic oscillations', *Journal of General Microbiology*. Available at: www.microbiologyresearch.org (Accessed: 2 July 2019).

Asquith, B. *et al.* (2009) 'Lymphocyte kinetics in health and disease.', *Trends in immunology*, 30(4), pp. 182–9. doi: 10.1016/j.it.2009.01.003.

Bandyopadhyay, K. K. and Ghose, T. K. (1982) 'Studies on immobilizedSaccharomyces cerevisiae. III. Physiology of growth and metabolism on various supports', *Biotechnology and Bioengineering*, 24(4), pp. 805–815. doi: 10.1002/bit.260240405.

Baserga R (1965) 'The relationship of the cell cycle to tumour growth and control of cell division: a review', *Cancer research*, 25(5), p. 581.

Borzani, W., Gregori, R. E. and Vairo, M. L. R. (1977) 'Some observations on oscillatory changes in the growth rate ofSaccharomyces cerevisiae in aerobic continuous undisturbed culture', *Biotechnology and Bioengineering*. Wiley-Blackwell, 19(9), pp. 1363–1374. doi: 10.1002/bit.260190909.

Brook, A. (1974) 'No Title', *Acc Chemical Research*, 7, pp. 77–84.

Bruinenberg, P. M., Van Dijken, J. P. and Scheffers, W. a. (1983) 'A Theoretical Analysis of NADPH Production and Consumption in Yeasts', *Microbiology*, 129(4), pp. 953–964. doi: 10.1099/00221287-129-4-953.

Burnetti, A. J., Aydin, M. and Buchler, N. E. (2016) 'Cell cycle Start is coupled to entry into the yeast metabolic cycle across diverse strains and growth rates', *Molecular biology of the cell*, 27(1), pp. 64–74. doi: 10.1091/mbc.E15-07-0454.

Chandra, F. A., Buzi, G. and Doyle, J. C. (2011) 'Glycolytic Oscillations and Limits on Robust Efficiency', *Science*. American Association for the Advancement of Science, 333(6039), pp. 187–192. doi: 10.1126/SCIENCE.1200705.

Chen, C. and McDonald, K. A. (1990) 'Oscillatory behavior ofSaccharomyces cerevisiae in continuous culture: II. Analysis of cell synchronization and metabolism', *Biotechnology and Bioengineering*, 36(1), pp. 28–38. doi: 10.1002/bit.260360105.

Chen, Z. *et al.* (2007) 'Restriction of DNA replication to the reductive phase of the metabolic cycle protects genome integrity.', *Science (New York, N.Y.)*, 316(5833), pp. 1916–9. doi: 10.1126/science.1140958.

Choi, J. and Antoniewicz, M. R. (2011) 'Tandem mass spectrometry: a novel approach for metabolic flux analysis.', *Metabolic engineering*. Elsevier, 13(2), pp. 225–33. doi:

10.1016/j.ymben.2010.11.006.

Choi, J., Grossbach, M. T. and Antoniewicz, M. R. (2012) 'Measuring complete isotopomer distribution of aspartate using gas chromatography/tandem mass spectrometry.', *Analytical chemistry*, 84(10), pp. 4628–32. doi: 10.1021/ac300611n.

Christensen, B. and Nielsen, J. (1999) 'Isotopomer analysis using GC-MS.', *Metabolic engineering*, 1(4), pp. 282–90. doi: 10.1006/mben.1999.0117.

Cohen, A. *et al.* (1983) 'Purine and Pyrimidine Metabolism in Human T Lymphocytes', *Journal of Biological Chemistry*, 258, p. 12334.

Collart, M. A. and Oliviero, S. (2001) 'Preparation of yeast RNA.', *Current protocols in molecular biology / edited by Frederick M. Ausubel ... [et al.]*, Chapter 13, p. Unit13.12. doi: 10.1002/0471142727.mb1312s23.

Cooper, S. (2003) 'Rethinking synchronization of mammalian cells for cell cycle analysis', *Cellular and molecular life sciences : CMLS*, 60(6), pp. 1099–1106. doi: 10.1007/s00018-003-2253-2.

Daran-Lapujade, P. *et al.* (2004) 'Role of Transcriptional Regulation in Controlling Fluxes in Central Carbon Metabolism of Saccharomyces cerevisiae: A CHEMOSTAT CULTURE STUDY', *Journal of Biological Chemistry*. AMER SOC BIOCHEMISTRY MOLECULAR BIOLOGY INC, 9650 ROCKVILLE PIKE, BETHESDA, MD 20814-3996 USA, 279(10), pp. 9125–9138. doi: 10.1074/jbc.M309578200.

DeBerardinis, R. J. *et al.* (2008) 'Brick by brick: metabolism and tumor cell growth', *Current Opinion in Genetics & Development*. Elsevier Current Trends, 18(1), pp. 54–61. doi: 10.1016/J.GDE.2008.02.003.

Deberardinis, R. J. and Chandel, N. S. (2016) 'Fundamentals of cancer metabolism: introduction and overarching principles', *Advancement of Science*, (2), p. e1600200. doi: 10.1126/sciadv.1600200.

Defoiche, J. *et al.* (2009) 'Measurement of ribosomal RNA turnover in vivo by use of deuterium-labeled glucose.', *Clinical chemistry*, 55(10), pp. 1824–33. doi: 10.1373/clinchem.2008.119446.

Defontaine, A., Lecocq, F. M. and Hallet, J. N. (1991) 'A rapid miniprep method for the preparation of yeast mitochondrial DNA', *Nucleic Acids Research*. Narnia, 19(1), pp. 185–185. doi: 10.1093/nar/19.1.185.

Droste, P. *et al.* (2011) 'Visualizing multi-omics data in metabolic networks with the software Omix-A case study', *BioSystems*. Elsevier Ireland Ltd, 105(2), pp. 154–161. doi: 10.1016/j.biosystems.2011.04.003.

Finn, R. K. and Wilson, R. E. (1954) 'Fermentation Process Control, Population Dynamics of a Continuous Propagator for Microorganisms', *Journal of Agricultural and Food Chemistry*. American Chemical Society, 2(2), pp. 66–69. doi: 10.1021/jf60022a003.

Förster, J. *et al.* (2003a) 'Genome-scale reconstruction of the Saccharomyces cerevisiae metabolic network.', *Genome research*. Cold Spring Harbor Laboratory Press, 13(2), pp. 244–53. doi: 10.1101/gr.234503.

Förster, J. *et al.* (2003b) 'Genome-scale reconstruction of the Saccharomyces cerevisiae metabolic network.', *Genome research*, 13(2), pp. 244–53. doi: 10.1101/gr.234503.

Frick, O. and Wittmann, C. (2005) 'Characterization of the metabolic shift between oxidative and fermentative growth in Saccharomyces cerevisiae by comparative 13C flux analysis', *Microbial Cell Factories*, 4(1), p. 30. doi: 10.1186/1475-2859-4-30.

Furukawa, K., Heinzle, E. and Dunn, I. J. (1983) 'Influence of oxygen on the growth of Saccharomyces cerevisiae in continuous culture.', *Biotechnology and bioengineering*, 25(10), pp. 2293–2317. doi: 10.1002/bit.260251003.

Gombert, A. K. *et al.* (2001) 'Network identification and flux quantification in the central metabolism of Saccharomyces cerevisiae under different conditions of glucose repression.', *Journal of bacteriology*, 183(4), pp. 1441–51. doi: 10.1128/JB.183.4.1441-1451.2001.

Gustavsson, A.-K. *et al.* (2014) 'Heterogeneity of glycolytic oscillatory behaviour in individual yeast cells', *FEBS Letters*, 588(1), pp. 3–7. doi: 10.1016/j.febslet.2013.11.028.

von der Haar, T. (2008) 'A quantitative estimation of the global translational activity in logarithmically growing yeast cells.', *BMC systems biology*, 2(1), p. 87. doi: 10.1186/1752-0509-2-87.

Hans, M. A., Heinzle, E. and Wittmann, C. (2003) 'Free intracellular amino acid pools during autonomous oscillations in Saccharomyces cerevisiae', *Biotechnology and Bioengineering*, 82(2), pp. 143–151. doi: 10.1002/bit.10553.

Harrison, D. E. F. and Topiwala, H. H. (1974) 'Transient and oscillatory states of continuous culture', in. Springer, Berlin, Heidelberg, pp. 167–219. doi: 10.1007/3-540-06546-6_6.

Vander Heiden, M. G., Cantley, L. C. and Thompson, C. B. (2009) 'Understanding the Warburg effect: the metabolic requirements of cell proliferation.', *Science*. American Association for the Advancement of Science, 324(5930), pp. 1029–33. doi: 10.1126/science.1160809.

Heinzle, E. *et al.* (1983) 'Modelling of sustained oscillations observed in continuous culture of saccharomyces cerevisiae', *Modelling and COntrol of Biotechnical Processes*, p. 57. doi: 10.1016/B978-0-08-029978-5.50012-4.

Ho, D. D. *et al.* (1995) 'Rapid turnover of plasma virions and CD4 lymphocytes in HIV-1 infection.', *Nature*. Nature Publishing Group, 373(6510), pp. 123–6. doi: 10.1038/373123a0.

Holm, C. *et al.* (1986) 'A rapid, efficient method for isolating DNA from yeast', *Gene*, 42(2), pp. 169–173. doi: 10.1016/0378-1119(86)90293-3.

Hsu, P. P. and Sabatini, D. M. (2008) 'Cancer Cell Metabolism: Warburg and Beyond', *Cell*. Cell Press, 134(5), pp. 703–707. doi: 10.1016/J.CELL.2008.08.021.

Kanehisa, M. and Goto, S. (2000) 'KEGG: kyoto encyclopedia of genes and genomes.', *Nucleic acids research*, 28(1), pp. 27–30. Available at: http://www.ncbi.nlm.nih.gov/pubmed/10592173 (Accessed: 30 August 2018).

Kaspar von Meyenburg, H. (1969) 'Energetics of the budding cycle of Saccharomyces cerevisiae during glucose limited aerobic growth', *Archiv fuer Mikrobiologie*, 66(4), pp. 289–303. doi: 10.1007/BF00414585.

Kaspar von Meyenburg, H. (1973) 'Stable synchrony oscillations in continuous cultures of saccharomyces cerevisiae under glucose limitation', *Biological and Biochemical Oscillators*. Academic Press, pp. 411–417. doi: 10.1016/B978-0-12-167872-2.50036-4.

Klevecz, R. R. *et al.* (2004) 'A genomewide oscillation in transcription gates DNA replication and cell cycle.', *Proceedings of the National Academy of Sciences of the United States of America*, 101(5), pp. 1200–5. doi: 10.1073/pnas.0306490101.

Lai, Z., Kind, T. and Fiehn, O. (2017) 'Using Accurate Mass Gas Chromatography–Mass Spectrometry with the MINE Database for Epimetabolite Annotation', *Analytical Chemistry*. American Chemical Society, 89(19), pp. 10171–10180. doi: 10.1021/acs.analchem.7b01134.

Lange, H. C. and Heijnen, J. J. (2001) 'Statistical reconciliation of the elemental and molecular biomass composition of Saccharomyces cerevisiae', *Biotechnology and Bioengineering*, 75(3), pp. 334–344. doi: 10.1002/bit.10054.

Lunt, S. Y. and Vander Heiden, M. G. (2011) 'Aerobic Glycolysis: Meeting the Metabolic Requirements of Cell Proliferation', *Annu. Rev. Cell Dev. Biol*, 27, pp. 441–464. doi: 10.1146/annurev-cellbio-092910-154237.

Macallan, D. C. *et al.* (2009) 'Measurement of proliferation and disappearance of rapid turnover cell populations in human studies using deuterium-labeled glucose.', *Nature protocols*. Nature Publishing Group, 4(9), pp. 1313–27. doi: 10.1038/nprot.2009.117.

Malloy, C. R. *et al.* (1987) 'Carbon flux through citric acid cycle pathways in perfused heart by 13C NMR spectroscopy'. Available at: https://febs.onlinelibrary.wiley.com/doi/pdf/10.1016/0014-5793%2887%2981556-9 (Accessed: 13 August 2018).

Miccheli, A. *et al.* (2006a) 'Metabolic profiling by 13C-NMR spectroscopy: [1,2-13C2]glucose reveals a heterogeneous metabolism in human leukemia T cells', *Biochimie*. Elsevier, 88(5), pp. 437–448. doi: 10.1016/J.BIOCHI.2005.10.004.

Miccheli, A. *et al.* (2006b) 'Metabolic profiling by 13C-NMR spectroscopy: [1,2-13C2]glucose reveals a heterogeneous metabolism in human leukemia T cells', *Biochimie*. Elsevier, 88(5), pp. 437–448. doi: 10.1016/J.BIOCHI.2005.10.004.

Miranda-Santos, I. *et al.* (2015) 'Mass Isotopomer Analysis of Nucleosides Isolated from RNA and DNA Using GC/MS.', *Analytical chemistry*, 87(1), pp. 617–23. doi: 10.1021/ac503305w.

De Monte, S. *et al.* (2007) 'Dynamical quorum sensing: Population density encoded in cellular dynamics'. Available at: www.pnas.orgcgidoi10.1073pnas.0706089104 (Accessed: 2 July 2019).

Murray, D. B. *et al.* (1999) 'Involvement of glutathione in the regulation of respiratory oscillation during a continuous culture of Saccharomyces cerevisiae', *Microbiology*. Microbiology Society, 145(10), pp. 2739–2745. doi: 10.1099/00221287-145-10-2739.

Murray, D. B., Beckmann, M. and Kitano, H. (2007) 'Regulation of yeast oscillatory dynamics.', *Proceedings of the National Academy of Sciences of the United States of America*, 104(7), pp. 2241–6. doi: 10.1073/pnas.0606677104.

Nöh, K., Droste, P. and Wiechert, W. (2015) 'Visual workflows for 13C-metabolic flux analysis.', *Bioinformatics (Oxford, England)*, 31(3), pp. 346–354. doi: 10.1093/bioinformatics/btu585.

Orata, F. (2012) 'Derivatization reactions and reagents for gas chromatography analysis', *Advanced Gas Chromatography*. Edited by M. A. Mohd. InTech. Available at: http://forensicscienceeducation.org/wp-content/uploads/2013/02/Analytical-derivatization-.pdf (Accessed: 22 May 2014).

Otero, J. M. *et al.* (2010) 'Whole genome sequencing of Saccharomyces cerevisiae: from genotype to phenotype for improved metabolic engineering applications.', *BMC genomics*. BioMed Central Ltd, 11(1), p. 723. doi: 10.1186/1471-2164-11-723.

Pavlova, N. N. and Thompson, C. B. (2016) 'The Emerging Hallmarks of Cancer Metabolism', *Cell Metabolism*, 23(1), pp. 27–47. doi: 10.1016/j.cmet.2015.12.006.

Porro, D. *et al.* (1988) 'Oscillations in continuous cultures of budding yeast: A segregated parameter analysis', *Biotechnology and Bioengineering*, 32(4), pp. 411–417. doi: 10.1002/bit.260320402.

Poulsen, A. K., Petersen, M. Ø. and Olsen, L. F. (2007) 'Single cell studies and simulation of cell–cell interactions using oscillating glycolysis in yeast cells', *Biophysical Chemistry*. Elsevier, 125(2–

3), pp. 275–280. doi: 10.1016/J.BPC.2006.08.009.

Quinlivan, E. P. and Gregory, J. F. (2008) 'DNA digestion to deoxyribonucleoside: a simplified one-step procedure.', *Analytical biochemistry*, 373(2), pp. 383–5. doi: 10.1016/j.ab.2007.09.031.

Rao, A. R. and Pellegrini, M. (2011) 'Regulation of the yeast metabolic cycle by transcription factors with periodic activities', *BMC Systems Biology*, 5, p. 160. doi: 10.1186/1752-0509-5-160.

Rühl, M. *et al.* (2012) 'Collisional fragmentation of central carbon metabolites in LC-MS/MS increases precision of ^{13}C metabolic flux analysis.', *Biotechnology and bioengineering*, 109(3), pp. 763–71. doi: 10.1002/bit.24344.

Satroutdinov, A. D., Kuriyama, H. and Kobayashi, H. (1992) 'Oscillatory metabolism of Saccharomyces cerevisiae in continuous culture.', *FEMS microbiology letters*, 77(1–3), pp. 261–7. Available at: http://www.ncbi.nlm.nih.gov/pubmed/1334018 (Accessed: 18 June 2014).

Sauer, U. (2006) 'Metabolic networks in motion: 13C-based flux analysis.', *Molecular systems biology*. EMBO Press, 2(1), p. 62. doi: 10.1038/msb4100109.

Savinell, J. M. and Palsson, B. O. (1992) 'Optimal selection of metabolic fluxes for in vivo measurement. I. Development of mathematical methods', *Journal of Theoretical Biology*, 155(2), pp. 201–214. doi: 10.1016/S0022-5193(05)80595-8.

Schneider, K. (2011) 'Auswirkungen der MAE1-Gendeletion auf den Zentralstoffwechsel von Saccharomyces cerevisiae unter verschiedenen Physiologien', pp. 1–311.

Shupletsov, M. S. *et al.* (2014) 'OpenFLUX2: 13C-MFA modeling software package adjusted for the comprehensive analysis of single and parallel labeling experiments', *Microbial Cell Factories*, 13(1), pp. 1–25. doi: 10.1186/s12934-014-0152-x.

Silverman, S. J. *et al.* (2010) 'Metabolic cycling in single yeast cells from unsynchronized steady-state populations limited on glucose or phosphate', *Proceedings of the National Academy of Sciences*, 107, pp. 6946–6951. doi: 10.1073/pnas.1002422107.

Slavov, N. *et al.* (2011) 'Metabolic cycling without cell division cycling in respiring yeast', *Proceedings of the National Academy of Sciences*, 108(47), pp. 19090–19095. doi: 10.1073/pnas.1116998108.

Slavov, N. and Botstein, D. (2011) 'Coupling among growth rate response, metabolic cycle, and cell division cycle in yeast.', *Molecular biology of the cell*, 22(12), pp. 1997–2009. doi: 10.1091/mbc.E11-02-0132.

T.Gregg, C. *et al.* (1973) 'Substantial replacement of mammalian body carbon with carbon-13', *Life Sciences*, 13(7), pp. 775–782. doi: https://doi.org/10.1016/0024-3205(73)90068-4.

Tu, B. P. *et al.* (2005) 'Logic of the Yeast Metabolic Cycle ':, *Science (New York, N.Y.)*, 310(November), pp. 1152–1158.

Tu, B. P. *et al.* (2007) 'Cyclic changes in metabolic state during the life of a yeast cell.', *Proceedings of the National Academy of Sciences of the United States of America*, 104(43), pp. 16886–91. doi: 10.1073/pnas.0708365104.

Tummler, K., Kühn, C. and Klipp, E. (2015) 'Dynamic metabolic models in context: biomass backtracking', *Integr. Biol.*, 7(8), pp. 940–951. doi: 10.1039/C5IB00050E.

Vallino, J. J. and Stephanopoulos, G. (1993) 'Metabolic Flux Distributions in Corynebacterium glutamicum During Growth and Lysine Overproduction', 41, pp. 633–646.

Varma, A. and Palsson, B. O. (1993) 'Metabolic capabilities of E. coli: I. synthesis of biosynthetic precursors and cofactors', *Journal of Theoretical Biology*, 165, p. 477.

Velagapudi, V. R. *et al.* (2006) 'Metabolic screening of Saccharomyces cerevisiae single knockout strains reveals unexpected mobilization of metabolic potential', *Process Biochemistry*, 41(10), pp. 2170–2179. doi: 10.1016/j.procbio.2006.06.016.

Verduyn, C. (1991) 'Physiology of yeasts in relation to biomass yields.', *Antonie van Leeuwenhoek*, 60(3–4), pp. 325–353. doi: 10.1007/BF00430373.

Verduyn, C. *et al.* (1992) 'Effect of benzoic acid on metabolic fluxes in yeasts: a continuous-culture study on the regulation of respiration and alcoholic fermentation.', *Yeast (Chichester, England)*, 8(7), pp. 501–17. doi: 10.1002/yea.320080703.

Warburg, O. (1924) 'Über den Stoffwechsel der Carcinomzelle', *Die Naturwissenschaften*, 12(50), pp. 1131–1137. doi: 10.1007/BF01504608.

Warburg, O. (1956) 'On the origin of cancer cells.', *Science (New York, N.Y.)*, 123(3191), pp. 309–14. Available at: http://www.ncbi.nlm.nih.gov/pubmed/13298683.

Wegner, A. *et al.* (2014) 'Fragment formula calculator (FFC): determination of chemical formulas for fragment ions in mass spectrometric data.', *Analytical chemistry*, 86(4), pp. 2221–8. doi: 10.1021/ac403879d.

Wei, X. *et al.* (1995) 'Viral dynamics in human immunodeficiency virus type 1 infection.', *Nature*, 373(6510), pp. 117–22. doi: 10.1038/373117a0.

Weitzel, M. *et al.* (2013) '13CFLUX2--high-performance software suite for (13)C-metabolic flux analysis.', *Bioinformatics (Oxford, England)*, 29(1), pp. 143–5. doi: 10.1093/bioinformatics/bts646.

Wiechert, W. *et al.* (1997) 'Bidirectional reaction steps in metabolic networks .2. Flux estimation and statistical analysis', *Biotechnology and Bioengineering*, 55, pp. 118–135. doi: 10.1002/(SICI)1097-0290(19970705)55:1<118::AID-BIT13>3.0.CO;2-I.

Wiechert, W. *et al.* (1999) 'Bidirectional reaction steps in metabolic networks: III. Explicit solution and analysis of isotopomer labeling systems.', *Biotechnology and bioengineering*, 66(2), pp. 69–85. Available at: http://www.ncbi.nlm.nih.gov/pubmed/10567066.

Wiechert, W. (2001) '13C metabolic flux analysis.', *Metabolic engineering*, 3(3), pp. 195–206. doi: 10.1006/mben.2001.0187.

Wiechert, W. *et al.* (2001) 'A Universal Framework for 13C Metabolic Flux Analysis', *Metabolic Engineering*, 3(3), pp. 265–283. doi: 10.1006/mben.2001.0188.

Wiechert, W. (2007) 'The Thermodynamic Meaning of Metabolic Exchange Fluxes'. doi: 10.1529/biophysj.106.099895.

Wiechert, W. and de Graaf, a a (1996) 'In vivo stationary flux analysis by 13C labeling experiments.', *Advances in biochemical engineering/biotechnology*, 54, pp. 109–154. doi: 10.1007/BFb0102334.

Wiechert, W. and Graaf, A. a (1997) 'Bidirectional Reaction Steps in Metabolic Networks Part I : Modelling and Simulation of Carbon Isotope Labelling Experiments', *Biotechnol. Bioeng.*, 5, pp. 101–117.

van Winden, W. a *et al.* (2002) 'Correcting mass isotopomer distributions for naturally occurring isotopes.', *Biotechnology and bioengineering*, 80(4), pp. 477–9. doi: 10.1002/bit.10393.

van Winden, W. a *et al.* (2005) 'Metabolic-flux analysis of Saccharomyces cerevisiae CEN.PK113-7D based on mass isotopomer measurements of (13)C-labeled primary metabolites.', *FEMS yeast research*, 5(6–7), pp. 559–68. doi: 10.1016/j.femsyr.2004.10.007.

Wittmann, C., Hans, M. and Heinzle, E. (2002) 'In vivo analysis of intracellular amino acid labelings by GC/MS.', *Analytical biochemistry*, 307(2), pp. 379–82. Available at: http://www.ncbi.nlm.nih.gov/pubmed/12202258.

Wittmann, C. and Heinzle, E. (1999) 'Mass spectrometry for metabolic flux analysis.', *Biotechnology and bioengineering*, 62(6), pp. 739–750. doi: 10.1002/(SICI)1097-0290(19990320)62:6<739::AID-BIT13>3.0.CO;2-E.

Zamboni, N. *et al.* (2009) '(13)C-based metabolic flux analysis.', *Nature protocols*. Nature Publishing Group, 4(6), pp. 878–92. doi: 10.1038/nprot.2009.58.

Zamboni, N., Fischer, E. and Sauer, U. (2005) 'FiatFlux--a software for metabolic flux analysis from 13C-glucose experiments.', *BMC bioinformatics*, 6, p. 209. doi: 10.1186/1471-2105-6-209.

8|Supplementary information

8.1| XML SCRIPT OF SIMPLIFIED MODEL "ONE POPULATION"

XML for 13CFlux2 suite.

```xml
<?xml version="1.0" encoding="UTF-8"?>
<fluxml xmlns="http://www.13cflux.net/fluxml"
xmlns:xsi="http://www.w3.org/2001/XMLSchema-instance"
xsi:schemaLocation="http://www.13cflux.net/fluxml
http://www.13cflux.net/fluxml">
  <info>
    <name>single population</name>
    <date>2019-10-10 15:37:12</date>
  </info>
  <reactionnetwork>
    <metabolitepools>
      <pool atoms="3" id="_3PG">
        <annotation name="name">3PG</annotation>
      </pool>
      <pool atoms="9" id="AICAR"/>
      <pool atoms="8" id="AIR"/>
      <pool atoms="2" id="AcCoA"/>
      <pool atoms="6" id="CITICIT"/>
      <pool atoms="1" id="CO2"/>
      <pool atoms="1" id="CTHF">
        <annotation name="kegg.compound">C00143</annotation>
      </pool>
      <pool atoms="3" id="DHAP"/>
      <pool atoms="4" id="Ery4P"/>
      <pool atoms="6" id="Fru6P"/>
      <pool atoms="6" id="FruBP"/>
      <pool atoms="3" id="GA3P"/>
      <pool atoms="7" id="GAR"/>
      <pool atoms="6" id="GLC"/>
      <pool atoms="2" id="GLY"/>
      <pool atoms="6" id="Glc6P"/>
      <pool atoms="4" id="MAL"/>
      <pool atoms="4" id="OAA"/>
      <pool atoms="5" id="ORO"/>
      <pool atoms="3" id="PEP"/>
      <pool atoms="3" id="PYR"/>
      <pool atoms="5" id="Rib5P"/>
      <pool atoms="5" id="Rul5P"/>
      <pool atoms="3" id="SER"/>
      <pool atoms="7" id="Sed7P"/>
      <pool atoms="2" id="ThPPGA"/>
      <pool atoms="9" id="PYRD"/>
      <pool atoms="5" id="Xyl5P"/>
      <pool atoms="10" id="PUR"/>
      <pool atoms="5" id="OGLU"/>
      <pool atoms="6" id="GLC12"/>
      <pool atoms="6" id="TreGalGlyc"/>
      <pool atoms="2" id="Acet_EtOH">
        <annotation name="name">Acet/EtOH</annotation>
      </pool>
      <pool atoms="1" id="CO2out"/>
```

```
        <pool atoms="10" id="TMP"/>
        <pool atoms="2" id="AA14"/>
        <pool atoms="2" id="AA15"/>
        <pool atoms="4" id="AA8"/>
        <pool atoms="2" id="Glxlate"/>
    </metabolitepools>
    <reaction bidirectional="false" id="upt">
      <annotation name="pathway">Glucose Input </annotation>
      <reduct cfg="C#1@1 C#2@1 C#3@1 C#4@1 C#5@1 C#6@1" id="GLC"/>
      <rproduct cfg="C#1@1 C#2@1 C#3@1 C#4@1 C#5@1 C#6@1" id="Glc6P"/>
    </reaction>
    <reaction id="gly1">
      <annotation name="pathway">Glycolysis</annotation>
      <reduct cfg="C#1@1 C#2@1 C#3@1 C#4@1 C#5@1 C#6@1" id="Glc6P"/>
      <rproduct cfg="C#1@1 C#2@1 C#3@1 C#4@1 C#5@1 C#6@1" id="Fru6P"/>
    </reaction>
    <reaction id="gly2">
      <annotation name="pathway">Glycolysis</annotation>
      <reduct cfg="C#1@1 C#2@1 C#3@1 C#4@1 C#5@1 C#6@1" id="Fru6P"/>
      <rproduct cfg="C#1@1 C#2@1 C#3@1 C#4@1 C#5@1 C#6@1" id="FruBP"/>
    </reaction>
    <reaction id="gly3">
      <annotation name="pathway">Glycolysis</annotation>
      <reduct cfg="C#1@1 C#2@1 C#3@1 C#4@1 C#5@1 C#6@1" id="FruBP"/>
      <rproduct cfg="C#4@1 C#5@1 C#6@1" id="GA3P"/>
      <rproduct cfg="C#1@1 C#2@1 C#3@1" id="DHAP"/>
    </reaction>
    <reaction id="gly4">
      <annotation name="pathway">Glycolysis</annotation>
      <reduct cfg="C#1@1 C#2@1 C#3@1" id="DHAP"/>
      <rproduct cfg="C#3@1 C#2@1 C#1@1" id="GA3P"/>
    </reaction>
    <reaction id="gly5">
      <annotation name="pathway">Glycolysis</annotation>
      <reduct cfg="C#1@1 C#2@1 C#3@1" id="GA3P"/>
      <rproduct cfg="C#1@1 C#2@1 C#3@1" id="_3PG"/>
    </reaction>
    <reaction id="gly6">
      <annotation name="pathway">Glycolysis</annotation>
      <reduct cfg="C#1@1 C#2@1 C#3@1" id="_3PG"/>
      <rproduct cfg="C#1@1 C#2@1 C#3@1" id="PEP"/>
    </reaction>
    <reaction bidirectional="false" id="gly7">
      <annotation name="pathway">Glycolysis</annotation>
      <reduct cfg="C#1@1 C#2@1 C#3@1" id="PEP"/>
      <rproduct cfg="C#1@1 C#2@1 C#3@1" id="PYR"/>
    </reaction>
    <reaction bidirectional="false" id="ppp1">
      <annotation name="pathway">Pentose Phosphate Pathway </annotation>
      <reduct cfg="C#1@1 C#2@1 C#3@1 C#4@1 C#5@1 C#6@1" id="Glc6P"/>
      <rproduct cfg="C#1@1" id="CO2"/>
      <rproduct cfg="C#2@1 C#3@1 C#4@1 C#5@1 C#6@1" id="Rul5P"/>
    </reaction>
    <reaction id="ppp2">
      <annotation name="pathway">Pentose Phosphate Pathway </annotation>
      <reduct cfg="C#1@1 C#2@1 C#3@1 C#4@1 C#5@1" id="Rul5P"/>
      <rproduct cfg="C#1@1 C#2@1 C#3@1 C#4@1 C#5@1" id="Xyl5P"/>
    </reaction>
```

```
<reaction id="ppp3">
  <annotation name="pathway">Pentose Phosphate Pathway </annotation>
  <reduct cfg="C#1@1 C#2@1 C#3@1 C#4@1 C#5@1" id="Rul5P"/>
  <rproduct cfg="C#1@1 C#2@1 C#3@1 C#4@1 C#5@1" id="Rib5P"/>
</reaction>
<reaction id="ppp4">
  <annotation name="pathway">Pentose Phosphate Pathway </annotation>
  <reduct cfg="C#1@1 C#2@1 C#3@1 C#4@1 C#5@1" id="Xyl5P"/>
  <rproduct cfg="C#3@1 C#4@1 C#5@1" id="GA3P"/>
  <rproduct cfg="C#1@1 C#2@1" id="ThPPGA"/>
</reaction>
<reaction id="ppp5">
  <annotation name="pathway">Pentose Phosphate Pathway </annotation>
  <reduct cfg="C#1@1 C#2@1 C#3@1 C#4@1 C#5@1" id="Rib5P"/>
  <reduct cfg="C#1@2 C#2@2" id="ThPPGA"/>
  <rproduct cfg="C#1@2 C#2@2 C#1@1 C#2@1 C#3@1 C#4@1 C#5@1" id="Sed7P"/>
</reaction>
<reaction id="ppp6">
  <annotation name="pathway">Pentose Phosphate Pathway </annotation>
  <reduct cfg="C#1@1 C#2@1 C#3@1 C#4@1 C#5@1 C#6@1 C#7@1" id="Sed7P"/>
  <reduct cfg="C#1@2 C#2@2 C#3@2" id="GA3P"/>
  <rproduct cfg="C#4@1 C#5@1 C#6@1 C#7@1" id="Ery4P"/>
  <rproduct cfg="C#1@1 C#2@1 C#3@1 C#1@2 C#2@2 C#3@2" id="Fru6P"/>
</reaction>
<reaction id="ppp7">
  <annotation name="pathway">Pentose Phosphate Pathway </annotation>
  <reduct cfg="C#1@1 C#2@1 C#3@1 C#4@1" id="Ery4P"/>
  <reduct cfg="C#1@2 C#2@2" id="ThPPGA"/>
  <rproduct cfg="C#1@2 C#2@2 C#1@1 C#2@1 C#3@1 C#4@1" id="Fru6P"/>
</reaction>
<reaction bidirectional="false" id="pf1">
  <annotation name="pathway">Pyruvate Fate</annotation>
  <reduct cfg="C#1@1 C#2@1 C#3@1" id="PYR"/>
  <rproduct cfg="C#2@1 C#3@1" id="AcCoA"/>
  <rproduct cfg="C#1@1" id="CO2"/>
</reaction>
<reaction bidirectional="false" id="pf2">
  <annotation name="pathway">Pyruvate Fate</annotation>
  <reduct cfg="C#1@1 C#2@1 C#3@1" id="PYR"/>
  <rproduct cfg="C#1@1" id="CO2"/>
  <rproduct cfg="C#2@1 C#3@1" id="Acet_EtOH"/>
</reaction>
<reaction bidirectional="false" id="acs">
  <annotation name="pathway">Pyruvate Fate</annotation>
  <reduct cfg="C#1@1 C#2@1" id="Acet_EtOH"/>
  <rproduct cfg="C#1@1 C#2@1" id="AcCoA"/>
</reaction>
<reaction bidirectional="false" id="pf3">
  <annotation name="pathway">Pyruvate Fate</annotation>
  <reduct cfg="C#1@1 C#2@1 C#3@1" id="PYR"/>
  <reduct cfg="C#1@2" id="CO2"/>
  <rproduct cfg="C#1@1 C#2@1 C#3@1 C#1@2" id="OAA"/>
</reaction>
<reaction id="tcc1">
  <annotation name="pathway">TCAcycle</annotation>
  <reduct cfg="C#1@1 C#2@1 C#3@1 C#4@1" id="OAA"/>
  <reduct cfg="C#1@2 C#2@2" id="AcCoA"/>
  <rproduct cfg="C#4@1 C#3@1 C#2@1 C#2@2 C#1@2 C#1@1" id="CITICIT"/>
```

```
    </reaction>
    <reaction id="tcc2">
      <annotation name="pathway">TCAcycle</annotation>
      <reduct cfg="C#1@1 C#2@1 C#3@1 C#4@1 C#5@1 C#6@1" id="CITICIT"/>
      <rproduct cfg="C#6@1" id="CO2"/>
      <rproduct cfg="C#1@1 C#2@1 C#3@1 C#4@1 C#5@1" id="OGLU"/>
    </reaction>
    <reaction id="tcc4">
      <annotation name="pathway">TCAcycle</annotation>
      <reduct cfg="C#1@1 C#2@1 C#3@1 C#4@1" id="MAL"/>
      <rproduct cfg="C#1@1 C#2@1 C#3@1 C#4@1" id="OAA"/>
    </reaction>
    <reaction bidirectional="false" id="gss1">
      <annotation name="pathway">Glycine/Serine System </annotation>
      <reduct cfg="C#1@1 C#2@1 C#3@1" id="_3PG"/>
      <rproduct cfg="C#1@1 C#2@1 C#3@1" id="SER"/>
    </reaction>
    <reaction id="gss2">
      <annotation name="pathway">Glycine/Serine System </annotation>
      <reduct cfg="C#1@1 C#2@1 C#3@1" id="SER"/>
      <rproduct cfg="C#1@1 C#2@1" id="GLY"/>
      <rproduct cfg="C#3@1" id="CTHF"/>
    </reaction>
    <reaction id="gss3">
      <annotation name="pathway">Glycine/Serine System </annotation>
      <reduct cfg="C#1@1" id="CTHF"/>
      <reduct cfg="C#1@2" id="CO2"/>
      <rproduct cfg="C#1@2 C#1@1" id="GLY"/>
    </reaction>
    <reaction bidirectional="false" id="texc1">
      <annotation name="pathway">TCAcycle exchanges</annotation>
      <reduct cfg="C#1@1 C#2@1 C#3@1 C#4@1" id="OAA"/>
      <rproduct cfg="C#1@1 C#2@1 C#3@1" id="PEP"/>
      <rproduct cfg="C#4@1" id="CO2"/>
    </reaction>
    <reaction bidirectional="false" id="texc2">
      <annotation name="pathway">TCAcycle exchanges</annotation>
      <reduct cfg="C#1@1 C#2@1 C#3@1 C#4@1" id="MAL"/>
      <rproduct cfg="C#1@1 C#2@1 C#3@1" id="PYR"/>
      <rproduct cfg="C#4@1" id="CO2"/>
    </reaction>
    <reaction bidirectional="false" id="purb1">
      <annotation name="pathway">PURine Biosynthesis </annotation>
      <reduct cfg="C#1@1 C#2@1 C#3@1 C#4@1 C#5@1" id="Rib5P"/>
      <reduct cfg="C#1@2 C#2@2" id="GLY"/>
      <rproduct cfg="C#1@2 C#2@2 C#1@1 C#2@1 C#3@1 C#4@1 C#5@1" id="GAR"/>
    </reaction>
    <reaction bidirectional="false" id="purb2">
      <annotation name="pathway">PURine Biosynthesis </annotation>
      <reduct cfg="C#1@1 C#2@1 C#3@1 C#4@1 C#5@1 C#6@1 C#7@1" id="GAR"/>
      <reduct cfg="C#1@2" id="CTHF"/>
      <rproduct cfg="C#1@1 C#2@1 C#1@2 C#3@1 C#4@1 C#5@1 C#6@1 C#7@1"
id="AIR"/>
    </reaction>
    <reaction bidirectional="false" id="purb3">
      <annotation name="pathway">PURine Biosynthesis </annotation>
      <reduct cfg="C#1@1 C#2@1 C#3@1 C#4@1 C#5@1 C#6@1 C#7@1 C#8@1" id="AIR"/>
      <reduct cfg="C#1@2" id="CO2"/>
```

```
      <rproduct cfg="C#1@1 C#2@1 C#1@2 C#3@1 C#4@1 C#5@1 C#6@1 C#7@1 C#8@1"
id="AICAR"/>
    </reaction>
    <reaction bidirectional="false" id="purb4">
      <annotation name="pathway">PURine Biosynthesis </annotation>
      <reduct cfg="C#1@1 C#2@1 C#3@1 C#4@1 C#5@1 C#6@1 C#7@1 C#8@1 C#9@1"
id="AICAR"/>
      <reduct cfg="C#1@2" id="CTHF"/>
      <rproduct cfg="C#1@2 C#1@1 C#2@1 C#3@1 C#4@1 C#5@1 C#6@1 C#7@1 C#8@1
C#9@1" id="PUR"/>
    </reaction>
    <reaction bidirectional="false" id="pyrb1">
      <annotation name="pathway">PYRimidine Biosynthesis </annotation>
      <reduct cfg="C#1@1 C#2@1 C#3@1 C#4@1" id="OAA"/>
      <reduct cfg="C#1@2" id="CO2"/>
      <rproduct cfg="C#1@2 C#4@1 C#3@1 C#2@1 C#1@1" id="ORO"/>
    </reaction>
    <reaction bidirectional="false" id="pyrb2">
      <annotation name="pathway">PYRimidine Biosynthesis </annotation>
      <reduct cfg="C#1@1 C#2@1 C#3@1 C#4@1 C#5@1" id="ORO"/>
      <reduct cfg="C#1@2 C#2@2 C#3@2 C#4@2 C#5@2" id="Rib5P"/>
      <rproduct cfg="C#1@1 C#2@1 C#3@1 C#4@1 C#1@2 C#2@2 C#3@2 C#4@2 C#5@2"
id="PYRD"/>
      <rproduct cfg="C#5@1" id="CO2"/>
    </reaction>
    <reaction id="lpb1">
      <annotation name="pathway">LiPids Biosynthesis </annotation>
      <reduct cfg="C#1@1 C#2@1" id="AcCoA"/>
    </reaction>
    <reaction bidirectional="false" id="aab14">
      <annotation name="pathway">AA Biosynthesis </annotation>
      <reduct cfg="C#1@1 C#2@1 C#3@1" id="PYR"/>
      <rproduct cfg="C#1@1" id="CO2"/>
      <rproduct cfg="C#2@1 C#3@1" id="AA14"/>
    </reaction>
    <reaction id="aab2">
      <annotation name="pathway">AA Biosynthesis </annotation>
      <reduct cfg="C#1@1 C#2@1 C#3@1 C#4@1" id="OAA"/>
    </reaction>
    <reaction id="aab3">
      <annotation name="pathway">AA Biosynthesis </annotation>
      <reduct cfg="C#1@1 C#2@1 C#3@1 C#4@1 C#5@1" id="OGLU"/>
    </reaction>
    <reaction id="aab5">
      <annotation name="pathway">AA Biosynthesis </annotation>
      <reduct cfg="C#1@1 C#2@1 C#3@1 C#4@1 C#5@1" id="Rib5P"/>
    </reaction>
    <reaction id="aab6">
      <annotation name="pathway">AA Biosynthesis </annotation>
      <reduct cfg="C#1@1 C#2@1 C#3@1 C#4@1" id="Ery4P"/>
    </reaction>
    <reaction id="oneCM1">
      <annotation name="pathway">One Carbon Metabolism</annotation>
      <reduct cfg="C#1@1" id="CO2"/>
      <rproduct cfg="C#1@1" id="CTHF"/>
    </reaction>
    <reaction id="aab7">
      <annotation name="pathway">AA Biosynthesis </annotation>
```

```
        <reduct cfg="C#1@1 C#2@1 C#3@1" id="PEP"/>
    </reaction>
    <reaction id="aab4">
      <annotation name="pathway">AA Biosynthesis </annotation>
      <reduct cfg="C#1@1 C#2@1" id="AcCoA"/>
    </reaction>
    <reaction id="pyrb3">
      <annotation name="pathway">PYRimidine Biosynthesis </annotation>
      <reduct cfg="C#1@1 C#2@1 C#3@1 C#4@1 C#5@1 C#6@1 C#7@1 C#8@1 C#9@1"
id="PYRD"/>
    </reaction>
    <reaction id="purb5">
      <annotation name="pathway">PURine Biosynthesis </annotation>
      <reduct cfg="C#1@1 C#2@1 C#3@1 C#4@1 C#5@1 C#6@1 C#7@1 C#8@1 C#9@1
C#10@1" id="PUR"/>
    </reaction>
    <reaction id="tcc3___1 tcc3___2">
      <annotation name="pathway">TCAcycle</annotation>
      <annotation name="name">tcc3</annotation>
      <reduct cfg="C#1@1 C#2@1 C#3@1 C#4@1 C#5@1" id="OGLU"/>
      <rproduct id="MAL">
        <variant cfg="C#2@1 C#3@1 C#4@1 C#5@1"/>
        <variant cfg="C#5@1 C#4@1 C#3@1 C#2@1"/>
      </rproduct>
      <rproduct cfg="C#1@1" id="CO2"/>
    </reaction>
    <reaction id="upt12">
      <annotation name="pathway">Mixture Input </annotation>
      <reduct cfg="C#1@1 C#2@1 C#3@1 C#4@1 C#5@1 C#6@1" id="GLC12"/>
      <rproduct cfg="C#1@1 C#2@1 C#3@1 C#4@1 C#5@1 C#6@1" id="GLC"/>
    </reaction>
    <reaction id="stcb1">
      <annotation name="pathway">StorageCarbohydrates</annotation>
      <reduct cfg="C#1@1 C#2@1 C#3@1 C#4@1 C#5@1 C#6@1" id="Glc6P"/>
      <rproduct cfg="C#1@1 C#2@1 C#3@1 C#4@1 C#5@1 C#6@1" id="TreGalGlyc"/>
    </reaction>
    <reaction id="stcb2">
      <annotation name="pathway">StorageCarbohydrates</annotation>
      <reduct cfg="C#1@1 C#2@1 C#3@1 C#4@1 C#5@1 C#6@1" id="TreGalGlyc"/>
    </reaction>
    <reaction id="pf4">
      <annotation name="pathway">Pyruvate Fate</annotation>
      <reduct cfg="C#1@1 C#2@1" id="Acet_EtOH"/>
    </reaction>
    <reaction id="coOut">
      <annotation name="pathway">CO2 OUTput </annotation>
      <reduct cfg="C#1@1" id="CO2out"/>
    </reaction>
    <reaction bidirectional="false" id="pyrb4">
      <annotation name="pathway">PYRimidine Biosynthesis </annotation>
      <annotation name="ec-code">2.1.1.45</annotation>
      <annotation name="kegg.reaction">R02101</annotation>
      <reduct cfg="C#1@1 C#2@1 C#3@1 C#4@1 C#5@1 C#6@1 C#7@1 C#8@1 C#9@1"
id="PYRD"/>
      <reduct cfg="C#1@2" id="CTHF"/>
      <rproduct cfg="C#1@1 C#2@1 C#3@1 C#4@1 C#1@2 C#5@1 C#6@1 C#7@1 C#8@1
C#9@1" id="TMP"/>
    </reaction>
```

```xml
    <reaction id="pyrb5">
      <annotation name="pathway">PYRimidine Biosynthesis </annotation>
      <reduct cfg="C#1@1 C#2@1 C#3@1 C#4@1 C#5@1 C#6@1 C#7@1 C#8@1 C#9@1
C#10@1" id="TMP"/>
    </reaction>
    <reaction id="aab9">
      <annotation name="pathway">AA Biosynthesis </annotation>
      <reduct cfg="C#1@1" id="CO2"/>
    </reaction>
    <reaction id="aab10">
      <annotation name="pathway">AA Biosynthesis </annotation>
      <reduct cfg="C#1@1 C#2@1 C#3@1 C#4@1 C#5@1 C#6@1 C#7@1 C#8@1 C#9@1
C#10@1" id="PUR"/>
    </reaction>
    <reaction id="aab11">
      <annotation name="pathway">AA Biosynthesis </annotation>
      <reduct cfg="C#1@1" id="CTHF"/>
    </reaction>
    <reaction id="aab12">
      <annotation name="pathway">AA Biosynthesis </annotation>
      <reduct cfg="C#1@1 C#2@1 C#3@1" id="SER"/>
    </reaction>
    <reaction id="aab13">
      <annotation name="pathway">AA Biosynthesis </annotation>
      <reduct cfg="C#1@1 C#2@1" id="GLY"/>
    </reaction>
    <reaction id="lpb2">
      <annotation name="pathway">LiPids Biosynthesis </annotation>
      <reduct cfg="C#1@1 C#2@1 C#3@1" id="DHAP"/>
    </reaction>
    <reaction id="aab1">
      <annotation name="pathway">AA Biosynthesis </annotation>
      <reduct cfg="C#1@1 C#2@1 C#3@1" id="PYR"/>
    </reaction>
    <reaction bidirectional="false" id="aab15">
      <annotation name="pathway">AA Biosynthesis </annotation>
      <reduct cfg="C#1@1 C#2@1 C#3@1" id="PEP"/>
      <rproduct cfg="C#1@1" id="CO2"/>
      <rproduct cfg="C#2@1 C#3@1" id="AA15"/>
    </reaction>
    <reaction bidirectional="false" id="aab8">
      <annotation name="pathway">AA Biosynthesis </annotation>
      <reduct cfg="C#1@1 C#2@1 C#3@1 C#4@1 C#5@1" id="OGLU"/>
      <rproduct cfg="C#1@1" id="CO2"/>
      <rproduct cfg="C#2@1 C#3@1 C#4@1 C#5@1" id="AA8"/>
    </reaction>
    <reaction id="aab14o">
      <annotation name="pathway">AA Biosynthesis </annotation>
      <reduct cfg="C#1@1 C#2@1" id="AA14"/>
    </reaction>
    <reaction id="aab15o">
      <annotation name="pathway">AA Biosynthesis </annotation>
      <reduct cfg="C#1@1 C#2@1" id="AA15"/>
    </reaction>
    <reaction id="aab8o">
      <annotation name="pathway">AA Biosynthesis </annotation>
      <reduct cfg="C#1@1 C#2@1 C#3@1 C#4@1" id="AA8"/>
    </reaction>
```

```
    <reaction bidirectional="false" id="coEf">
      <annotation name="pathway">CO2 OUTput </annotation>
      <reduct cfg="C#1@1" id="CO2"/>
      <rproduct cfg="C#1@1" id="CO2out"/>
    </reaction>
    <reaction id="gss4">
      <annotation name="pathway">Glycine/Serine System </annotation>
      <reduct cfg="C#1@1 C#2@1" id="Glxlate"/>
      <rproduct cfg="C#1@1 C#2@1" id="GLY"/>
    </reaction>
    <reaction id="glxc1___1 glxc1___2">
      <annotation name="pathway">GLyoXylate Cycle </annotation>
      <annotation name="name">glxc1</annotation>
      <reduct cfg="C#1@1 C#2@1 C#3@1 C#4@1 C#5@1 C#6@1" id="CITICIT"/>
      <rproduct cfg="C#1@1 C#2@1" id="Glxlate"/>
      <rproduct id="MAL">
        <variant cfg="C#6@1 C#3@1 C#4@1 C#5@1" ratio="0.5"/>
        <variant cfg="C#5@1 C#4@1 C#3@1 C#6@1" ratio="0.5"/>
      </rproduct>
    </reaction>
    <reaction id="glxc2">
      <annotation name="pathway">GLyoXylate Cycle </annotation>
      <reduct cfg="C#1@1 C#2@1" id="Glxlate"/>
      <reduct cfg="C#1@2 C#2@2" id="AcCoA"/>
      <rproduct cfg="C#1@1 C#2@1 C#2@2 C#1@2" id="MAL"/>
    </reaction>
  </reactionnetwork>
  <configuration name="config_fit_dnucleoside">
    <input pool="GLC12" type="isotopomer">
      <label cfg="110000" cost="0.0" purity="1.0">1.0</label>
    </input>
    <measurement>
      <mlabel>
        <date>2019-10-10 15:37:12</date>
      </mlabel>
      <model>
        <labelingmeasurement>
          <group id="ms_group_14" scale="auto">
            <textual>PUR#M0,1,2,3,4,5,6,7,8,9,10</textual>
          </group>
          <group id="ms_group_15" scale="auto">
            <textual>PUR[1-5]#M0,1,2,3,4,5</textual>
          </group>
          <group id="ms_group_16" scale="auto">
            <textual>PYRD[5-9]#M0,1,2,3,4,5</textual>
          </group>
          <group id="ms_group_17" scale="auto">
            <textual>PYRD[1-4]#M0,1,2,3,4</textual>
          </group>
          <group id="ms_group_18" scale="auto">
            <textual>TMP[1-5]#M0,1,2,3,4,5</textual>
          </group>
        </labelingmeasurement>
      </model>
      <data>
        <dlabel>
          <date>2019-07-19 20:11:52</date>
        </dlabel>
```

        <datum id="ms_group_14" stddev="0.0014350819543624154"
weight="0">0.031719995420069785</datum>
        <datum id="ms_group_14" stddev="0.00147451654618702"
weight="1">0.13283692796518656</datum>
        <datum id="ms_group_14" stddev="0.001310360619998012"
weight="2">0.26136302426883157</datum>
        <datum id="ms_group_14" stddev="0.0013142056473342968"
weight="3">0.26243363595353203</datum>
        <datum id="ms_group_14" stddev="0.0014576201499512168"
weight="4">0.16432261216805702</datum>
        <datum id="ms_group_14" stddev="0.001490277658707112"
weight="5">0.07978493942869021</datum>
        <datum id="ms_group_14" stddev="0.001491792630749814"
weight="6">0.03308751457628896</datum>
        <datum id="ms_group_14" stddev="0.0014911274476276245"
weight="7">0.013324053040415241</datum>
        <datum id="ms_group_14" stddev="0.0014910498417727062"
weight="8">0.007650917240562705</datum>
        <datum id="ms_group_14" stddev="0.001490998279546338"
weight="9">0.006802008311876879</datum>
        <datum id="ms_group_14" stddev="0.0014908689261455147"
weight="10">0.006674371626489119</datum>
        <datum id="ms_group_15" stddev="0.0020251864382446246"
weight="0">0.19376363175412845</datum>
        <datum id="ms_group_15" stddev="0.001734657292274592"
weight="1">0.3329419961420902</datum>
        <datum id="ms_group_15" stddev="0.0018556942496278294"
weight="2">0.2933305302315938</datum>
        <datum id="ms_group_15" stddev="0.002130038311413169"
weight="3">0.13000603141864736</datum>
        <datum id="ms_group_15" stddev="0.0021604766363987876"
weight="4">0.03747426149828103</datum>
        <datum id="ms_group_15" stddev="0.002158785588671181"
weight="5">0.012483548955259247</datum>
        <datum id="ms_group_16" stddev="6.412984987162851E-4"
weight="0">0.8251550645594964</datum>
        <datum id="ms_group_16" stddev="0.004731909267584373"
weight="1">0.04685827133087658</datum>
        <datum id="ms_group_16" stddev="0.004706951792430985"
weight="2">0.1095206739002582</datum>
        <datum id="ms_group_16" stddev="0.004702661148108066"
weight="3">0.009609552846652726</datum>
        <datum id="ms_group_16" stddev="0.004702450914892361"
weight="4">0.005739707425136421</datum>
        <datum id="ms_group_16" stddev="0.004701808580585281"
weight="5">0.0031167299375796805</datum>
        <datum id="ms_group_17" stddev="0.0012941644791380706"
weight="0">0.3315431007756188</datum>
        <datum id="ms_group_17" stddev="0.0015088269627625782"
weight="1">0.28430316033588365</datum>
        <datum id="ms_group_17" stddev="0.0015658069921230242"
weight="2">0.23518056248878333</datum>
        <datum id="ms_group_17" stddev="0.0016602333382709643"
weight="3">0.11621383406946574</datum>
        <datum id="ms_group_17" stddev="0.001678138977374947"
weight="4">0.03275934233024854</datum>
        <datum id="ms_group_18" stddev="0.004109102788248463"
weight="0">0.299162002598008</datum>

```xml
        <datum id="ms_group_18" stddev="0.004890014150961411"
weight="1">0.23994113461147074</datum>
        <datum id="ms_group_18" stddev="0.005067528465930151"
weight="2">0.20142146877252304</datum>
        <datum id="ms_group_18" stddev="0.005186688733466049"
weight="3">0.14465169115108562</datum>
        <datum id="ms_group_18" stddev="0.005206420413998105"
weight="4">0.11204476317898752</datum>
        <datum id="ms_group_18" stddev="0.005314445560935209"
weight="5">0.0027789396879250726</datum>
      </data>
    </measurement>
    <simulation method="auto" type="auto">
      <variables>
        <fluxvalue flux="aab12" type="net">0.36410598668549443</fluxvalue>
        <fluxvalue flux="aab13" type="net">0.7185582291196076</fluxvalue>
        <fluxvalue flux="aab14o" type="net">0.9987853924512077</fluxvalue>
        <fluxvalue flux="aab15o" type="net">0.2845215816373767</fluxvalue>
        <fluxvalue flux="aab2" type="net">0.5841668519647012</fluxvalue>
        <fluxvalue flux="aab3" type="net">0.696764080025324</fluxvalue>
        <fluxvalue flux="aab4" type="net">0.46114134450777544</fluxvalue>
        <fluxvalue flux="aab5" type="net">0.19256299042608108</fluxvalue>
        <fluxvalue flux="aab6" type="net">0.2845215816373767</fluxvalue>
        <fluxvalue flux="aab7" type="net">0.19312841497202152</fluxvalue>
        <fluxvalue flux="aab8o" type="net">0.19549964056177352</fluxvalue>
        <fluxvalue flux="aab9" type="net">0.09639120595772555</fluxvalue>
        <fluxvalue flux="gly1" type="net">5.899599999999999</fluxvalue>
        <fluxvalue flux="gss1" type="net">3.0</fluxvalue>
        <fluxvalue flux="gss3" type="net">2.0</fluxvalue>
        <fluxvalue flux="lpb1" type="net">1.809444778547385</fluxvalue>
        <fluxvalue flux="lpb2" type="net">0.07697965163525575</fluxvalue>
        <fluxvalue flux="pf1" type="net">4.0</fluxvalue>
        <fluxvalue flux="pf3" type="net">1.0</fluxvalue>
        <fluxvalue flux="pf4" type="net">0.0</fluxvalue>
        <fluxvalue flux="purb5" type="net">0.1000660142113296</fluxvalue>
        <fluxvalue flux="pyrb3" type="net">0.10746922652066192</fluxvalue>
        <fluxvalue flux="pyrb5" type="net">0.05</fluxvalue>
        <fluxvalue flux="tcc1" type="net">3.0</fluxvalue>
        <fluxvalue flux="tcc3___1" type="net">1.75</fluxvalue>
        <fluxvalue flux="tcc4" type="net">3.0</fluxvalue>
        <fluxvalue flux="upt12" type="net">10.0</fluxvalue>
        <fluxvalue flux="purb4" type="net">0.1541</fluxvalue>
        <fluxvalue flux="aab1" type="net">0.7492</fluxvalue>
        <fluxvalue flux="oneCM1" type="net">0.2334</fluxvalue>
        <fluxvalue flux="glxc1___1" type="xch">0.0</fluxvalue>
        <fluxvalue flux="glxc2" type="xch">0.0</fluxvalue>
        <fluxvalue flux="gly1" type="xch">1000.0</fluxvalue>
        <fluxvalue flux="gly2" type="xch">1000.0</fluxvalue>
        <fluxvalue flux="gly3" type="xch">1000.0</fluxvalue>
        <fluxvalue flux="gly4" type="xch">1000.0</fluxvalue>
        <fluxvalue flux="gly5" type="xch">1000.0</fluxvalue>
        <fluxvalue flux="gly6" type="xch">1000.0</fluxvalue>
        <fluxvalue flux="gss2" type="xch">0.0</fluxvalue>
        <fluxvalue flux="gss3" type="xch">1000.0</fluxvalue>
        <fluxvalue flux="gss4" type="xch">0.0</fluxvalue>
        <fluxvalue flux="oneCM1" type="xch">1000.0</fluxvalue>
        <fluxvalue flux="ppp2" type="xch">1000.0</fluxvalue>
        <fluxvalue flux="ppp3" type="xch">1000.0</fluxvalue>
```

```
        <fluxvalue flux="ppp4" type="xch">1000.0</fluxvalue>
        <fluxvalue flux="ppp5" type="xch">1000.0</fluxvalue>
        <fluxvalue flux="ppp6" type="xch">1000.0</fluxvalue>
        <fluxvalue flux="ppp7" type="xch">1000.0</fluxvalue>
        <fluxvalue flux="stcb1" type="xch">1000.0</fluxvalue>
        <fluxvalue flux="tcc1" type="xch">1000.0</fluxvalue>
        <fluxvalue flux="tcc2" type="xch">1000.0</fluxvalue>
        <fluxvalue flux="tcc4" type="xch">1000.0</fluxvalue>
        <fluxvalue flux="tcc3___1" type="xch">500.0</fluxvalue>
      </variables>
    </simulation>
  </configuration>
</fluxml>
```

8.2| LOG OF THE MFD ESTIMATION

Log of the estimation of MFD of one population model and deoxynucleosides experimental data.

```
validating configuration "config_fit_dnucleoside" ...
user requests 53 free fluxes (30 free net + 23 free xch).
size of stoichiometry is (38x70); exact rank is 38.
size of NET constraint system is (40x70); numerical rank is 40
size of XCH constraint system is (2x70); numerical rank is 2
validation succeeded!
using the following stoichiometry ...
            upt: net=         +10 (DEPD), xch=          0 (CONS)
           gly1: net=      +5.8996 (FREE), xch=       1000 (FREE)
           gly2: net=      +6.11966 (DEPD), xch=       1000 (FREE)
           gly3: net=      +6.11966 (DEPD), xch=       1000 (FREE)
           gly4: net=      +6.04269 (DEPD), xch=       1000 (FREE)
           gly5: net=      +12.1301 (DEPD), xch=       1000 (FREE)
           gly6: net=      +9.13012 (DEPD), xch=       1000 (FREE)
           gly7: net=      +8.91084 (DEPD), xch=          0 (CONS)
           ppp1: net=      +0.97649 (DEPD), xch=          0 (CONS)
           ppp2: net=     +0.220065 (DEPD), xch=       1000 (FREE)
           ppp3: net=     +0.756425 (DEPD), xch=       1000 (FREE)
           ppp4: net=     +0.220065 (DEPD), xch=       1000 (FREE)
           ppp5: net=     +0.252293 (DEPD), xch=       1000 (FREE)
           ppp6: net=     +0.252293 (DEPD), xch=       1000 (FREE)
           ppp7: net=    -0.0322284 (DEPD), xch=       1000 (FREE)
            pf1: net=          +4 (FREE), xch=          0 (CONS)
            pf2: net=      +3.64156 (DEPD), xch=          0 (CONS)
            acs: net=      +3.64156 (DEPD), xch=          0 (CONS)
            pf3: net=          +1 (FREE), xch=          0 (CONS)
           tcc1: net=          +3 (FREE), xch=       1000 (FREE)
           tcc2: net=      +4.39226 (DEPD), xch=       1000 (FREE)
           tcc4: net=          +3 (FREE), xch=       1000 (FREE)
           gss1: net=          +3 (FREE), xch=          0 (CONS)
           gss2: net=      +2.63589 (DEPD), xch=          0 (FREE)
           gss3: net=          +2 (FREE), xch=       1000 (FREE)
          texc1: net=     +0.258364 (DEPD), xch=          0 (CONS)
          texc2: net=      +1.47871 (DEPD), xch=          0 (CONS)
          purb1: net=       +0.1541 (DEPD), xch=          0 (CONS)
          purb2: net=       +0.1541 (DEPD), xch=          0 (CONS)
          purb3: net=       +0.1541 (DEPD), xch=          0 (CONS)
          purb4: net=       +0.1541 (FREE), xch=          0 (CONS)
          pyrb1: net=     +0.157469 (DEPD), xch=          0 (CONS)
          pyrb2: net=     +0.157469 (DEPD), xch=          0 (CONS)
           lpb1: net=      +1.80944 (FREE), xch=          0 (CONS)
          aab14: net=     +0.998785 (DEPD), xch=          0 (CONS)
           aab2: net=     +0.584167 (FREE), xch=          0 (CONS)
           aab3: net=     +0.696764 (FREE), xch=          0 (CONS)
           aab5: net=     +0.192563 (FREE), xch=          0 (CONS)
           aab6: net=     +0.284522 (FREE), xch=          0 (CONS)
         oneCM1: net=       +0.2334 (FREE), xch=       1000 (FREE)
```

```
    aab7: net=      +0.193128 (FREE), xch=            0 (CONS)
    aab4: net=      +0.461141 (FREE), xch=            0 (CONS)
   pyrb3: net=      +0.107469 (FREE), xch=            0 (CONS)
   purb5: net=      +0.100066 (FREE), xch=            0 (CONS)
 tcc3___1: net=          +1.75 (FREE), xch=          500 (FREE)
 tcc3___2: net=          +1.75 (DEPD), xch=          500 (DEPD)
   upt12: net=            +10 (FREE), xch=            0 (CONS)
   stcb1: net=        +3.12391 (DEPD), xch=         1000 (FREE)
   stcb2: net=        +3.12391 (DEPD), xch=            0 (CONS)
     pf4: net=             +0 (FREE), xch=            0 (CONS)
   coOut: net=        +16.2423 (DEPD), xch=            0 (CONS)
   pyrb4: net=           +0.05 (DEPD), xch=            0 (CONS)
   pyrb5: net=           +0.05 (FREE), xch=            0 (CONS)
    aab9: net=      +0.0963912 (FREE), xch=            0 (CONS)
   aab10: net=       +0.054034 (DEPD), xch=            0 (CONS)
   aab11: net=       +0.511094 (DEPD), xch=            0 (CONS)
   aab12: net=       +0.364106 (FREE), xch=            0 (CONS)
   aab13: net=       +0.718558 (FREE), xch=            0 (CONS)
    lpb2: net=      +0.0769797 (FREE), xch=            0 (CONS)
    aab1: net=         +0.7492 (FREE), xch=            0 (CONS)
   aab15: net=       +0.284522 (DEPD), xch=            0 (CONS)
    aab8: net=         +0.1955 (DEPD), xch=            0 (CONS)
  aab14o: net=       +0.998785 (FREE), xch=            0 (CONS)
  aab15o: net=       +0.284522 (FREE), xch=            0 (CONS)
   aab8o: net=         +0.1955 (FREE), xch=            0 (CONS)
    coEf: net=        +16.2423 (DEPD), xch=            0 (CONS)
    gss4: net=       -3.76324 (DEPD), xch=            0 (FREE)
 glxc1___1: net=      -0.696132 (DEPD), xch=            0 (FREE)
 glxc1___2: net=      -0.696132 (DEPD), xch=            0 (DEPD)
   glxc2: net=        +2.37097 (DEPD), xch=            0 (FREE)
tayloring simulation for measurement specifications ...
generating a REDUCED EMU network
Phase I  (generating a network with 10 levels)
Phase II (caching 833 non-zero elements)
evaluating objective function ...
eval #1: improved residual: 306861.9539062081
evaluation of objective function took 0.00540805s
```

«As raposas têm tocas e as aves do céu têm ninhos; mas o Filho do Homem não tem onde reclinar a cabeça.»

«Foxes have holes, and birds of the air have nests, but the Son of Man has nowhere to lay his head.»

Mt 8, 20

Ad Majorem Dei Gloria